

SEMI-AUTOMATIC IDENTIFICATION OF NEOGENIC DEPOSITS
BY USING HIGH RESOLUTION DIGITAL SURFACE MODELS IN
SOUTHEASTERN BRAZIL

Dissertation

der Mathematisch-Naturwissenschaftlichen Fakultät
der Eberhard Karls Universität Tübingen
zur Erlangung des Grades eines
Doktor der Naturwissenschaften
(Dr.rer.nat.)

vorgelegt von
MSc. Sonia Maria Lima Silva
aus Rio de Janeiro/Brazil

Tübingen, 2014

Tag der mündlichen Qualifikation:	12.01.2015
Dekan:	Prof. Dr. Wolfgang Rosenstiel
1.- Berichterstatter:	Prof. Dr. Volker Hochschild
2.- Berichterstatter:	Prof. Dr. Claudio Limeira Mello

Dedicated in memory of my parents
Norma and Morais, true examples of
dignity, generosity and honesty.

To my beloved husband Steffen for
his dedication, encouragement and
support.

ACKNOWLEDGMENTS

My deepest gratitude to the following people and institutions:

The *Coordenação de Aperfeiçoamento de Pessoal de Nível Superior* (CAPES) for granting a scholarship during the four years of my participation in the program, including an international scholarship for a PhD program in Germany, which enabled me to make my dream of achieving a doctorate come true.

The responsables of the Graduate Program in Geology/IGEO/UFRJ for accepting me and granting funds from PROAP/CAPES, as well as their assistance in the development of field activities.

The Geographic Institute of the Universität Tübingen for its great support, affection and friendship. And for making its infrastructure available to me at all times.

Professor Dr. Volker Hochschild (Universität Tübingen) for his support and the great opportunity he gave me to work in his research group, fostering not only me, but also all of the other foreigners; treating us with care, understanding, respect, tolerance and the awareness of cultural differences among countries.

Professor Dr. Claudio Limeira Mello (UFRJ) and Dr. José Duarte Correia (IBGE), for their guidance, friendship and motivation during this long journey. Both of them are examples of professionalism, ethics and dedication in all the activities they perform.

The Professors and all friends from the Geographisches Institute at the Universität Tübingen, who supported me at this important stage of my life. My special “Vielen Dank” for Dr. Michael Märker, Dr. Hans-Joachim Rosner, Dr. Jan Kropacek, Christian Bick, Christian Sommer, Elio Flores, Felix Bachofer,

Geraldine Quénéhervé, Mansour Mahamane, Reza Zakerinejad, Sandy-Cheril Manton and Silvia Duttle for all the help regarding several issues.

All Professors and staff of the Graduate Program in Geology/IGEO/UFRJ for their friendship and assistance in administrative matters.

The Professors and the entire staff of *Núcleo de Estudos do Quaternário* (NEQUAT)/Department of Geography /UFRJ for the friendly welcome.

The entire staff of the Division of Programs and Scholarships of the “*Pró-reitoria de Pós-graduação e Pesquisa*” of UFRJ, for their help in matters concerning the PhD abroad.

The staff of the Division of Covenants and International Relations Office of the *Gabinete do Reitor da Pró-reitoria de Pós-graduação e Pesquisa* of the UFRJ, for providing all necessary information regarding the envisaged transnational co-mentoring and their respective legal procedures.

The Japan Aeroespacial Agency (JAXA), that provided me the four triplets of ALOS/PRISM for free.

Steven Corr and the entire support staff of PCI Geomatics, for having given me the software license for the generation of DSMs and orthoimages free of charge for 3 months.

My unforgettable parents, to whom I dedicate this moment of my life, Norma Lima Silva and Morais Silva, who always encouraged me in all matters related to my personal and intellectual development. Without the sacrifices of you both, none of this would have been possible.

My dear and irreplaceable husband for his understanding and encouragement during this great challenge to develop a doctoral thesis. His calmness gave me balance to complete another chapter of our journey together.

Abstract

The Cenozoic deposits occupy large areas of the Brazilian territory with parts subject to intense human occupation. Nevertheless they are still little known and researched. One of the most important Cenozoic sedimentary units in Brazil corresponds to *Barreiras* Formation (Neogene), which is located along almost all of the Brazilian coast. Geomorphologically the deposits of the *Barreiras* Formation are associated with a relief of tabular forms, dissected into deep valleys with steep slopes. This research aims to develop a semi-automatic method of detailed scale mapping *Barreiras* Formation deposits by employing Digital Surface Models (DSMs) obtained from high resolution satellite images. The justification of this research is based on both: the lack of cartographic databases on the scale of 1:25.000, as well as the lack of maps representing these deposits in more detailed scale necessary for their proper description and interpretation. The selected area is located in the northern region of the State of *Rio de Janeiro*, between the city of *Campos dos Goytacazes* and the border to the State of *Espírito Santo*. In this area the most significant occurrence of *Barreiras* Formation deposits in the State of *Rio de Janeiro* is found. The main goal to be achieved in this research is the identification of such deposits by evaluating their geomorphological characteristics which are modeled by specific variables that represent these aspects. The study on the potential of the use of stereoscopic capabilities of high resolution images coming from ALOS/PRISM sensor, which made the generation of DSMs possible, together with the availability of Rational Polynomial Coefficients (RPCs), contributed to minimize the costs of acquiring field data, since most of the information needed to identify these deposits were obtained directly from these DSMs. The method used in this research consisted of: (1) the automatic generation and vertical accuracy control of DSMs; (2) the orthorectification of images and horizontal accuracy control of orthoimages; (3) the preparation of DSMs for the terrain analyses; (4) the terrain analyses; and (5) the generation and qualitative and quantitative evaluation of the final map. The generation of DSMs and the orthorectification of the images were carried out by using the empirical model of rational functions, using the RPCs available in the images. The terrain analyses

were based on the interpretation and combination of specific morphometric variables using two different methods: (a) combinatorial OR; and (b) maximum entropy. The best result was obtained with the first method, combining the four variables: altitude, slope, curvature and terrain roughness index. Beforehand, these variables were classified according to intervals representing the *Barreiras* Formation. The assessment of the final map was made by comparing such map to another one, generated by using visual interpretation method, in a scale comparable to the scale of the map generated in this research. The level of detail in drawing the boundaries of the deposits of *Barreiras* Formation in the final map was verified by comparing it to the map available at 1:250,000 scale, obtained from the Digital Terrain Models (DTMs) of the SRTM. The potential of the use of stereoscopic capabilities of high resolution images obtained from sensor ALOS/PRISM, together with the availability of RPCs reduced considerably the cost of acquisition of field data required for the generation of DSMs and orthoimages. The proposed methodology has brought clear benefits in terms of reducing the time spent in making a map in detail scale, compared to the time spent using the visual interpretation method.

Keywords: Cenozoic deposits; DSMs; ALOS/PRISM; RPCs; Southeastern Brazil.

Kurzfassung

Die känozoischen Ablagerungen bedecken einen großen, oftmals dicht besiedelten Teil der Landoberfläche Brasiliens. Dennoch sind diese Ablagerungen bis heute wenig bekannt und erforscht. Eine der wichtigsten känozoischen Sedimenteinheiten in Brasilien ist die „Barreiras Formation“ (Neogen), die entlang fast der gesamten brasilianischen Küste auftritt. Geomorphologisch sind die Ablagerungen der Barreiras Formation mit tafelförmigen Reliefs verbunden, zergliedert durch tiefe Täler mit steilen Berghängen. Diese Studie zielt auf die Entwicklung einer halbautomatischen Methode zur detaillierten Kartierung dieser Barreiras Formationen mit Hilfe von Digitalen Oberflächenmodellen („DOMs“), die aus hochauflösenden Satellitenbildern erstellt wurden, ab. Die Begründung für diese Studie ergibt sich sowohl aus dem Mangel an geographischen Datenbanken im Maßstab 1:25.000, als auch einem Mangel an detaillierteren Karten von diesen Ablagerungen, welche für ihre adäquate Beschreibung und Interpretation erforderlich sind. Das ausgewählte Gebiet zur Entwicklung der Studie befindet sich nördlich des Bundesstaates Rio de Janeiro, zwischen der Stadt Campos dos Goytacazes und der Grenze des Bundesstaates Espírito Santo. In diesem Gebiet befindet sich das bedeutendste Vorkommen von Ablagerungen im Bundesstaat Rio de Janeiro. Das Hauptziel dieser Studie war die Identifizierung dieser Ablagerungen durch Auswertung ihrer geomorphologischen Charakteristika, welche mit Hilfe von spezifischen Variablen modelliert werden, die diese Aspekte repräsentieren. Die Studie über das Potential des Einsatzes stereoskopischer Fähigkeiten von hochauflösenden Satellitenbildern, des ALOS/PRISM Sensors, welcher die Generierung von DOMs ermöglicht hat, verbunden mit der Verfügbarkeit Rationaler Polynom Koeffizienten (RPCs), trug zur Kostenminimierung bei der Akquisition von Felddaten bei, da die meisten der benötigten Informationen zur Identifizierung dieser Ablagerungen direkt von diesen Modellen erstellt wurden. Die eingesetzte Methode bestand aus: (1) Automatische Generierung und vertikale Validierung von DOMs. (2) Orthorektifizierung der Bilder und horizontale Validierung der Ortho-Bilder (3) Vorbereitung von DOMs für die Feldanalysen, (4) Feldanalysen und (5),

Generierung und qualitative und quantitative Evaluierung der finalen Karte. Die Erzeugung von DOMs und die Orthorektifizierung der Bilder wurde mit Hilfe des empirischen Modells der rationalen Funktionen anhand der in den Bildern verfügbaren rationalen Polynomkoeffizienten (RPCs) gemacht. Die Feldanalysen basierten auf der Interpretation und Kombination spezifischer morphometrischer Variablen mit zwei unterschiedlichen Ansätzen: (a) combinatorial OR; und (b) des Prinzips der Maximum-Entropie. Das beste Ergebnis wurde mit dem ersten Ansatz erzielt, nämlich der Kombination der vier Variablen Höhe, Neigung, Krümmung und Gelände-Rauheitsindex. Die Variablen wurden zuvor nach Intervallen, die die Barreiras Formation darstellen, eingestuft. Die Bewertung der in der Studie erzeugten "finalen Karte" wurde durch den Vergleich der finalen Karte mit einer anderen, durch die visuelle Interpretationsmethode erzeugten Karte in vergleichbarem Maßstab gemacht. Der Detailgrad bei der Festlegung der Grenzen der Barreiras Formation in der finalen Karte wurde durch den Vergleich mit der verfügbaren Karte im Maßstab 1:250.000 verifiziert, die von den Digitalen Geländemodellen ("DGMs") aus dem SRTM erstellt worden war. Das Potential der Verwendung von stereoskopischen Möglichkeiten von räumlich hochauflösenden Bildern von ALOS / PRISM, zusammen mit der Verfügbarkeit von RPCs reduzierte die Kosten für die Gewinnung von Felddaten erheblich, die für die Erzeugung von DOMs und Satellitenorthobildern erforderlich sind. Die vorgeschlagene Methodik zeigte deutliche Vorteile in Bezug auf die Zeiteinsparung der Kartenherstellung im Detail-Maßstab verglichen mit der Methodik der visuellen Interpretation.

Schlüsselwörter: Känozoischen Ablagerungen; DOMs; ALOS/PRISM; RPCs; Southeastern Brazil.

List of Figures

Figure 1	Contours of <i>Barreiras</i> Formation by: (a) Silva & Cunha (2001), scale of 1:500,000 and (b) Ribeiro (2010), scale of 1:250,000. A1, A2 and A3 represent areas with differences in the limits between <i>Barreiras</i> Formation and basement rocks as identified by these authors.....	25
Figure 2	Approaches and main methods used in the present study.....	28
Figure 3	Distribution of <i>Barreiras</i> Formation along the Brazilian coast.....	30
Figure 4	Representative deposits of <i>Barreiras</i> Formation outcropping on the northern Rio de Janeiro coast (region of <i>Barra de Itabapoana</i> , on the border with the State of <i>Espírito Santo</i>). Sandy sediments (facies Am, Aca, Ah) are prevalent and distributed in lenticular to tabular layers; the muddy sediments (facies La1 and La2), less expressive, are distributed in layers with lenticular geometry. Note post- <i>Barreiras</i> deposits on the top of the outcrop.....	33
Figure 5	Main geomorphological aspects associated with <i>Barreiras</i> Formation. Photography obtained near <i>Campos dos Goytacazes</i>	34
Figure 6	View of transitional landscape between the crystalline basement and <i>tabuleiros</i> of <i>Barreiras</i> Formation.....	35
Figure 7	Rose diagrams of lineaments frequency (left) and frequency plus length of lineaments (right) obtained for (a) Precambrian basement domain and (b) <i>Barreiras</i> Formation domain, in the region between the <i>Paraíba do Sul</i> and <i>Doce</i> rivers (between the north of the <i>Rio de Janeiro</i> State and the center-north of the State of <i>Espírito Santo</i>). There are two sets of predominant lineaments in the Precambrian basement domain (NE-SW and NW-SE). In the <i>Barreiras</i> Formation domain, NW-SE lineaments are predominant.....	36
Figure 8	Topographic profiles show the stepped behavior of <i>tabuleiros</i> ...	37

Figure 9	Location of the study area, with the representation of <i>Barreiras</i> Formation contour as Ribeiro (2010).....	39
Figure 10	Mosaic of topographic charts at 1:50,000 scale covering the study area.....	39
Figure 11	Main access roads in the study area.....	40
Figure 12	Map of structural provinces in central and southern Brazil, according to Bizzi et al. (2003), with the location of the study area in the context of the <i>Mantiqueira</i> Province.....	41
Figure 13	Geologic map of the northern portion of the state of <i>Rio de Janeiro</i> , where the study area is located.....	42
Figure 14	Geomorphological units in the northern <i>Rio de Janeiro</i> State, according to the geomorphological map of the state of <i>Rio de Janeiro</i> and height variation in the study area.....	44
Figure 15	Main landscape units in the study area. In the foreground, there is a alluvial plain of <i>Paraíba do Sul</i> River and small lacustrine bodies, in the limits of <i>Campos dos Goytacazes</i> . In the background, it can be observed the mountainous domain (<i>Serra do Mar</i>), and a hilly area on its foot. To the left, it is noticed an isolated massif.....	45
Figure 16	Effects of geometric distortions caused by the change of speed and change in the attitude of the platform.....	50
Figure 17	Distortion of orbital images related to Earth: (a) rotation; (b) curvature; and (c) topographic effects.....	51
Figure 18	Scattering of solar radiation in the atmosphere.....	52
Figure 19	Triplet observation mode of ALOS/PRISM.....	54
Figure 20	Automatic location of a homologous point in another image.....	58
Figure 21	Epipolar plan and the corresponding epipolar lines.....	59
Figure 22	Collinearity principle.....	60
Figure 23	Example of Triangulated Irregular Networks (TIN) structure.....	63
Figure 24	Example of Regular Grid structure.....	63
Figure 25	Displacement in raw image caused by the relief.....	67
Figure 26	(a) Precision (σ); (b) tendency (b-bias); and (c) accuracy getting together precision and tendency (RMSE).....	69

Figure 27	Normal Distribution.....	70
Figure 28	ALOS/PRISM satellite imagery covering the study area.....	75
Figure 29	Main processes of Remote Sensing approach.....	79
Figure 30	Processes involved in the Combinatorial Or and Maximum Entropy methods (Geomorphometry approach).....	85
Figure 31	Main processes involved in the Geographic Information System approach.....	90
Figure 32	Relationship between orthometric (H) and ellipsoid (h) heights N = geoid undulation.....	93
Figure 33	Plan and profile curvature and respective tangent vectors (t_h = horizontal tangent and t_v = vertical tangent).....	94
Figure 34	Effect of plan curvature on the water flow lines (A) concave curvature with convergent flow (in valley); (B) rectilinear; (C) convex curvature with divergent flow (on ridges).....	95
Figure 35	Scraps from the same detail area (triplet T1) of the DSMs generated by LPS and PCI GEOMATICS softwares. Several problems (noises) in the DSM generated with the LPS software, particularly in the area enclosed by the red circle can be noticed.....	99
Figure 36	Morphometric variables derived from DSM surface smoothed 10 times with window size of 15 by 15 pixels: Height; Slope; Curvature; Terrain Roughness Index (TRI); Multiresolution Index of Valley Bottom Flatness (MRVBF) and Multiresolution Index of Ridges Top Flatness (MRRTF). The main intervals related to <i>Barreiras</i> Formation, but not exclusively, are represented by the yellow color.....	103
Figure 37	Morphometric variables derived from DSM surface smoothed 14 times with window size of 15 by 15 pixels: Height; Slope; Curvature; Terrain Roughness Index (TRI); Multiresolution Index of Valley Botton Flatness (MRVBF) and Multiresolution Index of Ridges Top Flatness (MRRTF). The main intervals related to <i>Barreiras</i> Formation, but not exclusively, are represented by the yellow color.....	104

Figure 38	Figure 38: Morphometric variables derived from DSM surface smoothed 10 times with window size of 21 by 21 pixels: Height; Slope; Curvature; Terrain Roughness Index (TRI); Multiresolution Index of Valley Bottom Flatness (MRVBF) and Multiresolution Index of Ridges Top Flatness (MRRTF). The main intervals related to <i>Barreiras</i> Formation, but not exclusively, are represented by the yellow color.....	105
Figure 39	Map of <i>Barreiras</i> Formation generated from the combination of morphometric variables height, slope and curvature, and indices TRI, MRVBF and MRRTF, performed upon DSMs smoothed with a window size of 15 by 15 pixels and 10 iterations.....	107
Figure 40	Map of <i>Barreiras</i> Formationm generated from the combination of morphometric variables slope and curvature, and indices TRI, MRVBF, MRRTF, performed upon DSMs smoothed with a window size of 15 by 15 and 10 iterations.....	110
Figure 41	Map of <i>Barreiras</i> Formation generated from the combination of morphometric variables height, with two classes (<i>Barreiras</i> Formation and basement), slope and curvature, and indices TRI, MRVBF and MRRTF, performed upon DSMs smoothed with a window of 15x15 pixels and 10 iterations.....	112
Figure 42	Map of <i>Barreiras</i> Formation generated from the combination of morphometric variables height, with two classes (<i>Barreiras</i> Formation and basement), slope, curvature and TRI, performed upon DSMs smoothed with a window of 15x15 pixels and 10 iterations.....	114
Figure 43	Map of <i>Barreiras</i> Formation generated from the combination of morphometric variables height, with two classes (<i>Barreiras</i> Formation and basement.), slope, curvature and TRI, performed upon DSMs smoothed with a window of 15x15 pixels and 14 iterations.....	116
Figure 44	Map of <i>Barreiras</i> Formation generated from the combination of morphometric variables height - with two classes (<i>Barreiras</i>	

	Formation and basement), slope, curvature and TRI, performed upon DSMs smoothed with a window of 21x21 pixels and 10 iterations.....	118
Figure 45	Probability map of <i>Barreiras</i> Formation distribution generated by Maxent software, using 67 sample points collected in the field.....	120
Figure 46	Jackknife graph of Area Under the Curve (AUC), showing the importance of each variable to generate the probability map of <i>Barreiras</i> Formation distribution from 67 samples collected in the field.....	122
Figure 47	Probability map of <i>Barreiras</i> Formation distribution generated by Maxent software, using 46 samples collected from desktop..	124
Figure 48	Jackknife graph of Area Under the Curve (AUC), showing the importance of each variable to generate the probability map of <i>Barreiras</i> Formation distribution from 46 samples collected in the field.....	125
Figure 49	Probability map of <i>Barreiras</i> Formation distribution generated by Maxent software, using 151 samples collected from desktop	126
Figure 50	Jackknife graph of Area Under the Curve (AUC), showing the importance of each variable to generate the probability map of <i>Barreiras</i> Formation distribution from 151 samples collected in the field.....	127
Figure 51	Validation through spatial correlation analysis of the maps generated with combinatorial OR method upon DSM surface smoothed 10 times with windows 15 by 15 pixels, using the morphometric variables: (a) height, slope, curvature, TRI, MRVBF and MRRTF; (b) slope, curvature, TRI, MRVBF and MRRTF; and (c) height (<i>Barreiras</i> and basement interval classes), slope, curvature, TRI, MRVBF and MRRTF.....	131
Figure 52	Validation through spatial correlation analysis of the maps generated with combinatorial OR method using the morphometric variables: height (<i>Barreiras</i> and basement	

	interval classes), slope, curvature and TRI. (a) DSM surface smoothed 10 times with windows of 15 by 15 pixels; (b) DSM surface smoothed 14 times with windows of 15 by 15 pixels; and (c) DSM surface smoothed 10 times with windows of 21 by 21 pixels.....	132
Figure 53	Validation through spatial correlation analysis of the maps generated with maximum entropy method using the morphometric variables: height (<i>Barreiras</i> and basement interval classes), slope, curvature and TRI for the DSM surface smoothed 14 times with windows of 15 by 15 pixels. (a) Samples collected in field surveys; (b) 46 sample points collected from desktop; and (c) 151 sample points collected from desktop.....	133
Figure 54	Comparison between Silva (2014) and Chrismann (2014) maps and details of discrepancy areas (A1, A2, A3).....	135
Figure 55	Comparison between Silva (2014) and Ribeiro (2010) maps and details of discrepancy areas (A1, A2, A3).....	136

List of tables

Table 1	Description of the sources of error for the two categories and sub-categories.....	49
Table 2	Characteristics of ALOS/PRISM satellite imagery.....	54
Table 3	Differences between the two storage structures.....	64
Table 4	Values of the CE90 and horizontal RMSE in some Brazilian systematic mapping scales.....	72
Table 5	Values of the LE90 and vertical RMSE in some Brazilian systematic mapping scales.....	73
Table 6	Identification of scenes (triplets); acquisition date and scene code.....	75
Table 7	Number of ground control points used in vertical accuracy control for each triplet.....	81
Table 8	Number of ground control points used in horizontal accuracy control for each triplet.....	83
Table 9	Values of LE90 and RMSE of DSMs generated in LPS and their respective technical standard values established by the Brazilian Technical Standards of Cartography for the scale of 1:25,000 Class A.....	97
Table 10	Values of LE90 and RMSE of DSMs generated in PCI GEOMATICS and their respective technical standard values established by the Brazilian Technical Standards of Cartography for the scale of 1:25,000 Class A.....	98
Table 11	Values of CE90 and RMSE of orthoimages generated in PCI GEOMATICS and their respective technical standard values established by the Brazilian Technical Standards of Cartography for the scale of 1:25,000 Class A.....	100
Table 12	Class intervals of morphometric variables of <i>Barreiras</i> Formation for the three smoothed surfaces obtained by using the averaging technique FOCALMEAN.....	101
Table 13	Main characteristics of the combinatorial OR and maximum entropy methods.....	129

Abbreviations and Acronyms

ADS	Angular Displacement Sensor
ALOS	Advanced Land Observing Satellite
AOCS	Attitude and Orbit Control Subsystem
ATE	Automatic Terrain Extraction
CCD	Charged-Coupled Device
CEPERJ	<i>Fundação Centro Estadual de Estatísticas, Pesquisas e Formação de Servidores Públicos do Rio de Janeiro</i> (State Center for Statistics, Research and Training of Civil Servants of Rio de Janeiro)
CPRM	<i>Serviço Geológico do Brasil</i> (Brazilian Geological Services)
DBA	Database Administrator
DEGEO	<i>Departamento de Geologia</i> (Department of Geology)
DN	Digital Number
EORC	Earth Observation Research Center
ESRI	Environmental Systems Research Institute
GDTA	Groupement pour le Développement de la Télédétection Aérospatiale
GPS	Global Positioning System
IBGE	<i>Instituto Brasileiro de Geografia e Estatística</i> (Brazilian Institute for Geography and Statistics)
ICA	International Cartographic Association
IGEO	<i>Instituto de Geociências</i> (Geosciences Institute of UFRJ)
IRU	Inertial Reference Unit
ISE	<i>Índice Sócioeconômico</i> (Socioeconomic index)
JAXA	Japan Aerospace Exploration Agency

LPS	Leica Photogrammetry Suite
MAPGEO	<i>Mapa Geoidal</i> (Geoidal MAP)
DEM	Digital Elevation Model
DSM	Digital Surface Model
DTM	Digital Terrain Model
NEM	Numeric Elevation Model
MRRTF	Multiresolution index of Ridges Top Flatness
MRVBF	Multiresolution index of Valley Bottom Flatness
NEQUAT	<i>Núcleo de Estudos do Quaternário e Tecnógeno</i> (Research Group on Quaternary and Technogene)
NMAS	National Map Accuracy Standards
PRISM	Panchromatic Remote-sensing Instrument for Stereo Mapping
RADAR	Radar Detection And Ranging
RPC	Rational Polynomial Coefficient
SAGA	System for Automated Geoscientific Analysis
SAR	Synthetic Aperture Radar
SGBD	System Manager for Data Bases
GIS	Geographic Information System
SRTM	Shuttle Radar Topography Mission
STT	Star Tracker
TRI	Terrain Roughness Index
USGS	U.S. Geological Survey
UTM	Universal Transverse Mercator
VIR	Visible and Infrared

CONTENTS

ABSTRACT	vi
KURZFASSUNG	viii
LIST OF FIGURES	x
LIST OF TABLES	xvi
LIST OF ABBREVIATIONS AND ACRONYMS	xvii
1 INTRODUCTION	22
1.1 Problem Description.....	23
1.2 Research Deficit	26
1.3 Goals.....	26
1.4 Research Methods	27
2 THE BARREIRAS FORMATION	30
3 STUDY AREA	38
3.1 Location.....	38
3.2 Regional geology.....	40
3.2.1 Basement rocks.....	41
3.2.2 Cenozoic sedimentary deposits.....	42
3.3 Geomorphology.....	43
3.4 Climate, vegetation and occupation.....	46
4 RELEVANT CONCEPTS	48
4.1 Remote Sensing Imagery.....	48
4.1.1 Sources of geometric and radiometric distortions.....	48
4.1.2 Orbital images ALOS/PRISM.....	53
4.2 Geometric correction of imagery.....	55
4.3 Digital Elevation Models (DEMs).....	56
4.3.1 Automatic Generation of Digital Surface Models (DSMs).....	57
4.3.1.1 Matching images.....	58
4.3.1.2 Modeling of surface.....	61
4.3.1.3 Post-Processing.....	64
4.4 Orthoimagery.....	66
4.5 Quality control of remote sensing products.....	67
4.5.1 Positional Accuracy.....	68

4.5.2. Control of DSMs and Orthoimages in Brazil.....	70
4.5.2.1 Orthoimages horizontal control.....	71
4.5.2.2 DSMs vertical control.....	72
5 MATERIALS AND METHODS.....	74
5.1 Materials.....	74
5.1.1 ALOS/PRISM satellite imagery.....	74
5.1.2 Cartographic Products.....	75
5.1.3 Survey points.....	76
5.1.4 Software Applications.....	77
5.2 Methods.....	77
5.2.1 Remote Sensing approach.....	78
5.2.1.1 Digital Surface Models (DSMs) automatic generation.....	78
5.2.1.2 Orthorectification.....	82
5.2.2 Geomorphometry approach.....	83
5.2.2.1 Combinatorial OR.....	86
5.2.2.2 Maximum Entropy.....	87
5.2.3 Geographic Information System approach.....	89
5.2.3.1 DSMs post-processing.....	89
5.2.3.2 Morphometric variables generation.....	92
5.2.3.3 Map generalization, validation and visualization.....	96
6 RESULTS AND DISCUSSIONS.....	97
6.1 Results of accuracy control upon remote sensing products.....	97
6.1.1 Results of vertical accuracy control upon DSMs generated by LPS software.....	97
6.1.2 Results of vertical accuracy control upon DSMs generated by PCI GEOMATICS software.....	98
6.1.3 Qualitative evaluation of DSMs.....	98
6.1.4 Results of horizontal accuracy control upon orthoimages generated by PCI GEOMATICS software.....	100
6.2 Results of morphometric variables generation.....	100
6.3 Results of methods for identification of <i>Barreiras</i> Formation.....	106
6.3.1 Results obtained using the method of combinatorial OR.....	106
6.3.1.1 DSM smoothed 10 times with window size of 15 by 15	

pixels.....	106
6.3.1.2 DSM smoothed 14 times with window size of 15 by 15 pixels.....	115
6.3.1.3 DSM smoothed 10 times with window size of 21 by 21 pixels.....	117
6.3.2 Results of tests using method of maximum entropy.....	117
6.3.2.1 Samples collected in field survey.....	119
6.3.2.2 Set of samples collected from desktop.....	122
6.3.3 Evaluation of methods for identification of <i>Barreiras</i> Formation.....	127
6.4 Results of the output maps validation.....	129
6.5 Results of map visualization.....	134
7 CONCLUSIONS.....	137
REFERENCES.....	142

1 INTRODUCTION

The technological development in the field of Remote Sensing, with the availability of modern features of high resolution orbital sensors, and with the proven capability of three-dimensional mapping (Toutin et al, 2002a; 2002b), has modified and made more agile the processes of cartographic production. The launch of the IKONOS-2 satellite in 1999 by the American company Space Imaging initiated a phase of satellites of high resolution, which was revolutionary in terms of the detection of terrain details, making it a relevant source of data for mapping at various scales (Correia, 2008). With these sensors it has been possible to obtain cartographic bases in superior scales compared to those used in regional mapping, using simpler processes and achieving lower costs, which in the past was only possible through photogrammetric process.

Together with these advances, we can also mention the development of geo-technologies such as a Geographic Information System (GIS) and a Database Management System (DBMS). The first one is able to store a variety of graphical nature information, such as vectors and matrices, allowing, together with the DBMS, the manipulation and management of vast amounts of spatial and alphanumeric data, enabling the execution of various spatial analyses and the generation of basic or thematic intelligent maps (Aronoff, 1989, Burrough & McDonnell, 1998; Albrecht, 2007).

These technologies render mapping at scales of greater detail more efficiently, but they require new processes for the interpretation of these images in order to extract the maximum possible information, allowing either monitoring of important biophysical characteristics or the use/coverage of the terrain.

One method to gather information from the remote sensing products, known as Geomorphometry, involves the analysis of the land surface, with the operational focus on the extraction of the surface parameters from digital elevation models - DEMs (Pike et al., 2009). The morphometric analyses, with a view to measure the forms of relief through systematic and rational processes, have achieved great success since the late nineteenth century, particularly among researchers based in the Germanic countries, mainly in Austria, Germany and Switzerland (Christofoletti, 1980).

One of the groups of applications of the Geomorphometry in environmental and earth sciences refers to the Geomorphology, a field that has a long history of analyzing the data from digital elevation models to extract and classify landforms. Hengl & MacMillan (2009) quoted several authors who have elucidated ways to automatically classify landforms from DEMs, introducing techniques such as the concept of geometric signature, creating a set of measures that describe the topographic form well in order to distinguish geomorphologically distinct landscapes.

The present study intended to develop a process of semi-automatic identification of geologic units with remarkable geomorphological signature by integrating the geomorphometric analyses and the geotechnologies.

For this research an important Brazilian Cenozoic sedimentary unit named as *Barreiras* Formation, was selected. The *Barreiras* Formation is an important Cenozoic (Neogene) lithostratigraphic unit taking place along the Brazilian coast. Due to its wide spatial distribution, it is a particularly relevant unit for understanding the evolution of the Brazilian continental margin.

Besides, this sedimentary unit is always associated to a tabular relief and coastal cliffs. The smooth topographic conformation causes the land with *Barreiras* Formation to be preferentially occupied with an intense exploration of its mineral resources, especially clay as well as its water resources. In the area of research, in the region of *Campos dos Goytacazes* (northern portion of the State of *Rio de Janeiro*, in Southeastern Brazil), the *Barreiras* Formation is covered by grasslands, sugarcane plantations and eucalyptus reforestations.

The mapping of this unit in detailed scale is essential for planning the land use along the Brazilian coast.

1.1 Problem Description

Due to its wide spatial distribution, it is very difficult, time consuming and expensive to map the *Barreiras* Formation using the conventional methods (field surveys) or even by using visual interpretation methods upon images from remote sensors.

Throughout the eastern portion of Brazil several Cenozoic sedimentary units take place whose fragmentation in isolated patches was an essential

factor for the individualization of specific stratigraphic units by several researchers, despite the absence of clear criteria of differentiation (Saadi et al., 2005). Suguio & Nogueira (1999) pointed out that these sediments may be possibly correlated to the sedimentation of *Barreiras* Formation, which reinforces the need for further studies including detailed maps. The local analysis performed upon these detailed maps and the regional correlations are essential for the reconstitution of Neogene events in Brazil.

In the area of research, the *Barreiras* Formation has been documented by several authors, such as Martin *et al.* (1997), scale 1:200,000; Silva & Cunha (2001), scale 1:500,000; and Ribeiro (2010), 1:250,000 scale. Comparing the two most recent maps, there are significant differences perceived in tracing the contours of the limits of *Barreiras* Formation in contact with basement rocks (Figure 1). Such differences are not observed in contact between *Barreiras* Formation and the Quaternary deposits, probably for being easier to distinguish the two units with the methods and input data used. The lack of detail in the available maps can state a false reality of the actual location of this unit.

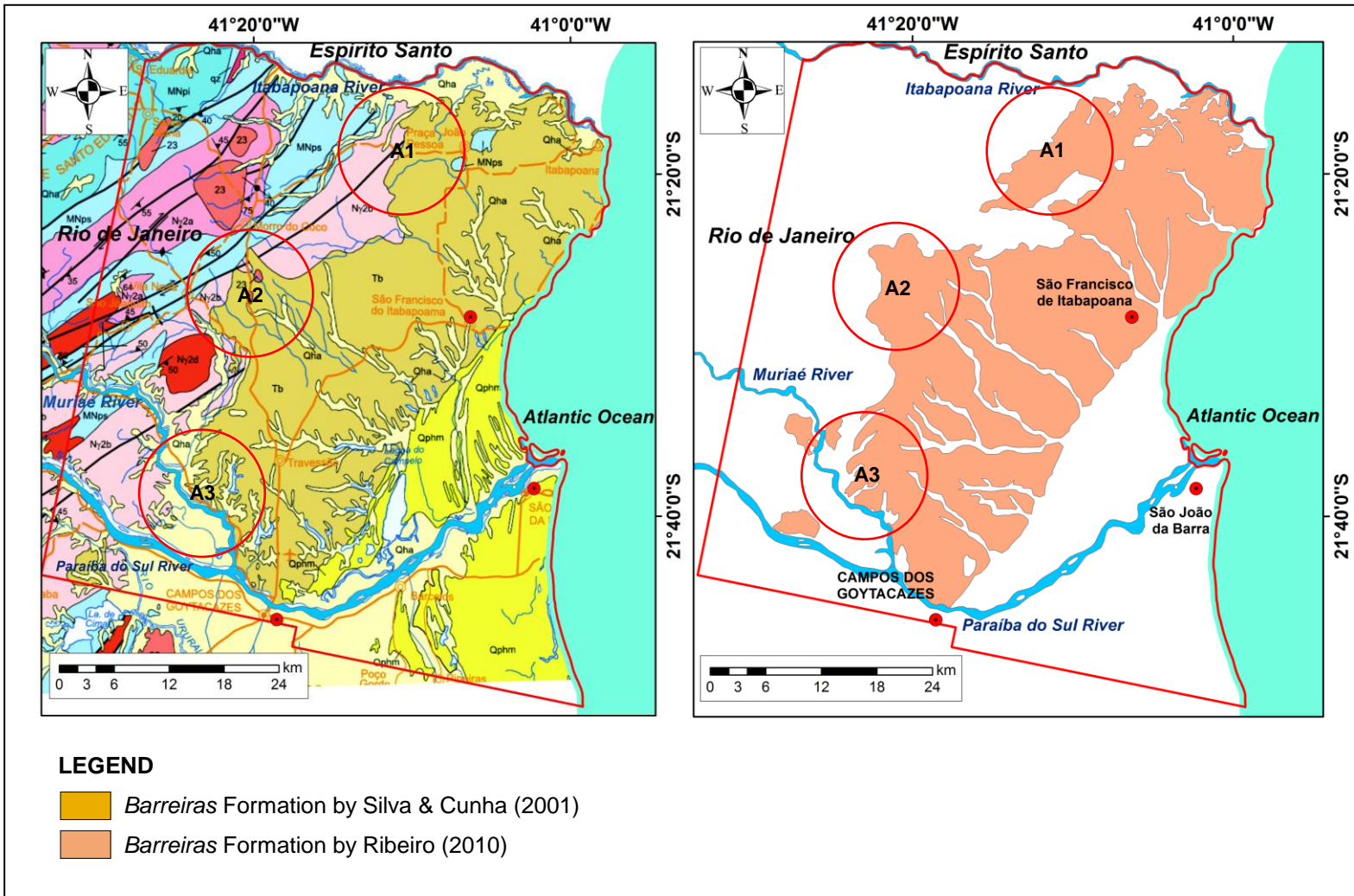


Figure 1: Contours of *Barreiras* Formation by: (a) Silva & Cunha (2001), scale of 1:500,000 and (b) Ribeiro (2010), scale of 1:250,000. A1, A2 and A3 represent areas with differences in the limits between *Barreiras* Formation and basement rocks as identified by these authors.

1.2 Research Deficit

Currently in Brazil, in terms of cartographic maps used in the thematic mapping in a more detailed scale, one of the difficulties arises from the fact that the country still does not have all its territory mapped in a scale greater than 1:100,000 scale. In a few states, including *Rio de Janeiro*, the mapping in scale of 1:25,000 is in process of development (IBGE, 2014a) employing aerial photos and photogrametric methods at high costs.

Regarding geological studies, although the Cenozoic deposits occupy a superficial extension of Brazil of 32.4 % (Bizzi *et al.*, 2003) and their areas are subject to intense occupation, they still remain little known and researched. The lack of topographic charts in appropriate scale makes the geological, geomorphological and pedological mapping in a detailed scale impossible.

Another aspect to be noticed is the absence of specific studies on *Barreiras* Formation in detailed scale based on its geomorphological characteristics. The contribution made by Valeriano (2001, 2003, 2005) and Valeriano & Carvalho Júnior (2003) for the identification studies of other forms of reliefs employing quantitative methods (Geomorphometry) is however worth being mentioned.

Moreover, there are no maps of *Barreiras* Formation on a larger scale than 1:250,000 nowadays that can provide greater details about its occurrence.

1.3 Goals

The main goal of this study is to develop a process of semi-automatic identification of the *Barreiras* Formation deposits and its mapping in detailed scale, employing digital surface models (DSMs) from high resolution optical satellite imagery and spatial data processing technologies.

A secondary goal is to assess the effectiveness of the rational functions model in the generation of DSMs in terms of its vertical and horizontal accuracy to achieve the Brazilian Cartographic Standards as well as the generation of

morphometric variables for the purpose of identification of *Barreiras* Formation deposits.

Both goals will contribute to reduce the aforementioned Research Deficit and consequently help to overcome the problem described above.

1.4 The Research Methods

The methods adopted in this research were based essentially on three integrated approaches (Figure 2): Remote Sensing, Geomorphometry and Geographic Information System.

The theoretical basis of Remote Sensing was present in all procedures used to acquire information about the research area without being in direct physical contact with the object of research as well as in the generation of DSMs and Orthoimages obtained from stereoscopic images of optical imagery systems.

The Geomorphometry approach involved all processes performed to quantitatively analyze the study area through the processing of information derived from the DSMs of the region.

The Geographic Information System approach established the connection with the two previous approaches from the use of a range of innovative ways of analysis, synthesis and presentation of information by using spatial visualization. The graphical representation of a place, phenomenon or process was made possible by the actions of powerful information processing (Dodge et al., 2008) such as those available in Geographic Information Systems.

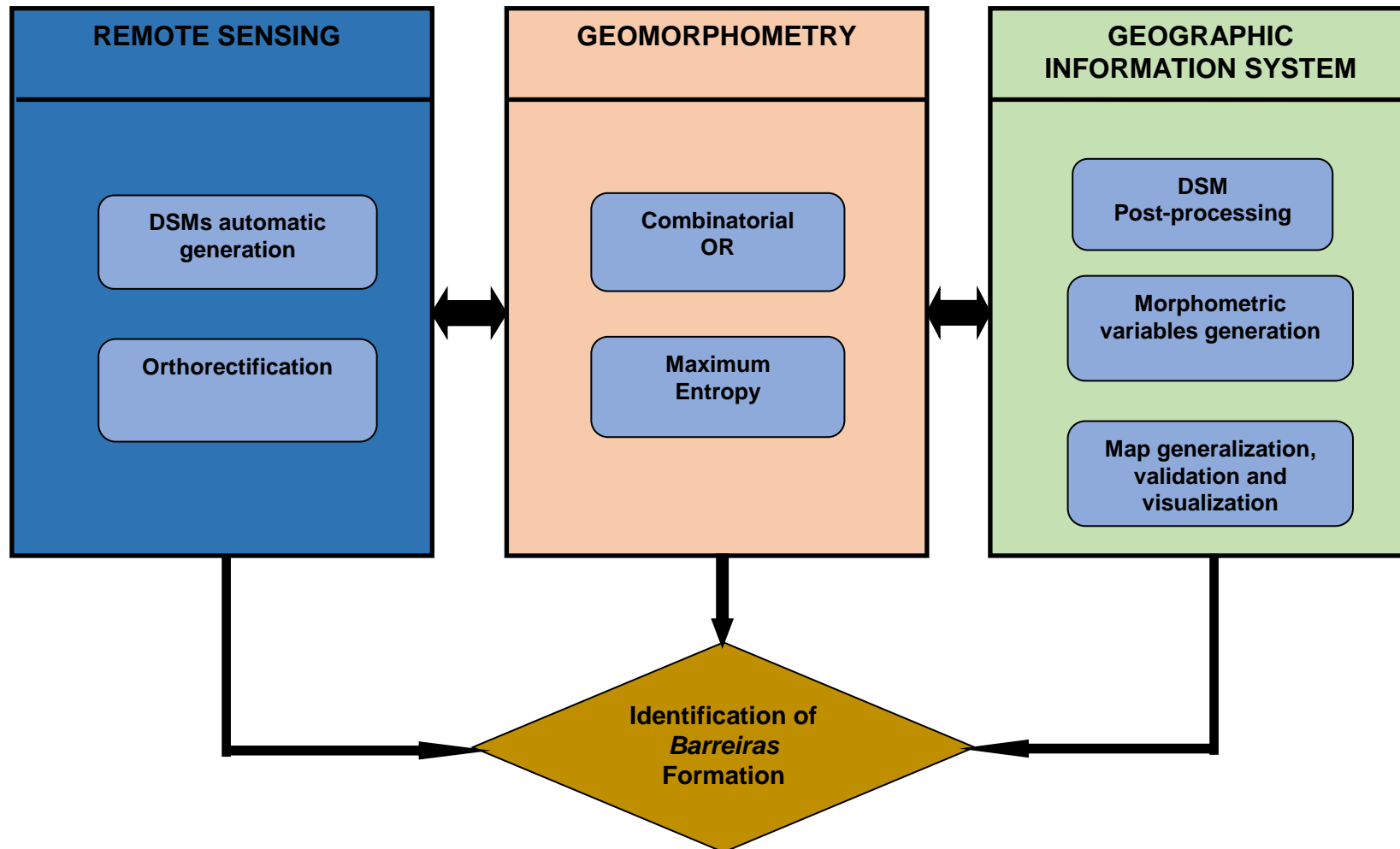


Figure 2: Approaches and main methods used in the present study.

The research will focus on the generation of DSMs from the high resolution images of the optical sensor ALOS/PRISM. These DSMs will be the source data for obtaining morphometric variables that best represent the geomorphology of *Barreiras* Formation deposits. The terrain analyses will be based on such morphometric variables using two different methods: (1) combinatorial OR; and (2) maximum entropy model.

Important targets to be achieved are: (1) the automatic generation of DSMs and vertical accuracy control; (2) the orthorectification of satellite images and horizontal accuracy control; (3) the preparation of DSMs for terrain analyses; (4) the terrain analyses; and (5) the generation and evaluation of the final map.

Additionally, the development of the research should answer the following issues on the basis of the available materials and the methods applied:

- what is the effective quality of DSMs automatically generated from high spatial resolution images by using the model of rational functions, in terms of its cartographic precision to achieve the Brazilian Cartographic Standards and for being used in the geomorphological analysis?
- what processes need to be made upon the DSMs to reach the stage of the generation of geomorphometric variables?
- what geomorphometric variables are most appropriate to represent the morphology of the *Barreiras* Formation?
- what are the gains achieved with the use of high spatial resolution images compared to the level of detail of the topic to be mapped, if compared to maps in the highest existent scale?

2 THE *BARREIRAS* FORMATION

The *Barreiras* Formation is an important Cenozoic (Neogene) lithostratigraphic unit taking place along the Brazilian coast, from the North to Southeast (Figure 3).

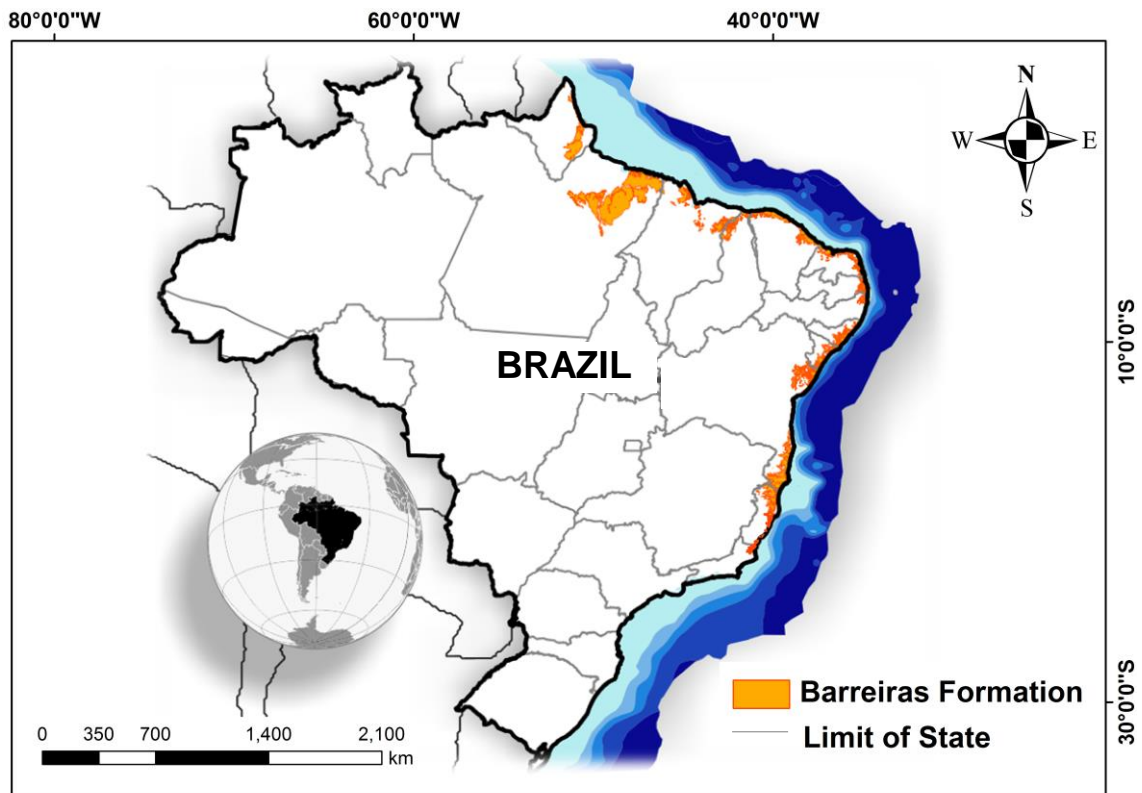


Figure 3: Distribution of *Barreiras* Formation along the Brazilian coast. Source: Bizzi *et al.* (2003).

This unit is composed of siliciclastic deposits, overlying Precambrian rocks and also Mesozoic sedimentary rocks of several marginal basins. It has been attributed to the time interval between the Miocene and Pliocene and corresponds to the substrate in which the large part of the Quaternary coastal deposits has been developed (Bezerra *et al.*, 2006).

The term *Barreiras* refers to coastal cliffs associated to the occurrence of these deposits along the Brazilian coast, having been reported since the description made by Pero Vaz de Caminha to the King of Portugal, D. Manuel I, when the discovery of Brazil in April 1500 (Suguio & Nogueira, 1999). Another

important geomorphological characteristic related to *Barreiras* Formation corresponds to a smooth hilly topography with tabular morphology, regionally named as coastal *tabuleiros* (Dantas, 2000; IBGE, 2009).

In Brazilian geological literature, the term *Barreiras* is used sometimes as *Formation* or as *Group*, having already been used once as *Series*. This last term is currently inappropriate for the denomination of the unit, as it represents a chronostratigraphic terminology, which is in this case not adequate, because the limits of its sedimentation in geologic time are not yet precisely defined (Nunes et al., 2011). Considering the aim of the present study, this discussion becomes rather unimportant and for this reason the term *Formation* will be adopted every time these deposits are mentioned, following the conception defended by Suguio & Nogueira (1999) and Morais (2001).

Several authors have studied the deposits of *Barreiras* Formation, and most of these researches are concentrated in the Northern and Northeastern regions of Brazil. In the Southeastern Brazil, these deposits are well represented in the northern part of the State of *Rio de Janeiro* and in the north part of the State of *Espírito Santo*. The most important occurrence in the State of *Rio de Janeiro* extends from *Campos dos Goytacazes* to the border with the State of *Espírito Santo* (Morais, 2001; Morais, 2007; Morais et al., 2006; Ribeiro, 2010), where the area of research is located.

The *Barreiras* Formation deposits predominantly consist of interbedded layers of sandstones and mudstones cemented by iron oxides/hydroxides. These deposits are related to fluvial deposition (Morais et al., 2006) or transitional environments (Rosseti, 2006).

Morais (2001), Morais et al. (2006) and Brêda (2012) have proposed facies descriptions and paleoenvironmental interpretations of *Barreiras* Formation deposits in the State of Rio de Janeiro. The method employed for facies characterization included the description of particle size, color, mineral composition and, especially, sedimentary structures and geometry of the layers. All authors emphasize the high degree of oxidation of the deposits, which imposed restrictions on the color description of the sediments and make the observation of primary sedimentary structures difficult.

Concerning paleoenvironmental interpretation of *Barreiras* Formation in the present studied area, Morais (2001) and Morais et al. (2006) interpreted these deposits as sandy distal braided fluvial environment, with a sedimentation dominated by tractive processes and less important suspensive processes. The deposits are predominantly composed by sandy sediments interbedded with muddy sediments, with minor participation of gravelly sediments (Figure 4). Generally, the layers show lenticular to tabular geometry. The color of the deposits is grayish-white, with a strong purplish-red mottling, including limonitic layers and well-developed ferruginous crusts.

In most of the study area, the *Barreiras* Formation deposits are unconformably covered by yellowish brown sandy-clayey sediments, showing a basal layer of quartz gravels and ferruginous fragments. This cover is recognized as post-*Barreiras* deposits (Morais et al., 2006).



Figure 4: Representative deposits of *Barreiras* Formation outcropping on the northern Rio de Janeiro coast (region of *Barra de Itabapoana*, on the border with the State of *Espírito Santo*). Sandy sediments (facies Am, Aca, Ah) are prevalent and distributed in lenticular to tabular layers; the muddy sediments (facies La1 and La2), less expressive, are distributed in layers with lenticular geometry. Note post-*Barreiras* deposits on the top of the outcrop. Source: Morais et al. (2006).

In terms of geomorphological aspects, the *Barreiras* Formation is associated to an expressive landform: large, elongated and smooth interfluves (named as *tabuleiros*), with relatively steep slopes, straight to concave base, limiting deep and flat valleys (Dantas, 2000; IBGE, 2009) - Figure 5.

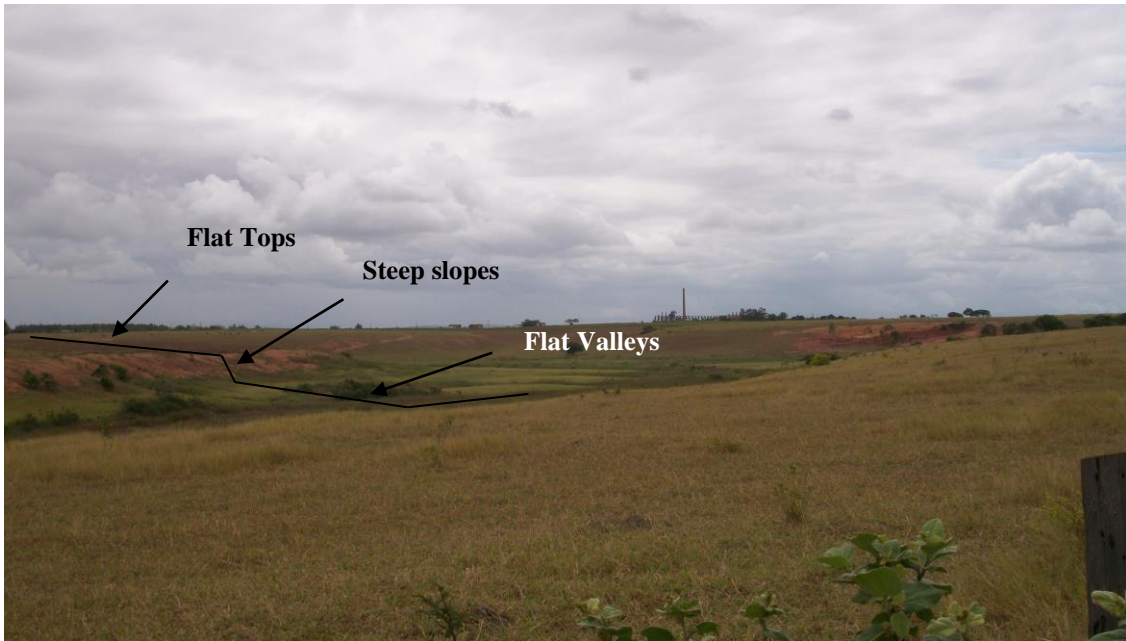


Figure 5: Main geomorphological aspects associated with *Barreiras* Formation. Photography obtained near *Campos dos Goytacazes*.

The *tabuleiros* constitute large areas with almost flat smooth topography, rising in general up to 50 m above the Quaternary plain, with higher elevations recorded near the contact with the crystalline hills. The *tabuleiros* are topographic intermediate level between the Quaternary plain and the crystalline basement, presenting general inclination towards the sea (Ramalho, 2005).

In the neighborhoods with the crystalline basement, *tabuleiros* are replaced by gently convex hills (Figure 6), more dissected by a denser network of drainage in comparison to the *tabuleiros* morphology.

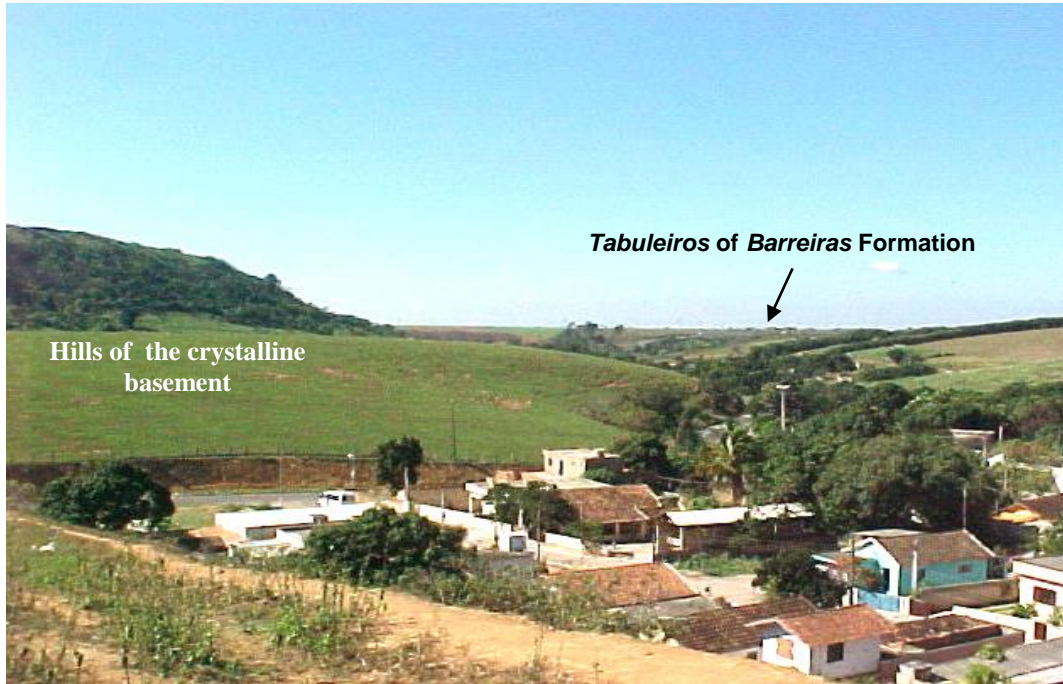


Figure 6: View of transitional landscape between the crystalline basement and *tabuleiros* of *Barreiras* Formation. Source: Ramalho (2005).

Ribeiro (2010) discussed the role of neotectonic mechanisms in the distribution of the *tabuleiros* of *Barreiras* Formation along the northern coast of Rio de Janeiro and the State of *Espírito Santo*, which includes the area of the present study, through the characterization of height variation and by analyzing morphostructural elements, topographic lineaments and the organization of the drainage network. Two main structural patterns were identified: NW-SE and NE-SW. The NW-SE lineaments are predominant in the *tabuleiros* of *Barreiras* Formation (Figure 7). As interpreted by Ribeiro (2010), these orientations express the action of neotectonic and the NW-SE structures limit different topographic compartments along the coast (Figure 8).

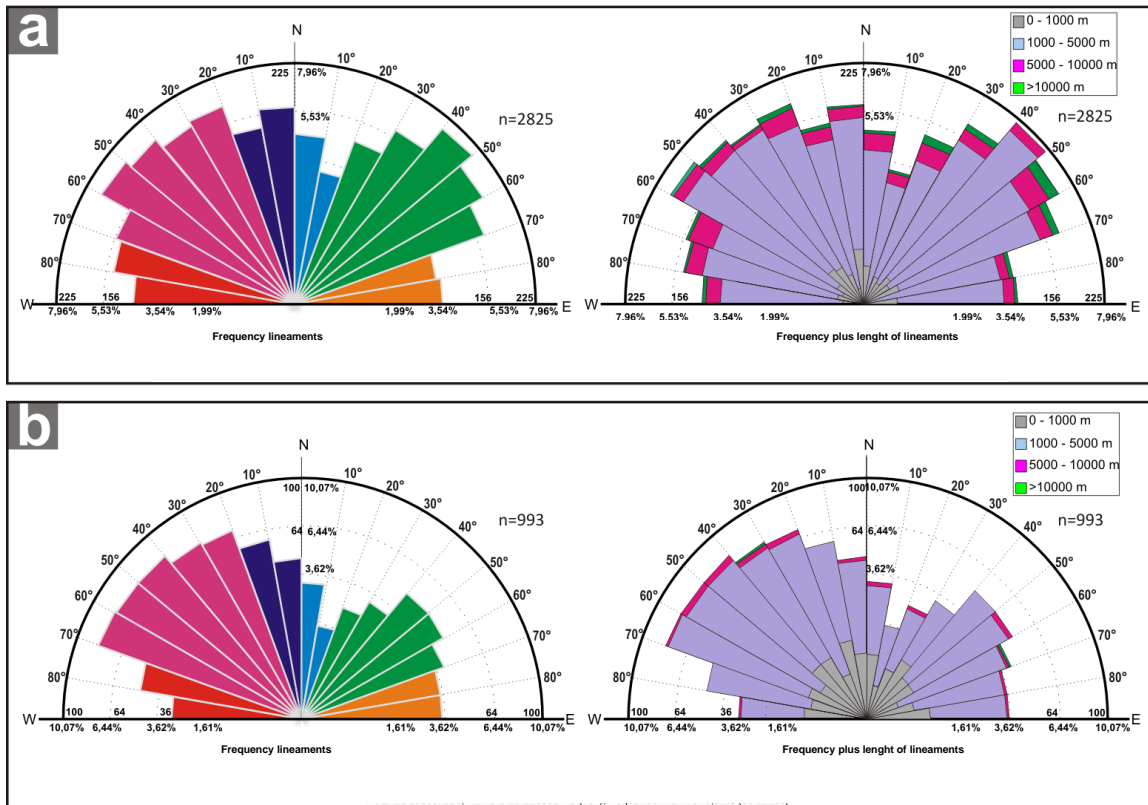


Figure 7: Rose diagrams of lineaments frequency (left) and frequency plus length of lineaments (right) obtained for (a) Precambrian basement domain and (b) *Barreiras* Formation domain, in the region between the Paraíba do Sul and *Doce* rivers (between the north of the *Rio de Janeiro* State and the center-north of the State of *Espírito Santo*). There are two sets of predominant lineaments in the Precambrian basement domain (NE-SW and NW-SE). In the *Barreiras* Formation domain, NW-SE lineaments are predominant. Source: Ribeiro (2010)

Ribeiro (2010) also evaluated the organization of the drainage network, through a characterization of the 4th-order drainage basin asymmetry and the tendency of flow direction of rivers draining the *Barreiras* Formation *tabuleiros*. An important control of NW-SE structures was also recognized.

The remarkable tectonic deformation that disturbs the tabular morphology associated to *Barreiras* Formation make its characterization difficult by means of geomorphological features isolated, making the mapping of its boundaries more difficult (Bezerra et al., 2006).

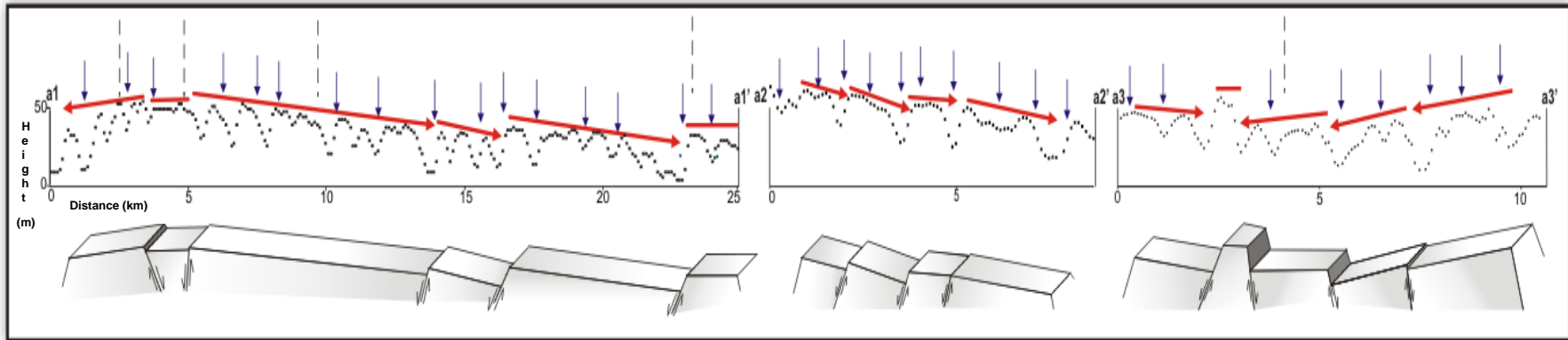


Figure 8: Topographic profiles show the stepped behavior of *tabuleiros*. Source: Ribeiro (2010).

3 STUDY AREA

3.1 Location

The area defined for this study is located in the northern State of *Rio de Janeiro*, between the city of *Campos dos Goytacazes* and the border with the State of *Espírito Santo* (Figure 9). This area is inserted in the onshore portion of the *Campos* Basin and displays the most extensive deposits of *Barreiras* Formation in the State of Rio de Janeiro. It was previously investigated by *Morais* (2001) for sedimentological characterization and paleoenvironmental interpretation of *Barreiras* Formation and also by *Ribeiro* (2010) for analysis of neotectonic control on the distribution of these deposits.

The boundaries of the study area are approximately between latitudes 21° 15' S and by the meridians 21° 50' S and 40° 50' W and 41° 35' W, being limited in the north by the political and administrative division between the states of *Rio de Janeiro* and *Espírito Santo*, and in the east by the Atlantic Ocean. The main cities in the area are *Campos dos Goytacazes*, *São João da Barra* and *São Francisco de Itabapoana*. The area is covered by eleven (11) sheets of the Brazilian systematic mapping (IBGE, 2014b) at 1:50,000 scale (Figure 10).

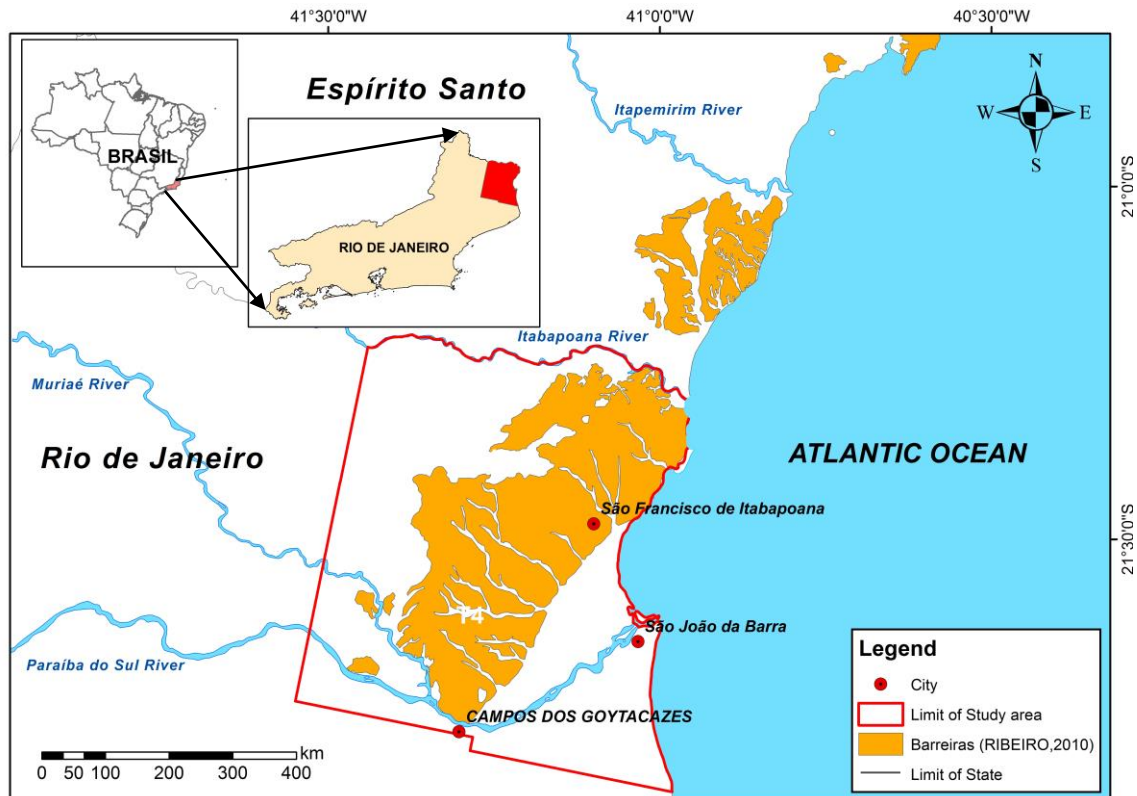


Figure 9: Location of the study area, with the representation of *Barreiras* Formation contour as Ribeiro (2010). Source of drainage, cities and highways: www.ibge.gov.br

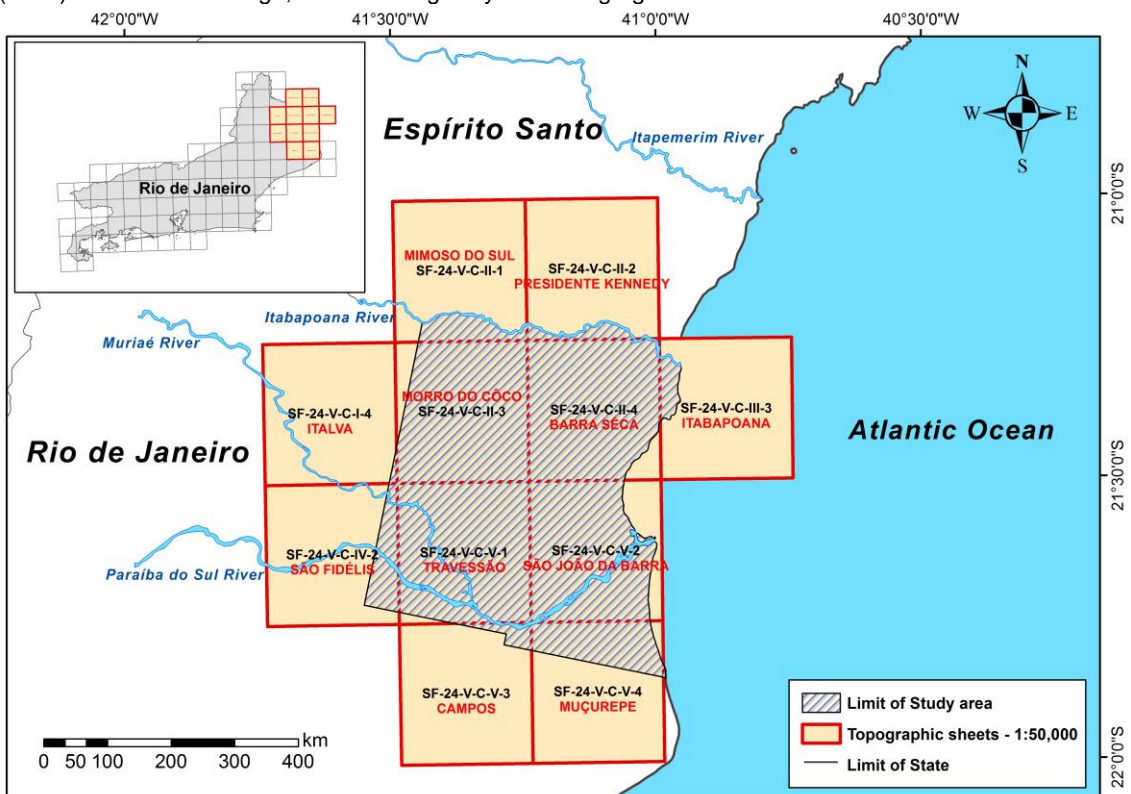


Figure 10: Mosaic of topographic charts at 1:50,000 scale covering the study area. Source: www.ibge.gov.br

The main access to the study area corresponds to the federal road BR-101, which crosses the entire length of the area in the NS direction, between the city of *Campos dos Goytacazes* and the border with the State of *Espírito Santo* (Figure 11). There are other important roads such as: BR-356, which connects *Campos dos Goytacazes* to *Itaperuna*, to the northwest, and to *São João da Barra*, to the northeast; RJ-492, which connects *Campos dos Goytacazes* to *São Fidélis*, and RJ-224, which connects *Campos dos Goytacazes* to *São Francisco de Itabapoana*.



Figure 11: Main access roads in the study area. Source: www.ibge.gov.br

3.2 Regional geology

The study area is characterized by two main geological domains: Precambrian/Eopaleozoic basement and Cenozoic sedimentary deposits (Martin et al., 1997).

3.2.1 Basement rocks

The basement rocks of the study area are related to the *Mantiqueira* Province (Figure 12), a Neoproterozoic to Early Paleozoic structural province (Almeida et al., 1981) formed when tectonic blocks of the Eastern and Western Gondwana (generated from the fragmentation of the Rodinia Supercontinent), joined in the so called Pan-African/Brazilian Event, which began 750-730 Ma and scored his last events at 490-480 Ma (Heilbron et al., 2004).

The *Mantiqueira* Province is located along the Atlantic coast, and extends over approximately 3000 km with NE-SW direction, bordering the eastern margins of the São Francisco and Rio de La Plata cratons (Silva & Cunha, 2001). It encompasses the *Araçuaí*, *Ribeira*, *Brasília Meridional* and *Dom Feliciano* orogens. The State of *Rio de Janeiro*, and consequently the study area, is located in the inner portion of the *Ribeira* orogen (Almeida et al., 1973).

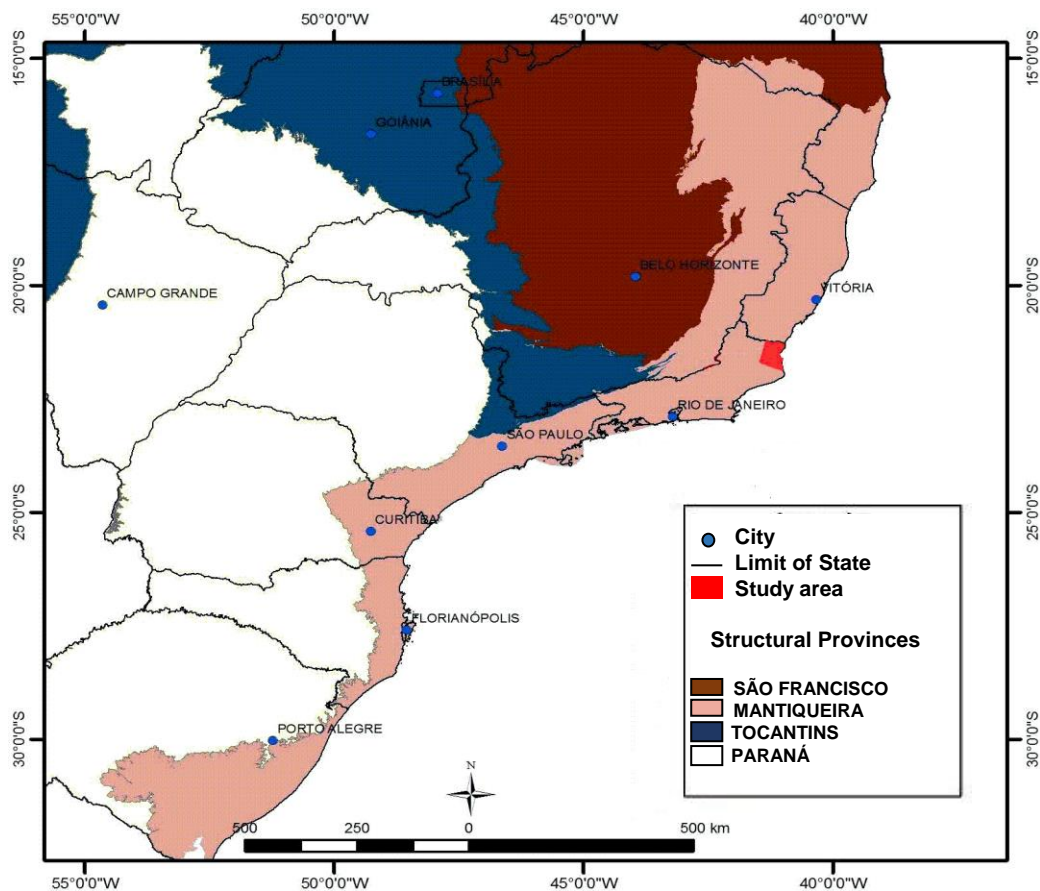


Figure 12: Map of structural provinces in central and southern Brazil, according to Bizzi et al. (2003), with the location of the study area in the context of the *Mantiqueira* Province.

According to Silva & Cunha (2001), the outcropping basement rocks in the study area correspond to Neoproterozoic paragneiss complexes (*Paraíba do Sul Complex/São Fidélis Unit* - garnetiferous biotite gneisses and migmatites, with sillimanite and locally cordierite) and Neoproterozoic to Paleozoic granitoid suites (*Desengano, Bela Joana* and *Angelim* suites), presenting a NE-SW structural orientation (Figure 13).

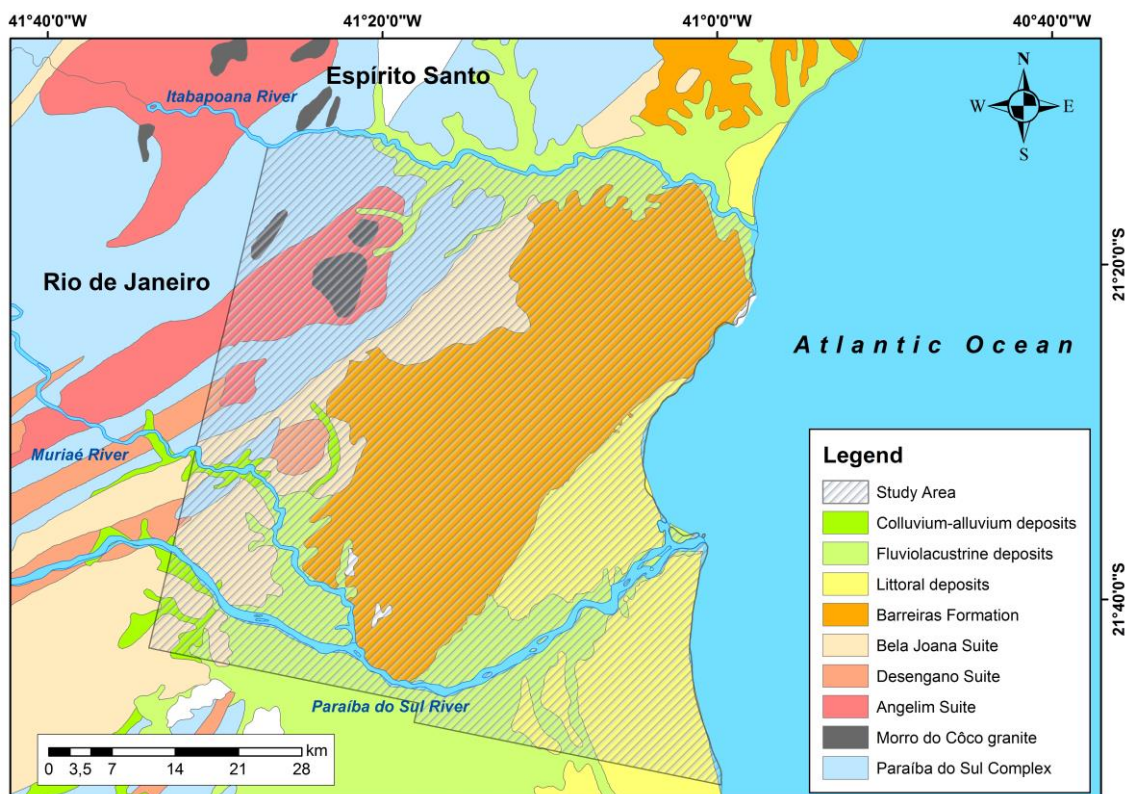


Figure 13: Geologic map of the northern portion of the state of *Rio de Janeiro*, where the study area is located. Source: <http://geobank.sa.cprm.gov.br>

3.2.2 Cenozoic sedimentary deposits

In the study area, the Cenozoic sedimentary units can be subdivided into *Barreiras* Formation deposits and Quaternary sediments.

The *Barreiras* Formation occupies an elongate range with NE-SW orientation, between areas of Precambrian rocks and Quaternary sediments (Figure 13), occupying large portions of the municipalities of *Campos dos Goytacazes* and *São Francisco de Itabapoana*. The best expositions are

distributed from the *Paraíba do Sul* River, near the City of *Campos dos Goytacazes*, up to the border with the State of *Espírito Santo*.

The Quaternary sediments are associated to continental, transitional and marine depositional systems. According to Martin et al. (1997), the Quaternary sedimentation in the study area can be subdivided into coastal marine deposits (Pleistocene and Holocene sand ridges), specially well developed in the *Paraíba do Sul* river mouth; Holocene swamp deposits; and Holocene colluvial and alluvial deposits, which are distributed along the river valleys.

3.3 Geomorphology

According to Dantas (2000), the relief of the State of *Rio de Janeiro* can be subdivided into two morphostructural units: the Atlantic Orogenic Belt and the Cenozoic Sedimentary Basins. These main geomorphologic domains include several relief units. The most representative landscape units and the height variation in the study area can be observed in Figure 14.

The Atlantic Orogenic Belt morphostructural unit involves sets of morphological units developed over Precambrian/Eopaleozoic metamorphic and igneous rocks. In this morphostructural unit, landforms present strong lithostructural control and a remarkable NE-SW orientation. The hilly domains show topographic amplitudes between 50 and 200 meters, gentle to medium gradients, convex-concave geometry and variable drainage patterns, presenting relatively thick alluvial/colluvial deposits; compartments of dissected hills, massifs and mountainous domains show amplitudes greater than 200 meters, medium to high gradient, concave and straight slope geometries, higher drainage density, presenting talus and colluvium deposits.

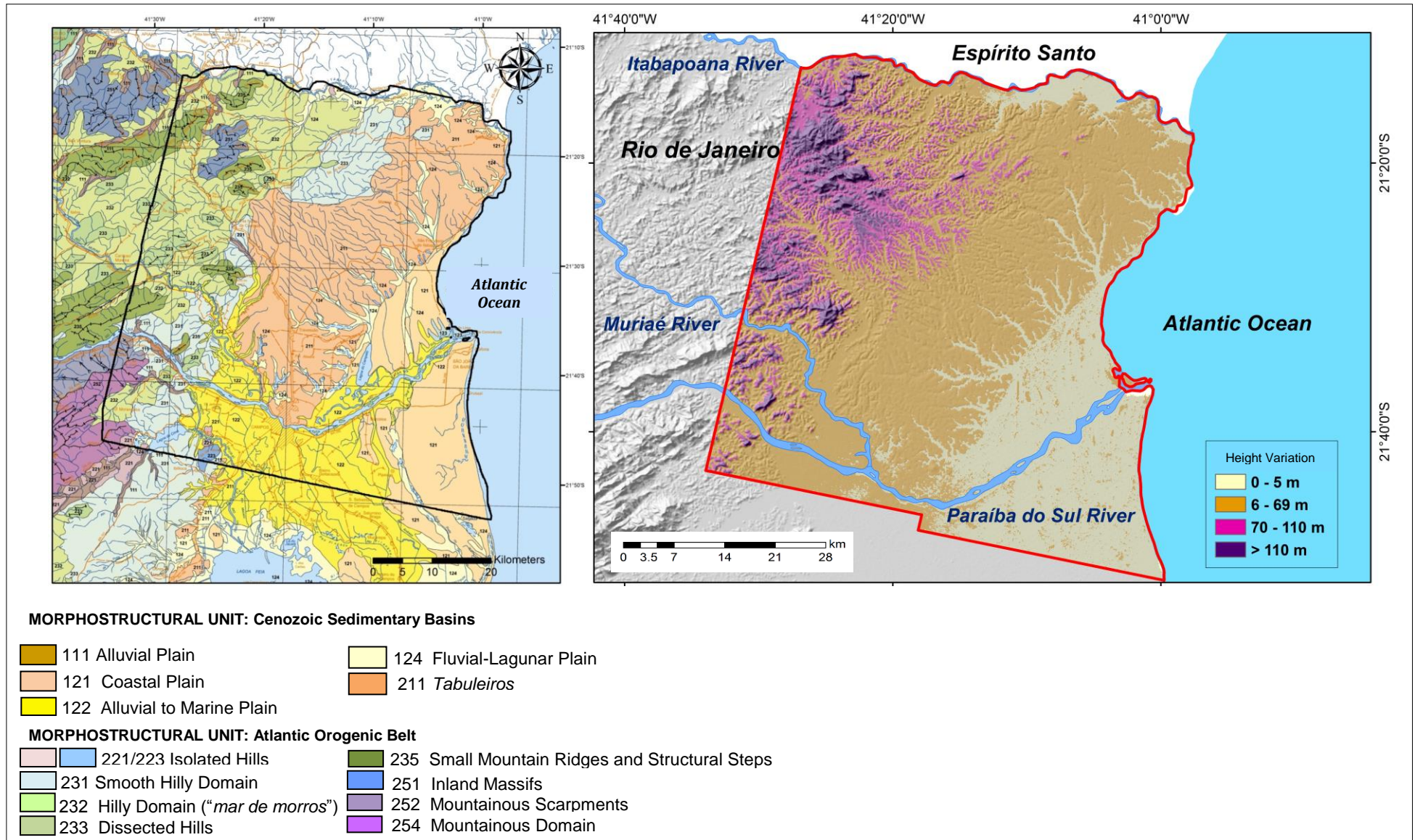


Figure 14: Geomorphological units in the northern *Rio de Janeiro* State, according to the geomorphological map of the state of *Rio de Janeiro* and height variation in the study area. Source of geomorphological map: Dantas (2000), original scale: 1:500,000.



Figure 15: Main landscape units in the study area. In the foreground, there is a alluvial plain of *Paraíba do Sul* River and small lacustrine bodies, in the limits of *Campos dos Goytacazes*. In the background, it can be observed the mountainous domain (*Serra do Mar*), and a hilly area on its foot. To the left, it is noticed an isolated massif. Source: www.camposfotos.blogspot.com.

The Cenozoic Sedimentary Basins morphostructural unit includes relief systems developed over Neogene and Quaternary deposits: *tabuleiros*; and marine, transitional and alluvial plains (Figure 13).

The *tabuleiros* are associated to the *Barreiras* Formation deposits, presenting relief amplitude between 10 and 50 meters, with very gentle gradient and gently convex to flat wide tops. This relief system was defined by Martin et al. (1997) as Tertiary Plateau, whose surface dips gently to the sea. The valleys in this relief system exhibits a "U" profile and a parallel drainage pattern.

The Alluvial to Marine Plain corresponds to a sub-horizontal surface related to the Quaternary alluvial and alluvial-marine sandy-clayey deposits. Wetlands are common, especially near the coast.

The Fluvio-Lagunar Plain represents a flat and poorly drained surface, covered by Holocene organic clay deposits.

The Coastal Plain is related to Pleistocene and Holocene sets of sand ridges presenting topographic amplitude less than 10 meters and covered by marine and eolian sand deposits, with a parallel drainage pattern.

3.4 Climate, vegetation and occupation

The State of *Rio de Janeiro* lies in the Tropical Central Brazil climatic zone, according to the classification of Nimer (1972, 1979). The topographic compartmentalization is a decisive factor in defining the climatic diversity of the State of *Rio de Janeiro*. Semi-humid tropical climate characterizes the coastal region, with an average annual temperature of 24°C; high-altitude tropical climate occurs in elevated areas that have a mean annual temperature of 18°C (CEPERJ, 2014).

Rainfall presents an uneven distribution throughout the region. It is observed an increasing gradient of annual averages from the coast towards the Atlantic Orogenic Belt, a fact associated to the absence of orographic barriers along the plains for retention of moist Atlantic winds. Where there is more regular rainfall, soils are less fertile and more susceptible to accelerated erosion. Rather, the low average of rainfall in the areas of floodplain results in more fertile soils (Ramalho, 2005).

The northern region of the *Rio de Janeiro* State has the lowest percentage of remaining Atlantic Forest, with 20% of its original forest cover. Due to population growth, it tends to suffer a great anthropogenic pressure (Gomes et al., 2009). The region is characterized by a pastoral and agricultural economy, with most of its vegetation removed, resulting in croplands and pasture (Ferreira et al., 2003). The original vegetation is composed by semi-deciduous forests and coastal forests (Rizzini, 1979). Currently, these areas are scattered in small forest fragments, mostly less than 10 ha.

The planting of sugarcane, that was introduced to Brazil in the sixteenth century, changed the landscape of the northern area of the State of *Rio de Janeiro*. Since the seventeenth century, the City of *Campos dos Goytacazes* has become the most important city of the northern region of *Rio de Janeiro* Paranhos (2000).

Carvalho & Totti (2006) highlight two important recent phases related to economic activities in the history of the northern region of *Rio de Janeiro*. One is related to the ethanol industry, which currently still exists but does not present so important economic levels as in the past, and the other one for the

oil industry, which influences the economy of some cities of this region, specially *Campos dos Goytacazes* and *Macaé*, placing the latter at the level of the municipalities with the highest Socioeconomic Index (ISE) in the region (8.3). The lowest index (2.8) corresponds to the city of *São Francisco de Itabapoana* (Totti et al., 2002).

4 RELEVANT CONCEPTS

In this chapter, relevant theoretical foundations for this study will be focused on. Its main objective is to facilitate the conceptual understanding of the data and methods used. For a more detailed knowledge about the mathematical formulation involved in some of the methods employed, it is recommended to consult the referenced bibliography and others related thereto.

4.1 Remote Sensing Imagery

4.1.1 Sources of geometric and radiometric distortions

The raw images often contain several geometric distortions and may not be directly integrated with other mapping products in a GIS environment, being necessary to apply either geometric as radiometric corrections, adapted to the nature and characteristics of image data (Toutin, 2004).

The sources of distortion can be grouped into two broad categories (Table 1). A more detailed description can be found in Jia & Richards (1999).

The first category is coming from the observer or from the acquisition system, such as the distortions of the platform, sensor and other measuring instruments. The second one is coming from the object being observed (target), such as those pertaining to the atmosphere and land surface (Toutin, 2004). Additionally, it is necessary to consider the deformations related to the projection system used to represent the maps, since they are referenced to a mathematical surface, usually an ellipsoid, and not the land surface itself.

Table 1: Description of the sources of error for the two categories and sub-categories. Source: adapted from Toutin (2004).

Category	Sub-category	Description of sources of errors
Observer or acquisition system	Platform (spaceborn or airborne)	Variation of the movement Variation in platform attitude (low to high frequencies)
	Sensor (VIR, SAR or HR)	Variation in sensor mechanisms (rate of scan, velocity of scanning, etc) Viewing/look angles Panoramic effect with field of view
	Measuring instruments	Time-variation or drift Clock synchronicity
Target	Atmosphere	Refraction and turbulence
	Earth	Curvature, rotation, topographic effect
	Projection System	Geoid to ellipsoid Ellipsoid to the projection system

In the case of satellite platforms, the variation of the altitude modifies the width of the imaged track, causing changes in the scale in the direction orthogonal to the path (cross-track), while the change in velocity along the trajectory leads to changes of scale in that direction.

Changes in the attitude of the platform can be described mathematically by parameters that represent the angles of yaw, pitch and roll. These errors cause the image rotation and shift in the direction of the trajectory and orthogonal to it. While these variations can be described by the three parameters above, it is necessary to know the information related to the physical reality of the viewing geometry, so you can calculate the magnitude of them for the purpose of correction (Richards & Jia, 1999).

The effects of variation in speed and changes in attitude of the platform are shown in Figure 16.

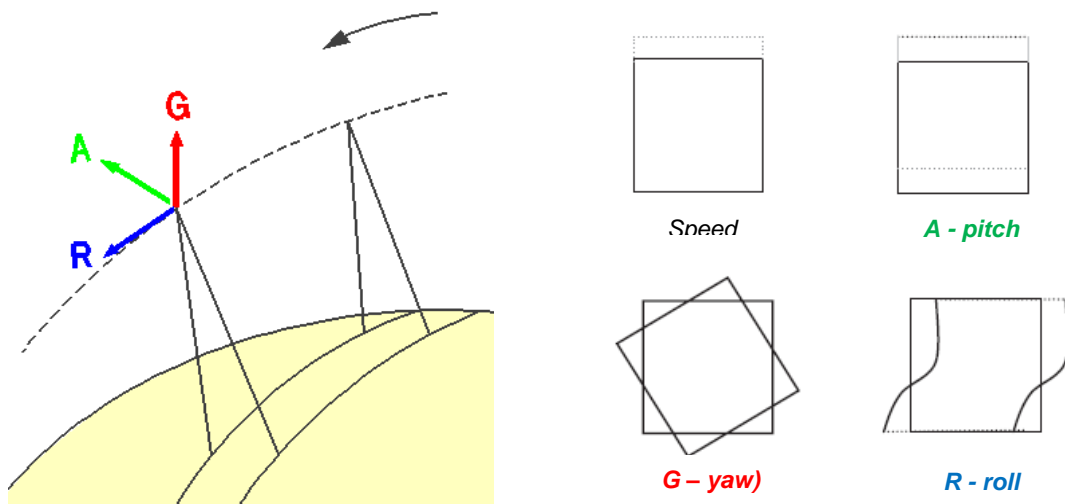
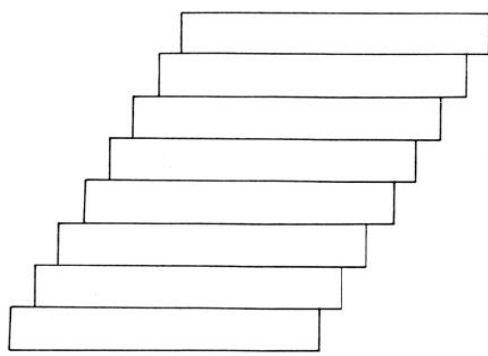
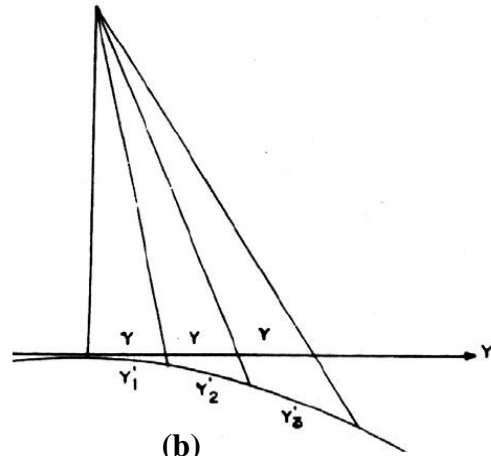


Figure 16: Effects of geometric distortions caused by the change of speed and change in the attitude of the platform. Sources: Modified Machado-Silva (1988) and Richards & Jia (1999)

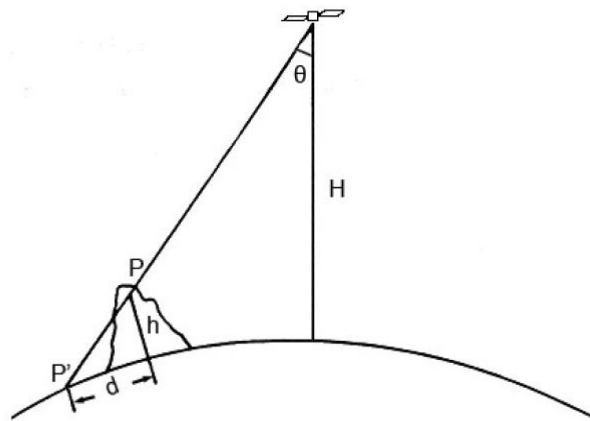
The distortion of the orbital images, related to Earth are those resulting from its rotation, curvature and the topographic effects. The distortions due to the rotation of Earth, which rotates from west to east, causing the displacement between successive scanings, so that each line imaged shifts to the left from the previous in terms of positioning on the ground. The distortions related to the curvature of the earth cause distortions due to lateral conical projection of each line of the image, relative to the cartographic representation plan. Finally, the distortions related to the topographic effects cause displacement (Figure 17).



(a)



(b)



$$d = R \cdot \left\{ \arcsen \left[\frac{\text{sen} \theta \cdot (R + H)}{R} \right] - \arcsen \left[\frac{\text{sen} \theta \cdot (R + H)}{R + h} \right] \right\}$$

d – relief displacement *H* – flying height
R – mean radius of the Earth *h* – relief height

(c)

Figure 17: Distortion of orbital images related to Earth: (a) rotation; (b) curvature; and (c) topographic effects. Source: Machado-Silva (1988).

Mechanisms that affect the measured brightness values of the pixels in an image can lead to radiometric distortions (Richards & Jia, 1999). The radiometry of images, obtained from passive remote sensing systems, can be affected by the presence of atmosphere due to the scattering or absorption of solar energy incident on the object on the Earth's surface by the particles of this atmosphere. In the absence of an atmosphere, the signal measured by the sensor will be a function of the level of solar irradiance incident on the object at the earth's surface and its reflectance properties.

The scattering (Figure 18) by atmospheric particles is the dominant mechanism that leads to radiometric distortion, through which the rays received by the sensor comes not only from the captured portion of the Earth by the image, but from numerous reflections in the atmosphere and other objects (GDTA, 1992). The atmospheric correction to be applied will depend on the wavelength bands and atmospheric conditions. The scattering is more severe in short wave lengths. Likewise, smoggy and dusty atmosphere, cause more diffusion than a dry and clear one (Lillesand & Kiefer, 1994; Richards & Jia, 1999), 1999; Sabins, 2000; Jensen, 2011). A detailed correction for the effects of scattering and absorption of air is often not required. As the necessary additional information, such as visibility and relative humidity, are not readily available and, whether the effect of the atmosphere is considered to be a problem for the image, approximate corrections can be made based on histograms generated for each band (Richards & Jia, 1999).

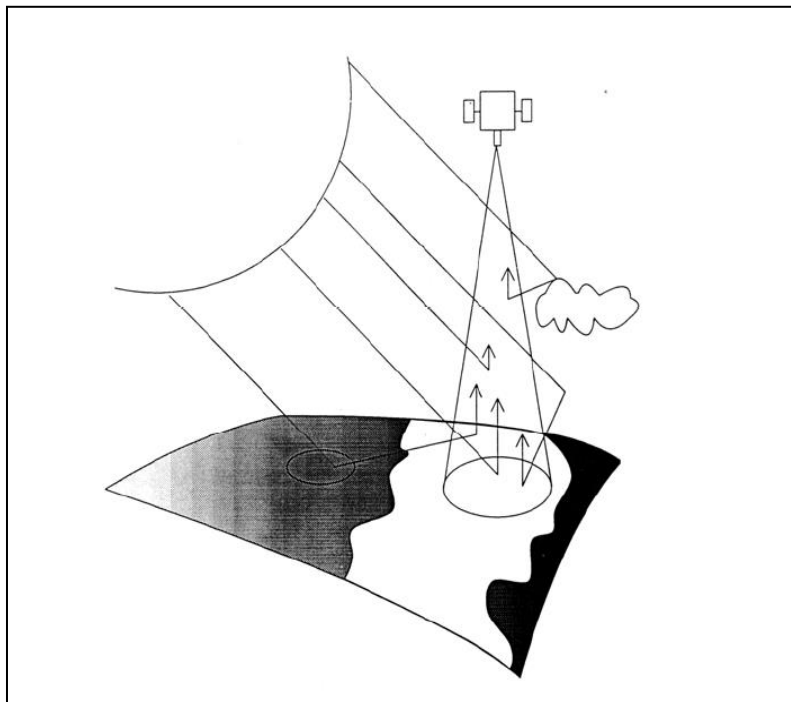


Figure 18: Scattering of solar radiation in the atmosphere. Source: GDTA (1992).

4.1.2 Orbital images ALOS/PRISM

The images used in this study are from the Advanced Land Observing Satellite (ALOS). The platform has three remote-sensing instruments for capture images, and the images used in this study were obtained from the Panchromatic Remote-sensing Instrument for Stereo Mapping (PRISM).

The ALOS platform leads on board a subsystem of attitude and orbit control (Attitude and Orbit Control Subsystem - AOCS), which allows accurate determination of the position and attitude of the satellite. The estimated position of the satellite is determined using dual-frequency GPS receivers (GPSR) while the attitude through the Star Tracker (STT) and an inertial reference unit - Inertial Reference Unit (IRU). The gyroscope allows the correction of the attitude and position of the satellite, while a reflector LASER is used to calibrate the position determined by GPS. Additionally, the Angular Displacement Sensor (ADS) records the oscillations of the PRISM sensor for capturing images (IWATA, 2003; JAXA, 2004).

The PRISM sensor is the push-broom type, in which the image is formed by scanning when the platform moves along its track (along-track scanning). The sensor has three independent optical systems for viewing nadir, forward and backward producing a stereoscopic image along the satellite's track (Figure 19). Each optical system uses a set of detectors (Charge Coupled Device - CCDs), 6 for nadir and 8 for forward and backward (4 for each one), arranged in a linear array in the focal plane formed by the lenses of the optical system. The bar detectors is positioned perpendicular to the trajectory of the platform. The swath width in triplet observation mode is 35 km (EORC/JAXA, 2007).

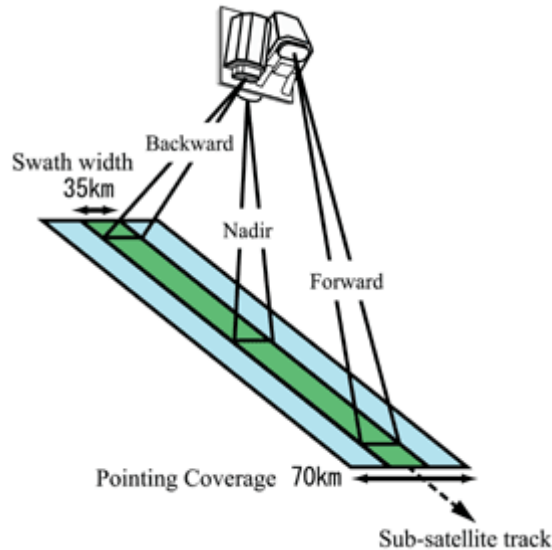


Figure 19: Triplet observation mode of ALOS/PRISM
Source: EORC/JAXA (2007).

The PRISM operates with one (1) panchromatic band in the wavelength range between 0.52 and 0.77 micrometers. The bit length is 8 bits and the spatial resolution is 2.5 m at nadir, allowing it to generate charts scale up to 1:25,000. The main characteristics of the sensor are presented in Table 2.

Table 2: Characteristics of ALOS/PRISM satellite imagery. Source: EORC/JAXA (2007).

Number of Bands	1 (Panchromatic)
Wavelength	0.52 a 0.77 micrometers
Number of Optics	3 (<i>Nadir; Forward; Backward</i>)
Base-to-Height ratio	1.0 (between Forward and Backward view)
Spatial Resolution	2.5 m (at Nadir)
Bit length	8 <i>bits</i>
Swath Width	35 km (Triplet mode)
Pointing Angle	-1.5 to +1.5 degree (Triplet mode, Cross-track direction=
Stereo angle	+/- 23.8 degree (F/B)
Flying height	691650 m
Focal length	1.939 m
Number of CCDs	6 (N) / 8 (F/B)
<i>Pixels</i> per CCD array	4992 (N)/4928 (F/B)

Images from the PRISM sensor can be delivered on different stages of processing: (1) Level 1A, corresponding to the raw image, without any correction; (2) level 1B1, at which images are radiometrically corrected; and (3) level 1B2, with radiometric and geometric corrections based on ephemeris data. For the latter level, the following correction options are available: (3a) 1B2R, where the image is georeferenced, the pixels are oriented in the direction of the trajectory of the satellite and the UTM projection parameters are attached and (3b) 1B2G, which corresponds to 1B2R image rotation, so that the pixels are designed and oriented along the grid north UTM (JAXA, 2007).

4.2 Geometric correction of imagery

The purpose of geometric correction of images consists of finding mathematical formulation that models the distortions contained in images obtained by remote sensors, whether airborne or orbital.

Toutin (2004; 2006) and Toutin *et al.* (2002a; 2002b) classifies the mathematical models to perform geometric correction of imagery such as: rigorous or photogrammetric and empirical models (such as polynomial and rational functions).

The rigorous or photogrammetric model represents the physical law of transformation from ground space to image space, since it considers the three-dimensional geometry of the acquisition of each line of the image expressed by the collinearity condition. By using the principle of collinearity, the model associates control points easily identifiable on the images to their respective in the field, tied to a reference ellipsoid (Toutin, 1995).

Although the rigorous model reflects the physical reality of the viewing geometry and correct the distortions inherent in the platform, the sensor and the earth, it is necessary to know the physical parameters of the sensor and platform (ephemeris and attitude), in the instant of acquisition image, which is not always the reality (Cheng & Toutin , 2001).

Unlike the rigorous model, empirical models do not model the geometry of the sensor. They are classified as: models of rational functions, using RPCs available in the image; models of rational functions in which RPCs are

calculated from the ground points (GCPs); and models of polynomial coefficients.

The model of rational functions, using Rational Polynomial Coefficients (RPCs) available in the image, is used when the parameters of the acquisition system are not provided by the satellite operators. These coefficients are determined from the calculated orbital data as well as the information from the sensor itself (Tommaselli & Medeiros, 2010).

These coefficients can also be calculated from control points (Ground Control Points - GCPs). Currently, many commercial software have functionality to import these coefficients, providing an alternative to the geometric image correction, since this model can be more accurate than polynomial models because it uses DEM or near elevation (Toutin , 2002a , 2004).

The mathematical formulation of the 3D model of rational functions can be found in Toutin (2002a, 2004).

The processing using the model of rational functions can be refined by adding a few control points (GCPs). If there is an availability of one or two points per image, you can perform a transformation of order 0, using 2D polynomial functions, which produces translation in x and y only. If three points are used per image, you can perform a 1st order transformation (affine transformation), which produces both translation and rotation of the model.

Studies by Bang et al. (2003), Tao & Hu (2004), and Takaku & Tadono (2009) with pictures Ikonos, Quickbird and PRISM, show that the images are more affected by errors of translation, so that the refinement of the empirical model of geometric correction using RPCs can be achieved with a polynomial transformation of order 0 , using one or two control points.

4.3 Digital Elevation Models (DEMs)

According to the U.S. Geological Survey (USGS), a DEM is a digital cartographic representation of the elevation of land at regularly spaced intervals in x and y directions, using z values referenced to a vertical datum (Maune et al., 2001a).

Other terms related to DEMs can be found in the literature. Felgueiras & Câmara (1999) use the term: Terrain Numerical Model (TNM) as a computational mathematical representation of the spatial distribution of a phenomenon that takes place within a region of the Earth's surface. In the context of these authors, the values may be beyond relief data, geological, meteorological, among others.

Felicísimo (1994) and Li et al. (2005) adopted the term Digital Terrain Model (DTM) to represent the spatial distribution of some feature of the terrain. Paparodits & Polidori (2002) and Jensen (2011) use the term DEM according to a more general character. According to these authors, the DEM differs according to the terms DTM and digital surface model (DSM), to represent, respectively, the elevations of bare ground, and elevations of landscape elements (bare ground, vegetation and buildings).

In this research, the term DEM will be used in a general sense. The product generated from satellite images is called DSM, since the calculated values of elevation refer to the top surfaces of buildings, trees, towers and other features and thus above the ground surface itself. For products whose elevation values refer to the land surface itself (bare ground), the term DTM will be used.

4.3.1 Automatic Generation of Digital Surface Models (DSMs)

The DSMs of this research were generated from stereoscopic pairs from optical satellite imagery. The natural phenomenon of stereoscopy comes from binocular vision, which provides depth perception based on the observation of a scene under two different angles of incidence. The stereoscopic parallax is related to the displacement in the apparent position of an object in an observed scene, viewed along two different lines of sight (Lillesand & Kiefer, 1994; Wolf & Dewitt, 2004). The principle of stereoscopy was used to calculate the elevation of the terrain, which was obtained from measurements of parallax between a pair of stereoscopic images.

The automatic generation of DEMs from stereo images, follows three steps: matching of images for obtaining homologous points of the stereo pair; modeling and surface reconstruction for interpolating values of elevation; and post-processing for editing and quality control model (Li et al., 2005).

4.3.1.1 Matching images

The first step employs a fundamental principle of photogrammetry, which is the identification and measurement of homologous points in two or more overlapping images (Figure 20). The matching of images is involved in virtually all digital photogrammetric processes, such as the orientation of images, generation of digital terrain models and automatic feature extraction (Costa, 2006).



Figure 20: Automatic location of a homologous point in another image. Source: CEFETES (2012)

According to Coelho & Brito (2007), most of the images' auto correlation applications work with two cuts: one corresponding to the area of the reference

image (left image) and the other one corresponding to the area of the second image (right image) where it is expected to find a similar image standard to the reference image.

The correlation coefficient expresses the correlation value and may be understood as a measure of the degree of linear relationship between two random variables. This value can range between -1 and 1, and the value 0 indicating no correlation between the variables, while the value of 1 indicates maximum correlation, which may be positive or negative (Coelho & Brito, 2007).

A major problem of the correlation of images is the definition of the search space. If the search region for homologous features is not restricted, the computational cost as well as the chance of having ambiguity is higher, which increases the risk of obtaining incorrect matches. So, as to avoid unnecessary calculations and reduce the computational cost, we need to restrict the search space (Wolf & Dewitt, 2004). One way to reduce the search space is applying the principle of epipolar geometry, where the search area is reduced to epipolar lines which are collinear and parallel to the x axis of the image (Figure 21).

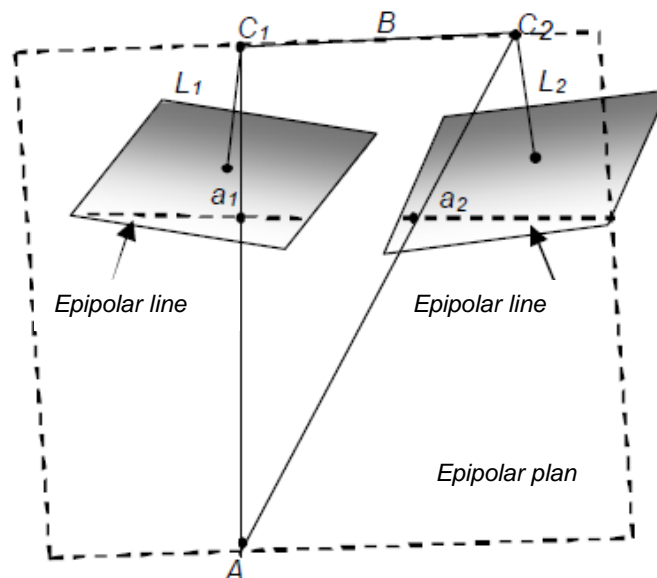


Figure 21: Epipolar plan and the corresponding epipolar lines.
Source: Mikhail *et al.* (2001)

Besides the issue of restricting the search space, another point to be noted is related to areas with vegetation cover, where the main failures in the process of digital correlation occur and occurrences of areas without elevation

value (empty). Moreover, the values of elevation determined are referenced to the top of the plant and not to the ground, as desired.

The process of geometric correction of satellite imagery is done by adopting a mathematical model for the geometric relationship between the coordinates of the image (image space) and their coordinates on the ground (object space), according to the Earth reference system and cartographic projection.

The rigorous models are based on the photogrammetric method, whose solution is obtained by rigorous adjustment by the least squares method. These models are based on the collinearity principle in which a point in the image space (p) its homologous in the object space (P) and the perspective center of the orbital image (CP_i) are collinear (Figure 22).

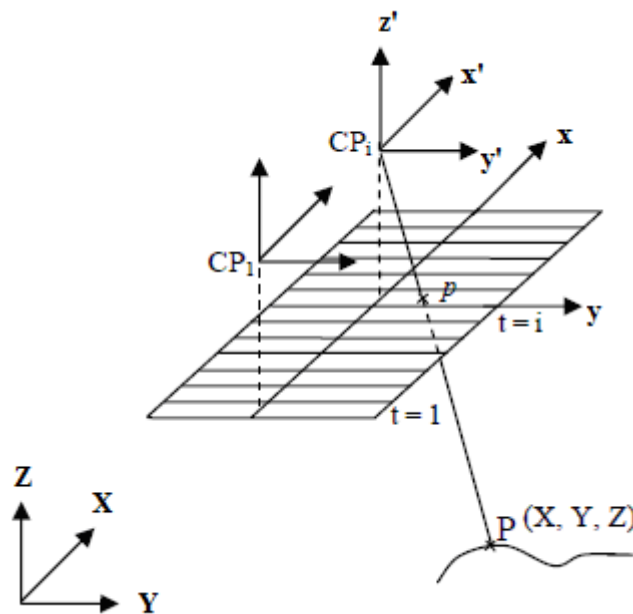


Figure 22: Collinearity principle. Source: Wolf & Dewitt (2004).

As already discussed in section 4.2 concerning the geometric correction of images, usually the information needed to make the orientation are not provided directly to the end user. Instead, the providers of images supply RPCs coefficients, whose information contained, allow the user to perform the steps

of geometric correction of model (Coelho & Brito, 2007). In this work, we adopted the model employing the RPCs supplied with the images.

The estimate of the accuracy of geometric correction is usually done through statistical RMS (Root Mean Square). Acquiring up checkpoints with quality and positioning them accurately on the image, you can get a low Root Mean Square Error (RMSE), often smaller than a pixel.

4.3.1.2 Modeling of surface

The next step of MDSs automatic generation process consists of elevation interpolation. This step uses interpolation functions to estimate the values of the elevation of any point, from the elevations of the sample. Although the interpolated surfaces demonstrate the variation of some phenomenon along three axes of data: x; y; and the axe of the interpolated attribute, they are not considered as three-dimensional representations (Burrough & McDonnell 1998).

The interpolation methods can be divided into two major groups: approximation models (global) and interpolation models (local). The first one employs analytical mathematical functions, such as polynomials, Fourier series and other spline functions, defining a continuous surface to represent the relief, from elevation data sample. The second one uses functions whose coefficients are defined by the samples of elevation points within a region of interest selected, taking as a choosing criteria, the distance or number of neighboring samples (Burrough & McDonnell, 1998; Felgueiras & Câmara,1999).

As for a large number of samples, it is quite difficult to define a polynomial function to adequately represent all the spatial variations of the phenomenon being modeled, it is very common to make use of local interpolation models to estimate the elevation value of each element of grid from a predetermined, number of neighboring samples.

The interpolation methods can also be classified into: deterministic and geostatistical. Deterministic methods are based directly on the values of elevation, measured from the neighborhood and/or mathematical formulations to estimate the elevation of any point. Geostatistical methods are statistical

probability models that include spatial correlation between the sample data to estimate the values of elevation (Burrough & McDonnell, 1998; Maune et al, 2001a).

The methods can also be classified according to the adjustment of the interpolated surface relative to the sample set, as adjusted or approximated. The first one creates a surface that passes through all points in the sample set. Unlike the first one, the approximated interpolation creates a surface which does not necessarily passes through the sampling points and typically indicates the trends of the surfaces (Burrough & McDonnell, 1998; El-Sheimy, 2005).

The interpolation method used in this study was bilinear. This is a method of local deterministic set range, which provides simplicity in the formulation, it is widely used in the generation of DSMs (Li et al., 2005). This method involves a series of successive interpolations, starting from a rough rectangular grid until a result of improvement in resolution, known as refining grid (Burrough & McDonnell, 1998; Felgueiras & Câmara,1999).

The choice of interpolation method for generating an DSM, largely depends on the purpose of its use. If the application is for hydrological modeling or mass movement, it is important to prepare an DSM that is hydrologically correct. However, if the purpose of use is for the generation of orthoimages or orthophotos, as in this study, the absolute accuracy of the altimetric values is more important (Hengl & Evans, 2009).

The interpolation of surface involves creating structures to store the data and the definition of surfaces to fit the elements of this structure.

The figures 23 and 24 show respectively the structures of the data used in practice to store the DSMs: Triangulated Irregular Networks (TIN); and Regular Grid. The last structure, used in this study, consists of a rectangular array of cells, regularly spaced and arranged along lines and columns. This structure can be interpreted as a discrete representation of a surface in which the entire cell assumes a value of elevation, changing only from the edge thereof (Maune et al. 2001a).

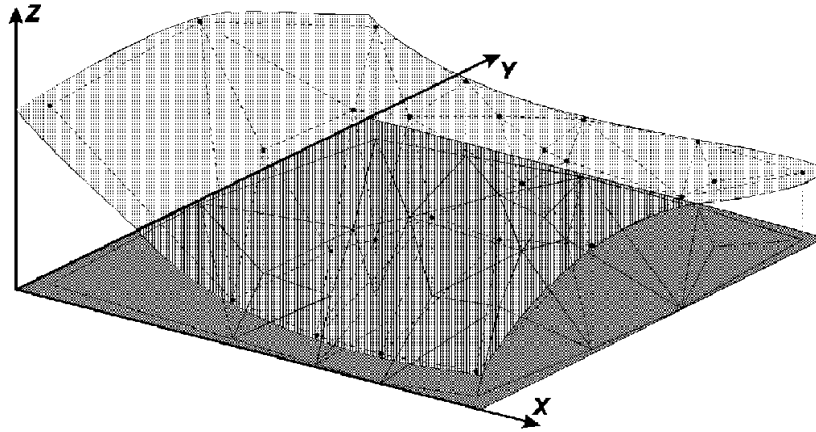


Figure 23: Example of Triangulated Irregular Networks (TIN) structure.
Source: Felgueiras & Câmara (1999).

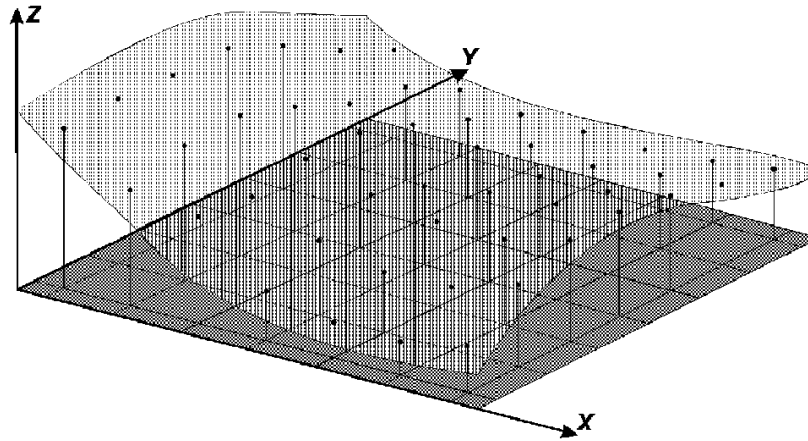


Figure 24: Example of Regular Grid structure. Source: Felgueiras & Câmara (1999).

The main differences between the two storage structures are shown in Table 3.

Table 3: Differences between the two storage structures. Source: Felgueiras & Câmara (1999)

Regular GRID	Triangulated Irregular Networks - TIN
Presents regularity in the spatial distribution of the vertices of cells.	Do not present regularity in the spatial distribution of the vertices of cells.
The vertices of the rectangles are estimated from samples.	The vertices of the triangles belong to the sample set.
Presents problems to represent surfaces with sharp local variations.	Represents better not homogeneous surfaces, with sharp local variations.
Simple data structure	More complex data structure
Topological relationships among the rectangles are explicit.	It is necessary to identify and store the topological relations between triangles.
Mostly used in qualitative applications and multilevel analyses in raster format.	Mostly used in quantitative applications.

The structure chosen to store the DSMs was the regular grid. The choice of the size of the grid cell, also called its spatial resolution, should take into consideration the purpose of the application, the accuracy of the data and the time spent for its generation. The choice of the size of a very dense grid will require more time for its creation. On the other hand a larger spacing may lead to the loss of information.

The bit length of DSMs, used in this study to represent the elevation variation was 32-bit Real.

4.3.1.3 Post-Processing

The last step of generating DSMs involves its post-processing for editing possible errors arising from the automatic process. The intended use of the DSMs in this study was not only to be used in the generation of orthoimages but also in the morphometric analysis.

The quality of DEMs influences the quality of the morphometric analysis. Even the most sophisticated algorithm used in morphometric analysis will not be able to correct severe errors in DEMs, used as basic inputs, being necessary to prepare them beforehand. The main objective of post-processing DEMs is to remove gross errors, improve the representation of the earth surface as well as the hydrological/ecological processes (Reuter et al., 2009).

The sensitivity of the local parameters in relation to the noise of DEM, as well as their dependence on grid resolution, increases in the following order (Shary et al., 2002):

1. Functions of first derivative (slope);
2. Linear functions of second derivative (single curvature); and
3. Square functions of second derivative (total curvature).

Errors in DEMs and their derived products can be grouped into: gross errors; systematic and random errors or noise (Wise, 2000, apud Reuter et al., 2009).

Gross errors are difficult to be detected in the elevation values of DEMs, but they can be easily identified visually as missing or unrealistic values, in DEM-derived products, generating features completely out of reality being modeled. As these errors produce erratic features, most of them can be detected using 3D views, using sun shading functions or even simple GIS functions (Reuter et al., 2009).

Systematic errors, however, are not easily detected visually, requiring statistical procedures. These errors can have causes such as: bias inherent in the method of data collection, limitations of the methods used to generate the DEMs or sensitivity of the algorithm used to compute the morphometric variables. An example of the latter arises from the use of too narrow search windows (Reuter et al., 2009).

Random errors are noise signal, often associated to measurement errors. Although they are significant for the DEMs generated from remote sensing imagery systems, they are inherent in any process of generating DEMs (Reuter et al., 2009). According to Sabins (2000) they occur as individual pixels with digital numbers (DNs) that are very different (higher or lower) from the values of its neighborhood, generating diffuse patches.

In general, DEMs from optical sensors require a number of steps of filtering to remove noise, interpolate empty cells, or reduce the effects of the influence of vegetation cover (Reuter et al., 2009). According to Gallant & Wilson (2000), any error in an MDE will be expanded in the calculated values of

the curvature, because this parameter is based on second derivative, which emphasizes local irregularities.

The most simple and widely used method to make the Spatial filtering of a discrete and continuous surface involves the use of a moving square window (known as the kernel or filter) on the surface and then calculating a new value of the center cell of the window as a function (f) of cell values covered by the window. This type of operation is commonly known as convolution. The window has frequently the size of 3 x 3 cells, but may also range from 5 x 5, 7 x 7 cells, or distance measurements (Crósta, 1992; Burrough & McDonnell, 1998).

The most common operations with windows (f) are the low-pass and high-pass filters. The low-pass filters have the function of eliminating the high frequencies (noise), maintaining the low and smoothing the surface. The effect is equivalent to the blurring of an image, causing the loss of detail information. The larger the size of the window, the greater the effect mentioned above.

Some of the most common types of low-pass filters are: mean, weighted mean, median and mode. The mean filter used in this study, is one of the simplest types of low-pass filters and its effect is to compute the elevation value for the cell at the center of the windows by using a simple arithmetic average of the values of its neighbors (Crósta, 1992).

The high-pass filter, unlike the previous one, eliminates low frequency while maintaining the high one and highlighting edges or boundaries between areas of different pixels values. Similarly to the one above, the size of the moving window influences the final result being that the smaller the window, the smaller the details to be highlighted in the image (Crósta, 1992).

4.4 Orthoimagery

The orthoimagery corresponds to images corrected by the displacements caused by relief, and are obtained through the orthorectification process.

The orthorectification becomes extremely necessary, especially if the images represent very irregular surfaces and steep slopes, since the satellite images are obtained through central perspective and therefore represented in

conical projections, causing the displacements shown in Figure 25 related to the right ortho position of a map projection.

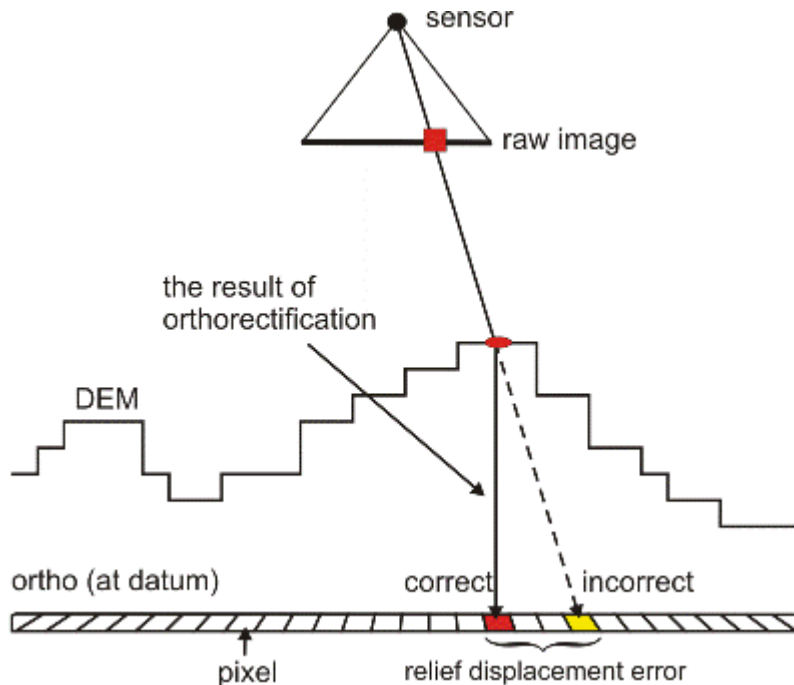


Figure 25: Displacement in raw image caused by the relief
Source: PCI Geomatics (2009a)

Jacobsen (2005) indicates the limitations of orthoimages generated from DSMs whose elevations values calculated refer to the top surfaces of buildings, trees, towers and other features and not to elevations of bare ground.

The orthorectification of images used in this study was performed using the Toutin (2004) approach, known as terrain independent. The corrections of distortions in raw images were done by using the Rational Functions model and their respective DSMs.

4.5 Quality control of remote sensing products

This subchapter will focus on positional accuracy, to have been this, one of the parameters used to assess the quality of DSMs and orthoimages generated.

4.5.1 Positional Accuracy

Positional accuracy was recognized in 1995 by the Committee on Spatial Data Quality ICA (International Cartographic Association), through the publication "Elements of Spatial Data Quality", as one of the seven (7) parameters defining the quality of geospatial data. The others are: lineage, loyalty attributes, completeness, logical consistency, semantic fidelity and temporality (Ramirez & Ali, 2003).

The quality control of cartographic documents is done generally by means of point features through their three-dimensional coordinates, obtained by topographic or geodetic surveys, or even from cartographic documents. The point features are usually called control points, or reference points and can be further classified according to their components horizontal and vertical. According to Merchant (1982), data used as reference to control cartographic documents must have an accuracy, at least, three times greater than the one of the product analyzed.

The main types of errors in measurements of physical quantities (point or linear) are: outliers, systematic and random errors. The outliers are easily detectable and can be eliminated when identified. Systematic errors are repeated with the same magnitude and the same signal, i.e., are cumulative and manifest themselves as a constant tendency that is external error. The random errors are related to the precision of a set of observations or dispersion of these observations about the mean, consists of internal error (Correia, 2008).

External error is calculated as the arithmetic mean of the differences between observations and their respective reference values.

Internal error is calculated using the Root mean squared error (RMSE), which is an estimator of standard deviation of a finite sample whose expression is given by Equation (1):

$$RMSE = \sqrt{\sum_{i=1}^n \frac{(l_i - l_v)^2}{n-1}} \quad (1)$$

where:

l_i - observed value

l_V - reference value

n - number of observations

The accuracy involves both the analysis of systematic errors as random errors and therefore get together the tendency - external error and the precision - internal error (Monico et al, 2009).

The concepts of precision, measured by the root mean square error of the sample; tendency represented by the average of sample value; and accuracy, get together precision and tendency of the sample are graphically shown in Figure 26.

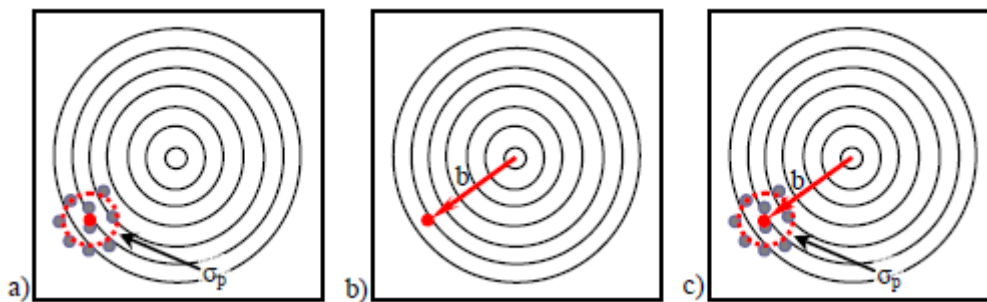


Figure 26: (a) Precision (σ); (b) tendency (b -bias); and (c) accuracy getting together precision and tendency (RMSE). Source: Monico et al. (2009).

Traditional methods, used in the analysis of errors measures, are based on the inherent assumption that most physical phenomena follows the normal (or Gaussian) distribution (Figure 27) of random errors (Smith, 2010), described by its parameters of mean and standard deviation. Calculating these two parameters from a sample set, it is possible to determine the probability of the true value of a quantity within certain confidence intervals (Andriotti, 2003).

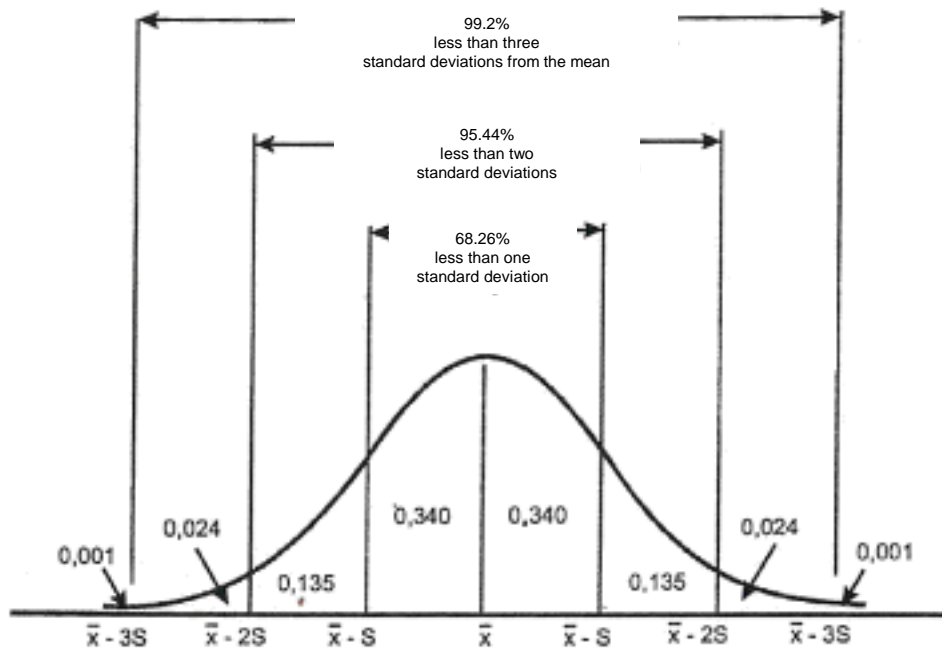


Figure 27: Normal Distribution. Source: Andriotti (2003).

where:

S - is the RMSE of the sample associated to the confidence level of 68.27% of the normal distribution

\bar{x} - is the average of observations

OBS: The 90% confidence level corresponds to 1.6449 times of S.

4.5.2. Control of DSMs and Orthoimages in Brazil

In Brazil, the same way as with the standard defined by National Map Accuracy Standards (NMAS), there is no expected minimum number of checkpoints of DEMs, since this standard was published before the emergence of these products (Maune et al., 2001b).

The lack of remote sensing standards in Brazil for accuracy controls implies the utilization of the Brazilian Cartographic Standards, established in Decree Law 89817 of June 20, 1984 used to evaluate the analog cartographic products (Brasil, 1984). These standards will be presented below.

4.5.2.1 Orthoimages horizontal control

Circular error 90% (CE90)

The parameter used in Brazil for the horizontal control is based on the circular error 90% (CE90) which correspond to the limit of the horizontal error of 90% of confidence level.

The horizontal (planimetry) error ep_i observed at each point i in terms of its UTM coordinates E and N, observed in the cartographic document being evaluated, compared to the respective coordinates taken as reference, is calculated by the Equation 2.

$$ep_i = \sqrt{(Eo_i - Ec_i)^2 + (No_i - Nc_i)^2} \quad (2)$$

where:

(Eo_i, No_i) - UTM coordinates of points measured in cartographic document

(Ec_i, Nc_i) - UTM coordinates of reference points

The calculation of the circular error (CE90) is made by ordering all n values of ep_i calculated. It then sets the limit value that contains 90% of n cases with value below or equal to this threshold. This limit value is the CE90 to be compared with the standards established for each scale mapping shown in Table 4 (Correia, 2008).

Horizontal RMSE

The horizontal root mean square error (RMSE) is calculated by the Equation 3.

$$\text{Horizontal RMSE} = \sqrt{\frac{\sum_{i=1}^n (Eo_i - Ec_i)^2 + \sum_{i=1}^n (No_i - Nc_i)^2}{n-1}} \quad (3)$$

The values of CE90 and horizontal RMSE in some scales of the Brazilian systematic mapping are shown in Tables 4, with bold emphasis to the scale of 1: 25,000, proposed in this study.

Table 4: Values of the CE90 and horizontal RMSE in some Brazilian systematic mapping scales. Source: Brasil (1984).

Scale	Class					
	A		B		C	
	CE90 (m)	RMSE (m)	CE90 (m)	RMSE (m)	CE90 (m)	RMSE (m)
1:250,000	125.0	75.0	200.0	125.0	250.0	150.0
1:100,000	50.0	30.0	80.0	50.0	100.0	60.0
1:50,000	25.0	15.0	40.0	25.0	50.0	30.0
1:25,000	12.5	7.5	20.0	12.5	25.0	15.0
1:10,000	5.0	3.0	8.0	5.0	10.0	6.0

The classification of any cartographic document in terms of its horizontal accuracy must reach both: the CE90 and the Horizontal RMSE, the former being associated to the tendency (systematic errors) of the observed data and the second with the precision (Correia, 2008; Oliveira, 2011).

4.5.2.2 DSMs vertical control

Linear error 90% (LE90)

The vertical (height) error of each isolated point of any cartographic document is calculated according to the Equation 4.

$$ea_i = H_{dci} - H_{ri} \quad (4)$$

where:

H_{dci} - height of point obtained by interpolation in the cartographic document

H_{ri} - height of reference point

Analogous to the procedure performed in the planimetry, the vertical LE90 can be obtained from the determination of the ordering of all the n values of e_{ai} calculated. Then it sets the limit value that contains 90% of n cases with value below or equal to this threshold and proceeds to the comparison with the reference value of the respective mapping scale, shown in Table 5 (Correia, 2008).

Vertical RMSE

The vertical root mean square error (RMSE) is calculated by the Equation 5.

$$\text{Vertical RMSE} = \sqrt{\frac{\sum_{i=1}^n (H_{dci} - H_{ri})^2}{n-1}} \quad (5)$$

The values of LE90 and vertical RMSE in some scales of the Brazilian systematic mapping are shown in Table 5, with bold emphasis to the scale of 1:25,000, proposed in this study.

Table 5: Values of the LE90 and vertical RMSE in some Brazilian systematic mapping scales. Source: Brasil (1984).

Scale	Eq* (m)	Class					
		A		B		C	
		LE90 (m)	RMSE (m)	LE90 (m)	RMSE (m)	LE90 (m)	RMSE (m)
1:250,000	100	50.0	33.4	60.0	40.0	75.0	50.0
1:100,000	50	25.0	16.7	30.0	20.0	37.5	25.0
	40	20.0	13.4	24.0	16.0	30.0	20.0
1:50,000	20	10.0	6.7	12.0	8.0	15.0	10.0
1:25,000	10	5.0	3.4	6.0	4.0	7.5	5.0
1:10,000	5	2.5	1.7	3.0	2.0	3.8	2.5

* Equidistance of contour lines, existing values in the Brazilian systematic topographic mapping.

As in the horizontal accuracy control, the classification of any cartographic document in terms of its vertical accuracy must reach both: the LE90 and the vertical RMSE.

5 MATERIALS AND METHODS

5.1 Materials

The data sources and software applications used in this study will be described in the following sections.

5.1.1 ALOS/PRISM satellite imagery

In this study, four scenes from the orbital sensor ALOS/PRISM were used. These scenes were cordially disposed through direct contact with JAXA. Each scene is composed of three images related to the viewing in the nadir direction as well as forward and backward directions (triplet observation mode).

The research of scenes covering the study area was taken from the JAXA website: <https://cross.restec.or.jp/cross-ex/topControl.action?language=en-US>. The selection of the scenes was visually performed, taking into account their sharpness, low cloud cover and best contrast. After preliminary analyses, the scenes shown in Figure 28 were selected. The JAXA's scene identifiers as well as their acquisition dates and the codes assigned in the present study to reference each scene are shown in Table 6. For simplicity, the codes will be used from now on to refer to each scene.

In addition to the images, RPC files containing information regarding the rational polynomial coefficients were delivered. The availability of these data for free has brought great savings for the research due to the high cost of high resolution satellite imagery.

The images were obtained with processing level of 1B2R. In the 1B2R level imagery, the CCDs of each viewing (Nadir, Forward and Backward) are joined to form a mosaic unlike the 1A and 1B1 level, where an image file is provided for each CCD. Other features related to the 1B2R level of processing are reported in section 4.1.2.

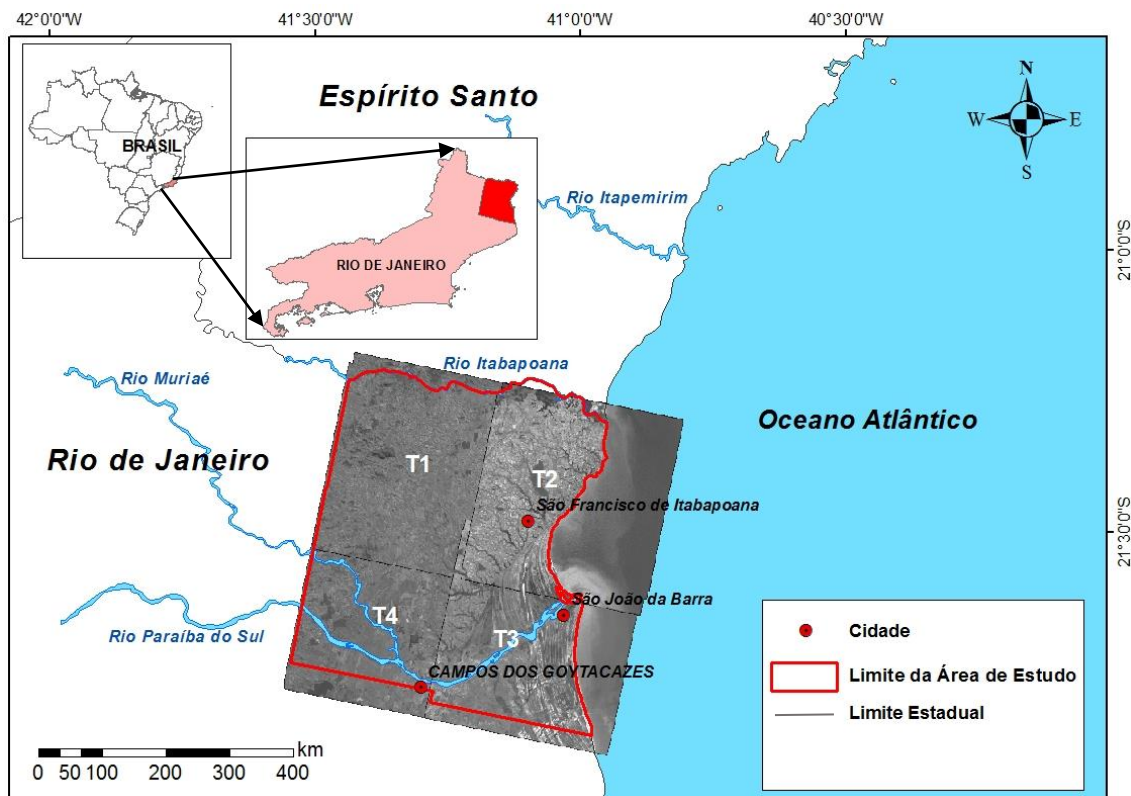


Figure 28: ALOS/PRISM satellite imagery covering the study area.

Table 6: Identification of scenes (triplets); acquisition date and scene code.

IDENTIFICATION SOURCE: JAXA	ACQUISITION DATE OF IMAGES	SCENE CODE
IMG-ALPSMN244254030	25/08/2010	T1
IMG-ALPSMN264384030	10/01/2011	T2
IMG-ALPSMN203994035	22/11/2009	T3
IMG-ALPSMN244254035	25/08/2010	T4

5.1.2 Cartographic Products

The products listed below correspond to all cartographic material used in this research. They helped both in the characterization of the investigated area as well as in the map validation processes.

- geological map from Silva & Cunha (2001);
- geomorphological map from Dantas (2000);
- thematic map from Ribeiro (2010); and
- thematic map from Chrismann (2014).

5.1.3 Survey points

The survey points were used to achieve two objectives: (1) generation and validation of DSMs and orthoimages for mapping purposes; and (2) generating of *Barreiras* Formation distribution map.

The points to achieve the first objective were obtained by IBGE. They are referenced to the national reference geodetic system SIRGAS 2000 (*Sistema de Referência Geocêntrico para as Américas*) and were obtained by GNSS relative positioning, resulting in half-meter accuracy.

To achieve the second objective, new survey points were collected in the research area. The survey visits had the following objectives: 1. understanding the geomorphology of the region; 2. identifying the *Barreiras* Formation deposits; and 3. collecting the coordinates of visited sites. Information about geomorphological, sedimentological and tectonic aspects were important to improve the understanding of the characteristics of these deposits and the regional morphology.

Several outcrops were visited throughout the research area, especially in the vicinity of the basement and the *Barreiras* Formation boundary. The sites were visited in distinct periods: (1) September 2011; (2) October 2011; and (3) March 2012. The material used in the field surveys included: mosaic of satellite imagery; and PDA Mio equipment, model P550B with ArcPad software v. 7.0.

Additionally, available survey points from Morais (2001) and Ribeiro (2010) were used.

5.1.4 Software applications

All of the software applications employed in this research are listed below:

- PCI GEOMATICS v. 2010 and v. 2013 - used for the automatic generation of DSMs and orthoimages. The first version is available on NEQUAT/Department of Geography/UFRJ and the second one was made available for free by contacting PCI Geomatics;
- Leica Geosystems/Leica Photogrammetry Suite (LPS) v. 9.2 - used for the automatic generation of DSMs and orthoimages. Available at the Institute of Geography/Universität Tübingen;
- Automated System for Geoscientific Analysis (SAGA) v. 2.0.8 - used for the preparation of DSMs and the generation of morphometric variables. Available for free at <http://www.saga-gis.org/>;
- Platform ArcGIS v. 9.3 and v. 10.1, including three applications: ArcCatalog, ArcMap, and ArcToolbox - used for the preparation of DSMs and the generation of morphometric variables as well as for the generation and display of maps. Available at NEQUAT/Department of Geography/UFRJ and at the Institute of Geography/Universität Tübingen;
- Mapgeo2010 v. 01 - used for the calculation of geoid heights. Available for free at www.ibge.gov.br; and
- Maxent v. 3.3.3 - used in modeling the spatial distribution of *Barreiras* Formation. Available at <http://www.cs.princeton.edu/~schapire/maxent> (free).

5.2 Methods

In this section, all methods involved in each of the three general approaches will be presented. The order of presentation of the processes was not done chronologically, but respecting the idea presented in the Introduction.

5.2.1 Remote Sensing approach

The general processes involved in this approach are shown in Figure 29. The input data were the ALOS/PRISM satellite imagery, the ground control points and the RPCs data. Details about each activity are described below.

5.2.1.1 Digital Surface Models (DSMs) automatic generation

As the atmospheric aerosols affect the radiometric quality of the images, hindering the process of auto-correlation, a fact to be considered when satellite imagery is used is the application of atmospheric correction in the raw images prior to start any processing. The atmospheric correction would only be recommended if the parameters needed to carry it out were made available to users. For not having been the case in this research, since the parameters were not available and as the correlation coefficients achieved in the correlation process met the desired accuracies, it was chosen not to apply atmospheric corrections in the raw images. Additionally, the pushbroom imagery systems, such as ALOS/PRISM, whose sensors are arranged linearly and perpendicular to the satellite track, allow capturing images with overlapping, almost simultaneously and with almost no variation in atmospheric conditions.

The generation of the DSMs was performed using the two different software applications PCI GEOMATICS and LPS for comparison purposes of the respective results. The initial tests were carried out using the OrthoEngine module from the PCI Geomatics software application.

The first process performed was the geometric correction of the images. In the classical Photogrammetry this is known as interior and exterior orientation.

The PCI/OrthoEngine offers five mathematical models for this purpose: (1) photogrammetric model; (2) model for optical sensors; (3) model for radar sensors; (4) polynomial models; and (5) spline model (PCI, 2009a). Due to the reduced number of control points and availability of RPC files, the model for optical sensors using rational functions was selected.

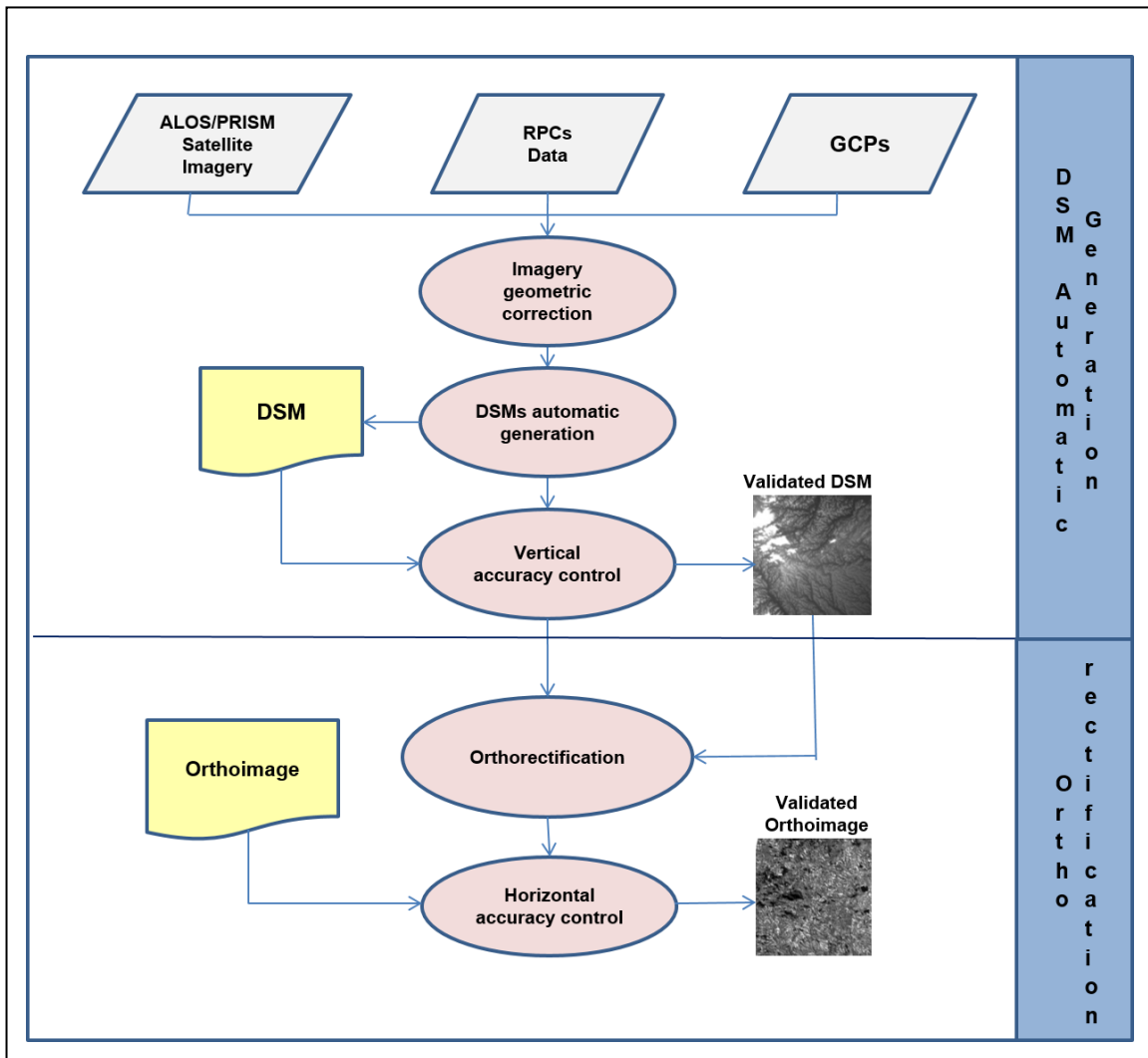


Figure 29: Main processes of Remote Sensing approach.

To compute the math model, three tests were performed: (1) with no control point; (2) using two control points and zero-order RPC-adjustment; and (3) with three control points using first-order RPC-adjustment. The last two options are recommended by PCI (2009a) in order to improve the accuracy.

The activities of identification of control points in the images that compose the triplet (Nadir, Forward and Backward) were performed using the GCP/TP Collection module. The choice of points took into consideration several criteria such as: proper identification in images; points closer to the ground surface, avoiding areas with vegetation cover, shadow and built; distribution in the image; and location in the area of overlap between two or more images.

Prior to the generation of DSMs, the epipolar images were created for each stereoscopic pair Backward-Nadir, Nadir-Forward and Backward-Forward in order to reduce the search space and improve the matching process. Epipolar images are stereo pairs that are re-projected so that the left and right images have a common orientation and the matching features between the images appear along a common X axis (PCI, 2009a).

The automatic generation of DSMs was performed using the so-called DEM from Stereo module by digital correlation of features in images with overlapping area. The DSMs were generated in DEM format, which corresponds to a regular grid format in which files of a panchromatic band are displayed in a gray scale, where the light color represents areas with higher height while dark areas represent the lower ones.

According to the pixel size, the DSMs were generated with a length of 10m due to the fairly flat terrain characteristic. Additional tests were performed with pixel size of 5 m with the demand of time far superior to the real gains in terms of vertical accuracy of DSMs.

The type of height values were set to real (32 bits). Gallant & Wilson (2000) reinforce that, in order to meet the requirements of shape-based applications, like in this research, the elevations of DEMs should be stored in real form (floating point). Another option available in the automatic generation process included the input of the approximate maximum and minimum height of the study area.

The procedures performed with LPS software were almost similar to the previous ones. The modules employed in the activities were the Project Manager and the Automatic Terrain Extraction (ATE). The LPS software offers five mathematical models including the photogrammetric, the rational functions and the polynomials. Like the tests with PCI, the model for optical sensors using rational functions was selected.

The identification of the control points in the three images of the triplet was performed using the Point Measurement function.

Unlike the PCI GEOMATICS, in the LPS software the creation of epipolar images is done automatically by the ATE module.

The LPS ATE module enables the combination of different strategies for calculating heights. These strategies can be set independently for each stereoscopic pair, both globally and locally, in the case of areas with significant differences in terms of variations in relief and occupation within the same stereo pair. The parameters for the type of terrain relief include: flat; undulating; and hilly. Regarding the type of occupancy, the available options are: rural; little or highly urbanized; and densely forested (LPS, 2008). Due to the relative homogeneous characteristics of the study area, both in relation to the relief and in relation to the type of occupation, the global strategy was used. The DSMs were generated with pixel size of 10 m.

The last process of automatic DSM generation was the vertical accuracy control in order to assess the quality of the output DSMs to meet the mapping requirements in the scale of 1:25,000. The number of ground control points used for this purpose for each triplet is shown in Table 7. The vertical accuracy of the ground control points, around 1 m, is in accordance with the value established by Merchant (1982). According to this author, the accuracy value of control ground points used in the accuracy control process should be less than 1/3 of the technical standard value RMSE, which in this study corresponds to the 1.1 m.

In order to carry out the validation process, the height of ground control points were compared to their respective values obtained from the output DSMs by using ArcGIS/ArcToolbox package tools. The ground control points used in the accuracy control of the DSMs did not include the points used in the generation of them.

Table 7: Number of ground control points used in vertical accuracy control for each *triplet*.

SCENE CODE (<i>Triplet</i>)	NUMBER OF GROUND CONTROL POINTS
T1	29
T2	26
T3	29
T4	28

The ellipsoid heights obtained from DSMs were converted into orthometric heights, employing the MAPGEO2010 program. Finally, the root mean square error (RMSE), mean and LE90 were calculated and the values obtained were compared to the respective reference values established by the Brazilian Technical Standards of Cartography (shown in item 4.5.2). For vertical accuracy control, Brazilian Technical Standards of Cartography establishes that 90% of isolated points whose heights are obtained by interpolation from contour lines should not have a larger error than those established for the standard LE90 value.

5.2.1.2 Orthorectification

The image orthorectification was also performed using two (2) different softwares: PCI GEOMATICS and LPS.

The orthoimages generated in this step were used for two purposes: (1) to evaluate the process of satellite imagery correction in terms of their horizontal accuracy, using the rational function model; and (2) as input for the visual interpretation of the *Barreiras* Formation deposits, which was carried out by Chrismann (2014). The output map generated by Chrismann (2014) served as reference for the validation process performed in this research.

The orthorectification process performed in the PCI Geomatics used the OrthoGeneration module. This module is based on the Independent Terrain approach of Toutin *et al.* (2002a, 2002b) and uses the height information from the DSMs. The orthoimages were resampled with pixel size of 2.5 m, using the method of bilinear interpolation.

Similarly, the orthoimages in LPS were generated using the software function OrthoRectification.

The next step included the evaluation of orthoimages in terms of their horizontal accuracy to meet the mapping on the scale of 1:25,000. The horizontal accuracy of the control points of IBGE, used as positional reference in horizontal accuracy control, around 0.5m, is in accordance with the value established by Merchant (1982). According to the author, the accuracy value of ground points used in the horizontal control process should be less than 1/3 of

the technical standard value RMSE, which in this study corresponds to the 2.5m.

The activities carried out included the ground control points identification upon orthoimages to obtain the coordinates E and N at their locations, using the ArcGIS editing tools. Similar to the procedure conducted in the vertical accuracy control, the root mean square error (RMSE), mean and CE90 were calculated. Subsequently, the results were compared with their respective reference values established by the Brazilian Technical Standards of Cartography (shown in item 4.5.2). The number of ground control points used for this purpose for each triplet is shown in Table 8. For horizontal accuracy control, 90% of well defined points on a cartographic map should not have larger errors than those established for the standard CE90 value.

Table 8: Number of ground control points used in horizontal accuracy control for each triplet.

SCENE CODE (Triplet)	NUMBER OF GROUND CONTROL POINTS
T1	15
T2	15
T3	16
T4	17

5.2.2 Geomorphometry approach

The vast distribution and the spatial variation of *Barreiras* Formation as well as the action of tectonic deformation result in risk for the use of isolated parts of this unit for purposes of its identification (Bezerra et al., 2006). For this reason, despite the use of high resolution images, it was decided to apply a more regional approach than a local one.

In this step, two different methods were used to identify the *Barreiras* Formation through combination of morphometric variables by using: (1) combinatorial OR; and (2) maximum entropy. The activities involved in each method are shown in Figure 30 and described as follows. The general input data were the layers containing the morphometric variables.

The criteria for choosing the variables took into account the geomorphological aspects of *Barreiras* Formation presented in Chapter 2. Moore et al. (1993) differentiates morphometric variables according to their achievement, as primary and secondary. Primary variables refer to those derived directly from DEM as slope, aspect, plan and profile curvature and others. Secondary variables involve the combination of primary variables, generally morphometric indices.

The variables selected to represent the geomorphological characteristics of *Barreiras* Formation were: height, slope and curvature, highlighted by Mitasova & Hofierka (1993) as key elements to describe the terrain surface. In addition to these variables, the following morphometric indices were chosen: terrain roughness index (TRI); multiresolution index of valley bottom flatness (MRVBF); and multiresolution index of ridge top flatness (MRRTF).

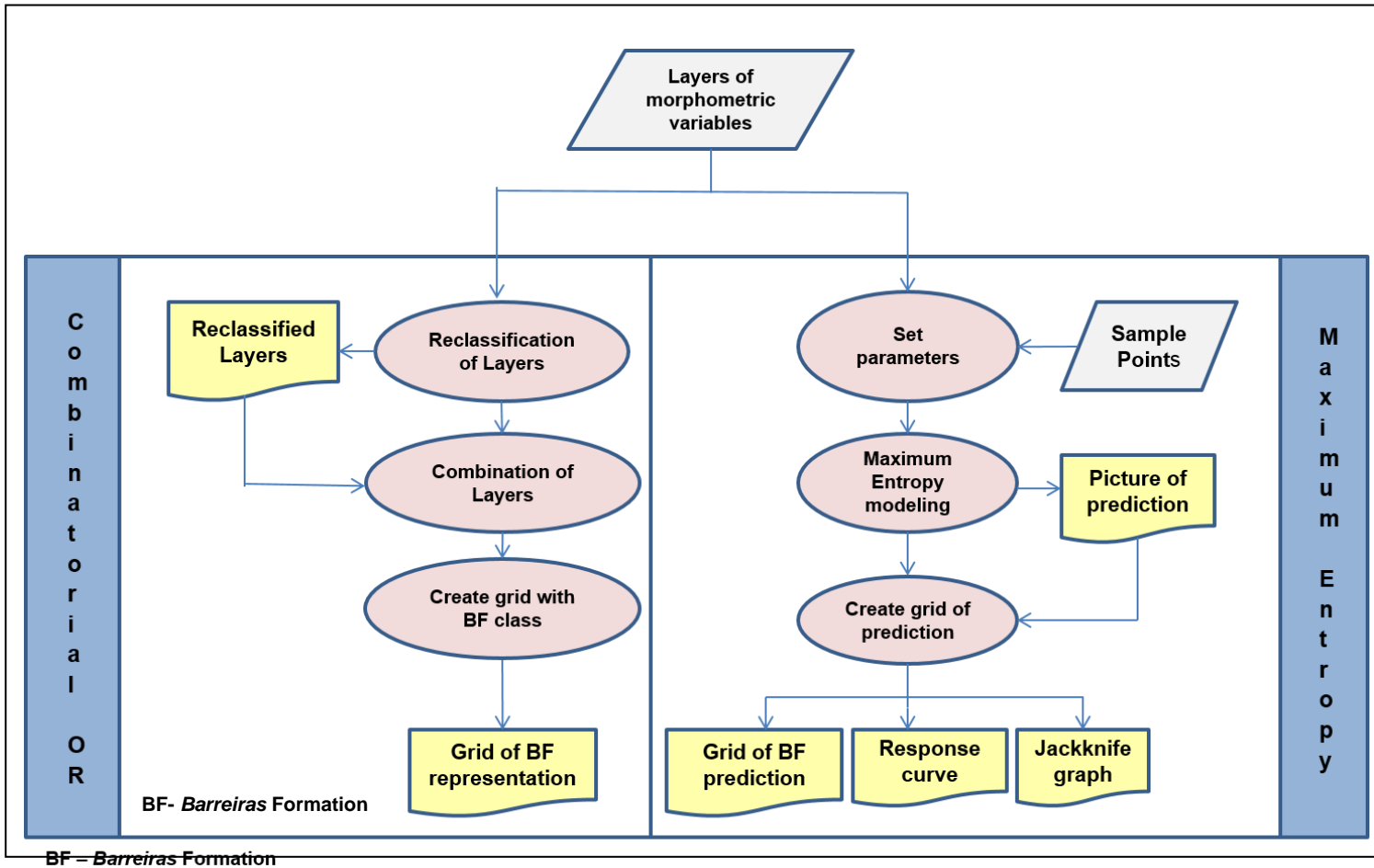


Figure 30: Processes involved in the Combinatorial OR and Maximum Entropy methods (Geomorphometry approach)

5.2.2.1 Combinatorial OR

The activities performed in this method included the classification of all layers of morphometric variables and subsequently the combination of all variables together.

The classification of each morphometric variable was done manually by using the classified function of ArcGIS in the layer properties. The map of Ribeiro (2010) was used as the reference for the successive approximations during the break values definition. Three classes were defined for each variable in order to represent the *Barreiras* Formation, the basement and the Quaternary plain.

The classes of each morphometric variable were combined all together using the Combine function from the ArcGIS/Spatial AnalystTool package. This function assigns a single output value to each unique combination of input values. The output is a file in raster format, containing integer values, representing each combination, recorded in the Value field of the attribute table (ESRI, 2013c).

The tests in the combinatorial OR were carried out using three smoothed surfaces of the studied area. The first smoothed surface used a window size of 15 by 15 pixels, smoothed 10 times; the second one used the same window size, smoothed 14 times; and the last one used a window size of 21 by 21 pixels, smoothed 10 times.

For the first smoothed surface, four tests were carried out. The first test involved the combination of all morphometric variables and indices (height, slope, curvature, TRI, MRVBF and MRRTF). Based on the results, further three tests were executed. In the second test, the height variable was excluded, keeping the other variables unchanged. As the complete exclusion of height variable caused the appearance of areas identified as *Barreiras* Formation upon the Quaternary deposits, it was decided to include it again but adding the basement class for the third test. The final test using the above mentioned DSM smoothed surface was carried out including the height variable with two classes (*Barreiras* Formation and basement), slope, curvature and TRI, excluding MRRTF and MRVBF indices.

The subsequent tests with the two other smoothed surfaces were performed using the last combination of variables due to its simplicity.

5.2.2.2 Maximum Entropy

The second method involved the application of a model developed in the Maxent software application. This model estimates a probability distribution of a target or studied phenomenon, searching for a probability distribution based on maximum entropy (as uniform as possible). The details of this model can be found in Phillips et al. (2006) and Phillips & Dudik (2008).

According to Elith et al. (2011), the model minimizes the relative entropy between two probability densities: one estimated from the occurrence data, defined in a covariate space, and another one originated from the landscape itself.

One of the advantages of the Maxent model, compared to other similar methods, is that it requires only the presence data to generate distribution models and it is suitable for all applications that have such data sets. Moreover, the performance forecast of Maxent is consistently competitive compared to other methods of best performance (Elith et al., 2011).

In addition to the presence data, the model uses a set of covariates, which, in this study, corresponded to morphometric variables. The model of Maxent, in particular, is more stable in relation to the use of correlated variables than other methods (e.g. gradual regression) so that there is little need to remove the correlated variables or even pre-process them, using Principal Component Analysis (Elith et al., 2011).

The Maxent model generates an output grid of prediction, showing the probability of occurrence in a continuous scale ranging from 0 to 1. Areas with higher values represent higher probability of occurrence of the phenomenon studied (Phillips et al, 2006; Phillips & Dudik, 2008).

To evaluate the distribution model, the software generates an index called Area Under the Curve (AUC) of the Receiver-Operator Characteristics (ROC) curve, which measures the fit degree of the model. Values close to one (1) indicate that the model is perfect in predicting the occurrence of the target,

while values near or below 0.5 values indicate that the model is no better than the random prediction.

Another feature available in the Maxent model for the evaluation of the results refers to the Jackknife graph, which can be analyzed based on percentile values of variables which had the greatest contribution to the generation of the distribution model and its importance when used alone (Phillips et al., 2006; Dudik & Phillips, 2008; Elith et al., 2011).

Although this approach is constantly used in the Biological Sciences for species distribution modeling, Phillips et al. (2004) describe it as a method of machine learning of general purpose, and with a simple and precise mathematical formulation, which employs maximum entropy techniques applied efficiently in different domains. For that reason this model was applied to predict the areas of highest probability of *Barreiras* Formation, based on its typical morphological characteristics, and modeled by different morphometric variables.

The tests performed in the present study used three data sets representing the occurrences of *Barreiras* Formation: the first one with 67 sample points; the second one with 46; and the third one with 151. Each sample point corresponded to a pair of E and N coordinates of sites visited during the field survey, where occurrences of these deposits were verified. As most of the field data was collected in the transition zone between the *Barreiras* Formation and the basement, it was necessary to identify new points to increase the sample set. These points were obtained through visual analysis upon the orthoimages using ArcGIS editing tools in well spatially distributed areas to avoid bias that could compromise the results, as reported by Phillips et al. (2004) and Elith et al. (2011).

The distribution model was built by selecting 80% of the samples containing the locations of occurrence of *Barreiras* Formation as training data, and the remainder (20 %) was used to test the resulting model.

5.2.3 Geographic Information System approach

The use of the Geographic Information System approach allowed performing the DSMs post-processing, the morphometric variables generation as well as the generalization, validation and visualization of the final map of *Barreiras* Formation (Figure 31).

5.2.3.1 DSMs post-processing

The DSMs post-processing aimed to improve their quality to meet the subsequent phase of morphometric variables generation. According to Wilson & Galant (2000), absolute measures of elevation errors do not provide a complete assessment of DSM quality, since most applications of DEMs depend on the representation of surface shape and drainage structure.

Even if the automatic generation option is adopted, it is necessary some editions of the DSMs to adapt the model in water masses and the elimination of random errors. Some computational applications offer smoothing functions for eliminating local noise and filling uncorrelated areas through interpolation based on the surrounding values (LPS, 2008; PCI, 2009b).

The activities of post-processing included, firstly, the visual evaluation of DSMs to identify spurious sinks or local depressions and their subsequent filling.

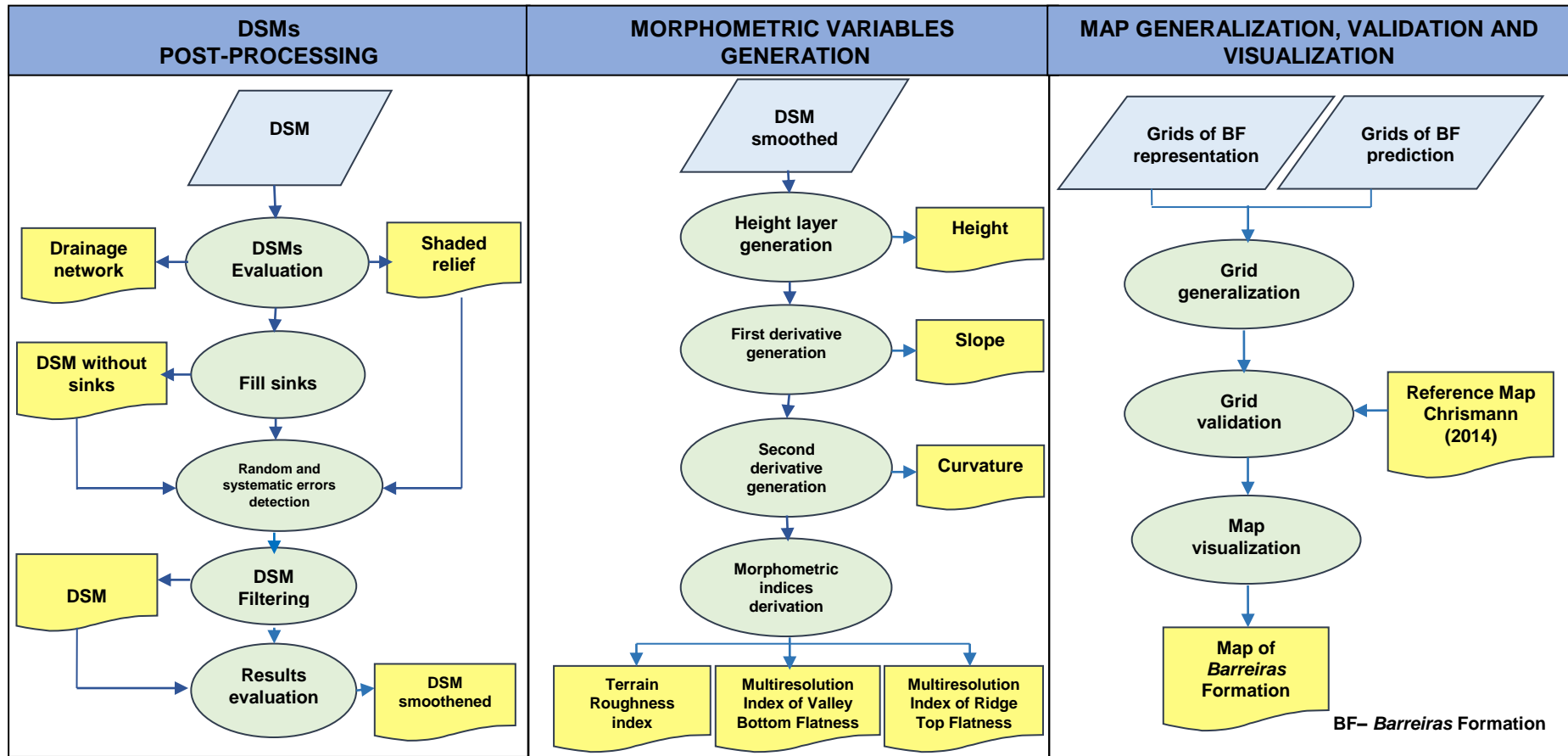


Figure 31: Main processes involved in the Geographic Information System approach

The next step was the detection of random and eventually systematic errors. The removal of DEMs noises is usually the first step in most algorithms for extracting morphometric variables. While DEMs provide a detailed analytical description of the terrain, pixel by pixel, morphometric analyses are developed in a more regional context, requiring digital filter applications to smooth the surface and therefore generalize the information obtained from DEMs (Correia, 2008).

An important question concerns the size of the moving windows used in the filtering process to recalculate the values of the attribute for each pixel (Crósta, 1992). Some software applications such as ArcGIS employ 3 by 3 pixels windows size. They are sensitive to tiny local variations for being small, being more suitable for regions with large height variations. Furthermore, as filtering operations require much time, one should avoid the use of small windows in large images.

Rana (2006) presents a discussion of the factors that limit the size of windows in relation to the dimensions of the studied features, and cites algorithms that work with different window sizes. This author warns about the fact that long-term smoothing of DEMs can affect their genuine topographic characteristics due to the gradual erosion of the features edges.

In several tests as to the identification of ridge and drainage lines, Rana (2006) found out the need to perform dozens of smoothing iterations applied to raw DEMs in order to obtain morphometric data with continuous and consistent values and without noise of local variations. In case of algorithms based on curvature, it is necessary to smooth DEMs before the calculation of this variable in order to avoid the effects of noises. Rana (2006) used a simple averaging technique built in the ArcGIS FOCALMEAN function and made ten (10) smoothing iterations for three DEMs with different cell sizes (i.e. 10m, 30m, 50m).

For this step, the low pass filter Gamma of PCI Geomatics and the simple averaging technique FOCALMEAN of ArcGIS were selected in order to compare the results.

The low pass filters reduce what is known as high frequency noise (speckling), but they can also degrade some finer details in the image, making it

unfocused (Crósta, 1992). As the low pass filter Gamma can preserve some of the linear image features such as edges (PCI, 2009b), filtering individual pixels in an image using the gray level values in a square window surrounding each pixel, this filter was selected for this step of the work.

The Gamma filter does not permit to use window sizes larger than 11 by 11 pixels (PCI, 2009b). Unlike, the FOCALMEAN function allows the use of different sizes of moving windows to calculate the statistics.

In addition to varying the size of moving windows, tests with successive applications of these filters were carried out with the aim of determining the appropriate number of iterations. The choice of the most suitable filter and the best combination of window size and number of iterations was done by evaluating the representation of three morphometric variables: height, slope and curvature, derived from each DSM smoothed surface.

5.2.3.2 Morphometric variables generation

In this step, the morphometric variables were derived from the DSMs. The activities were carried out using ArcGIS and SAGA software applications. The morphometric variables and indices used in this study were height, slope, curvature, TRI, MRVBF and MRRTF. A brief description of each variable is presented below.

Height refers to the variable that represents the distance measured along a perpendicular from one point on the ground surface and a reference surface (Maune *et al.*, 2001). The heights referenced to the geoid surface are known as orthometric heights. Unless explicitly stated, the term elevation used in DEMs refers to orthometric height (IBGE, 2014c).

The conversion process of the orthometric height (H) to ellipsoid height (h), referenced to a mathematical surface as the ellipsoid, implies the knowledge of the geoid undulation (N), as shown in Figure 32.

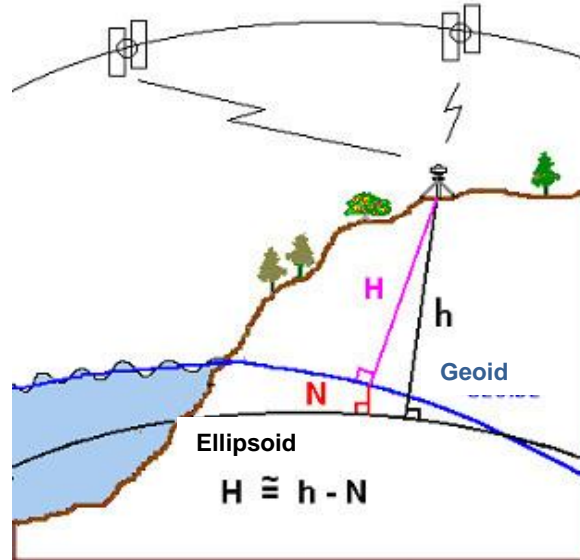


Figure 32: Relationship between orthometric (H) and ellipsoid (h) heights. N = geoid undulation. Source: adapted from IBGE (2014d).

As *Barreiras* Formation deposits outcrop at an intermediate height between the Quaternary and the basement, this variable becomes important in the identification of them when properly classified to reflect this height variation.

The slope corresponds to the rate of change of heights in the direction of steepest descent (Zevenbergen & Thorne, 1987; Wilson & Gallant, 2000). It is the first derivative of the height and is usually expressed in degrees, radians or percentage. The ArcGIS software application calculates this variable for each pixel using a window size of 3 by 3 pixels which moves successively along the map (ESRI 2013a). Regions with little height variation, such as the large flat interfluves associated to the *Barreiras* Formation, must present slope values around zero.

The curvature is based on the second derivative of the height and measures the rate of slope change. It can be represented by two components: the profile and plan curvatures (Figure 33). The most common units of curvature are degrees, percentages, or radians per unit distance. ArcGIS software application follows the mathematical formulation of Zevenbergen & Thorne (1987) and adopts the approach by a fourth order polynomial surface for each window of 3 by 3 pixels.

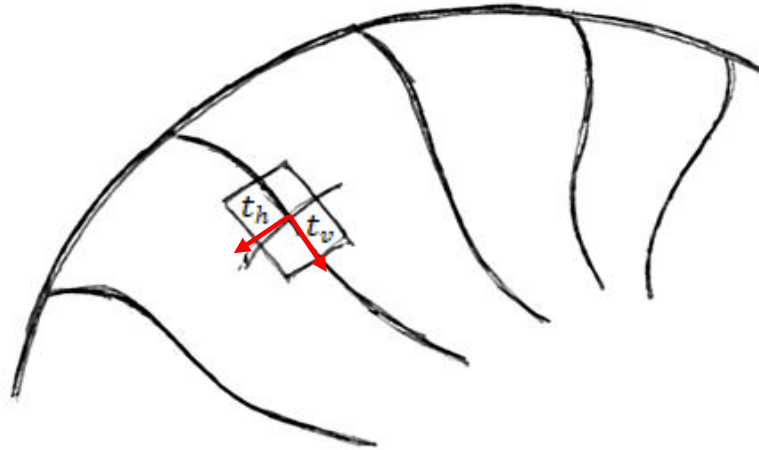


Figure 33: Plan and profile curvature and respective tangent vectors (t_h = horizontal tangent and t_v = vertical tangent). Source: Correia (2008)

The profile curvature is the rate of slope change down a flow line. It refers to the slope shape and may be convex, with negative values in the upper part of the slopes, where the slope increases; rectilinear, with value 0, where the change in slope is zero; or concave, with positive values at the lower of the slope. This variable is related to the dynamics of water flow in relation to acceleration, where the erosion process is associated to the acceleration of the flow in the straight and convex portions of the relief, while in the concave part the deceleration of flow favors depositional processes (Zevenbergen & Thorne, 1987; Wilson & Gallant, 2000; ESRI, 2013a, 2013b).

The plan curvature is the rate of aspect change along a contour and is linked to the characteristic of water to converge or diverge at if flows across the surface (Valeriano & Carvalho Júnior, 2003). The plan curvature shows negative values in the concave portions, where the water converges; null value in the straight stretches and positive values in the convex parts where there are divergent flows (Zevenbergen & Thorne, 1987; Wilson & Gallant, 2000; ESRI, 2013a, 2013b) as can be observed in Figure 34.

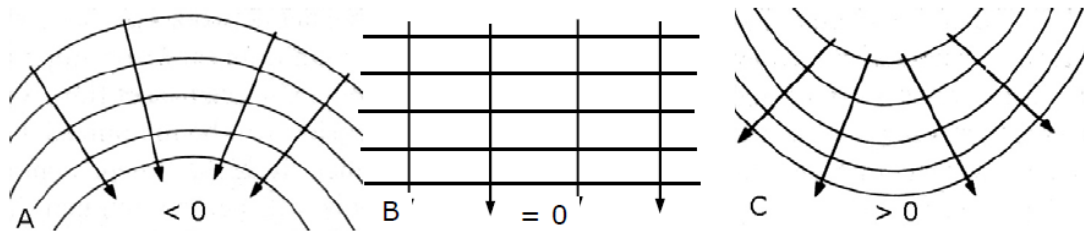


Figure 34: Effect of plan curvature on the water flow lines (A) concave curvature with convergent flow (in valley); (B) rectilinear; (C) convex curvature with divergent flow (on ridges). Source: modified from Summerfield (1991).

In this research, the total curvature was considered, for having achieved the best result in the identification of *Barreiras* Formation. Moreover, considering the characteristic of flat tops of these deposits, the plan curvature would not bring any benefit, if analyzed separately. The total curvature assumes positive or negative values, with zero curvature indicating that the surface is either flat or the convexity in one direction is balanced by the concavity in another direction (Wilson & Gallant, 2000). The flat tops of *Barreiras* Formation should present values around zero.

The Terrain Roughness Index (TRI) is a quantitative measure of topographic heterogeneity of the terrain. In this research, the calculation of this index was done using the function available in Morphometry module of SAGA software application, proposed by Riley et al. (1999). The method proposed by these authors employs the DoCELL function to calculate the sum of height differences between each pixel and its eight neighbors. In the case of *Barreiras* Formation, as this unit presents small height variations, this index has great potential to assist in its differentiation of basement domain.

The Multiresolution Index of Valley Bottom Flatness (MRVBF) is an index that can also be used to delineate hydrological and geomorphic units. The algorithm developed to calculate this index uses DEM to identify valley bottoms based on their topographic signature as flat low-lying areas. The algorithm uses slope and height to classify the degree of flattening of the valley bottoms. It operates at a range of scales (from coarser to finer resolutions) and combines the results at different scales into a single multiresolution index (Gallant & Dowling, 2003; Gallant et al., 2012).

There is a routine within the same algorithm that generates the MRVBF, which identifies the tops of the hills and calculates the Multiresolution Index of Ridges Top Flatness (MRRTF).

Although the algorithm for calculating these both indices has been developed using DEM spatial resolution of 25 m, the same algorithm can be used for any resolution with appropriate parameter settings. The connection between the size and flattening of the valley bottoms is incorporated into the algorithm by reducing the threshold value of the slope by a factor of 2 in each step (Gallant & Dowling, 2003; Gallant et al., 2012). The authors hypothesized that the relationship between these levels of slope, the spatial resolution of the DEM and the value of MRVBF does not vary between landscapes with different resolutions of DEMs. The threshold value of the slope should be adjusted to maintain the relationship between the slope and the resolution of DEM.

In this research, the two indices were calculated using the function available in the Morphometry module of the SAGA software application.

5.2.3.3 Map generalization, validation and visualization

The generalization activities aimed to aggregate cells based on the majority of their contiguous neighboring cells in order to obtain a more homogeneous representation of the *Barreiras* Formation deposits.

The output maps were validated using spatial correlation analysis comparing each map generated using both methods with a reference map. The map produced by Chrismann (2014) was established as reference data at this step of the study. The map that presented higher correlation with the reference map was compared to the map of Ribeiro (2010) in scale of 1:250,000 in order to evaluate the gains in identifying the *Barreiras* Formation using the proposed methodology and the high resolution images.

6 RESULTS AND DISCUSSIONS

This section will present the results obtained from all methods used in the three approaches and the discussions about them. In order to facilitate the understanding, the results will be presented in chronological order.

6.1 Results of accuracy control upon remote sensing products

6.1.1 Results of vertical accuracy control upon DSMs generated by LPS software

All digital surface models (DSMs) generated automatically using LPS software were evaluated by comparing their LE90 and RMSE values with the reference values established by the Brazilian Technical Standards of Cartography for the scale of 1:25,000 Class A. The best results of LE90 and RMSE values were selected and are shown in Table 9. Comparing the calculated values to the technical standards it is noticed that the DSMs are within the specified accuracy standard for the scale of 1: 25,000.

Table 9: Values of LE90 and RMSE of DSMs generated in LPS and their respective technical standard values established by the Brazilian Technical Standards of Cartography for the scale of 1:25,000 Class A.

<i>Triplet</i>	Scale/ Class	DSMs		Technical Standards	
		LE90(m)	RMSE(m)	LE90(m)	RMSE(m)
T1	1:25,000/A	3.259	1.891	5.0	3.4
T2	1:25,000/A	2.884	2.844	5.0	3.4
T3	1:25,000/A	1.887	1.216	5.0	3.4
T4	1:25,000/A	2.642	1.677	5.0	3.4

The DSMs were obtained using two (2) control points for the refinement of the rational function model and polynomial transformation of degree 0. The values of root mean square error (RMSE) of the automatic generation process, obtained from the refinement of the model, are lower than 1 pixel (2.5m).

6.1.2 Results of vertical accuracy control upon DSMs generated by PCI GEOMATICS software

As with the LPS Software, both a) the LE90 and RMSE values calculated from the DSMs generated automatically with PCI GEOMATICS software and b) the reference values established by the Brazilian Technical Standards of Cartography for the scale of 1:25,000 Class A are shown in Table 10.

Table 10: Values of LE90 and RMSE of DSMs generated in PCI GEOMATICS and their respective technical standard values established by the Brazilian Technical Standards of Cartography for the scale of 1:25,000 Class A.

<i>Triplet</i>	Scale/ Class	DSMs		Technical Standards	
		LE90(m)	RMSE(m)	LE90(m)	RMSE(m)
T1	1:25,000/A	3.219	2.259	5.0	3.4
T2	1:25,000/A	3.642	2.234	5.0	3.4
T3	1:25,000/A	2.628	1.399	5.0	3.4
T4	1:25,000/A	3.184	1.968	5.0	3.4

The best output DSMs, in terms of LE90 and RMSE values were generated employing two (2) ground control points for the refinement of the mathematical model (rational function) and by using polynomial transformation of degree 0. The values of the root mean square error (RMSE) obtained at the end of the DSMs automatic generation are lower than 1 pixel, except for the DSM related to the triplet T1, which presented RMSE error of 1.5 pixel.

6.1.3 Qualitative evaluation of DSMs

Although images from ALOS/PRISM sensor have specific problems of radiometric quality, causing gross errors in the image, the results of sensor orientation and correlation have a good level of accuracy (Gruen et al., 2007).

The problems regarding the presence of these noises as well as the good level of accuracy, verified by the excellent results of the correlation coefficients, lower or near 1 pixel, could be observed in almost all DSMs generated in the

test phase with both softwares. Most of the DSMs reached the mapping requirements of the scale of 1: 25,000, proposed in this study.

However, from a qualitative point of view almost all DSMs generated with the LPS software could not be used for the subsequent phase of morphometric variables derivation. Despite having excellent vertical accuracy as shown in Table 9, the DSMs generated with the LPS software presented several problems of noise that could compromise the morphometric analysis resulting in false interpretations.

Comparing the same clipping area of two DSMs generated by LPS and PCI GEOMATICS softwares (Figure 35), it is possible to notice such problems (noise) in DSMs generated by LPS. Although the figure shows an area of the DSM related to the triplet T1, the other three DSMs generated with the same software presented similar problems and, for this reason, were rejected on the subsequent stages.

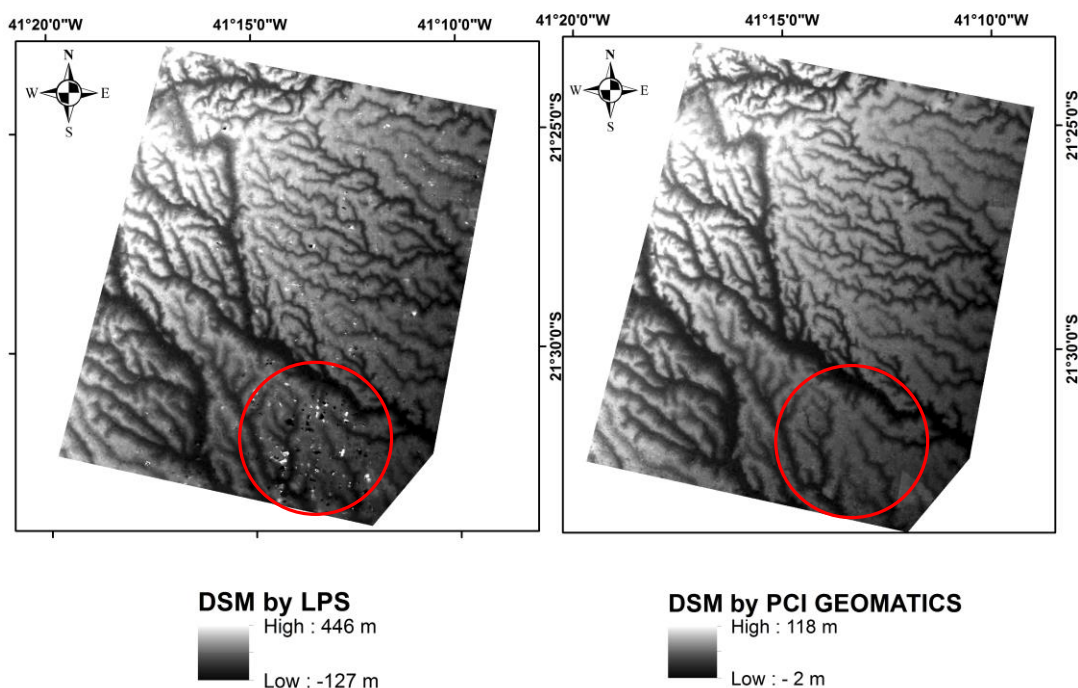


Figura 35: Scraps from the same detail area (triplet T1) of the DSMs generated by LPS and PCI GEOMATICS softwares. Several problems (noises) in the DSM generated with the LPS software, particularly in the area enclosed by the red circle can be noticed.

Due to the superior quality in terms of noise, the four DSMs generated with PCI GEOMATICS software (referring to triplets T1, T2, T3 and T4) were selected to generate the orthoimages. For this reason, only the results regarding the horizontal accuracy of orthoimages generated by this software will be presented.

6.1.4 Results of horizontal accuracy control upon orthoimages generated by PCI GEOMATICS software

The values of CE90 and RMSE calculated from the orthoimages generated automatically by using PCI GEOMATICS software and the technical standards established by the Brazilian Technical Standards of Cartography for the scale of 1:25,000 Class A, are shown in Table 11. Comparing the calculated values to the technical standards it is noticed that the orthoimages are within the specified accuracy standard for the scale of 1: 25,000.

Table 11: Values of CE90 and RMSE of orthoimages generated in PCI GEOMATICS and their respective technical standard values established by the Brazilian Technical Standards of Cartography for the scale of 1:25,000 Class A.

<i>Triplet</i>	Scale/ Class	Orthoimages		Technical Standards	
		CE90(m)	RMSE(m)	CE90(m)	RMSE(m)
T1	1:25,000/A	7.683	2.083	12.5	7.5
T2	1:25,000/A	5.686	2.049	12.5	7.5
T3	1:25,000/A	6.152	2.582	12.5	7.5
T4	1:25.000/A	5.217	2.019	12.5	7.5

6.2 Results of morphometric variables generation

The results of each morphometric variable generation were classified into interval classes and are shown in Figures 36, 37 and 38 that correspond respectively to different smoothed surfaces: 10 times with window size of 15 by 15 pixels; 14 times with window size of 15 by 15 pixels; and 10 times with window size of 21 by 21 pixels.

All morphometric variable distributions were classified according to three intervals, with the intermediate range associated to the major geomorphological features of *tabuleiros* of the *Barreiras* Formation. The class intervals of *Barreiras* Formation for the three smoothed surfaces are shown in Table 12.

The results, with few exceptions, showed little variation between the three smoothed surfaces and, in general, the surface smoothed 10 times with window size of 15 by 15 pixels presented best results.

Table 12: Class intervals of morphometric variables of *Barreiras* Formation for the three smoothed surfaces obtained by using the averaging technique FOCALMEAN.

Morphometric variable	Smoothed surface 15 by 15 pixels, 10 times	Smoothed surface 15 by 15 pixels, 14 times	Smoothed surface 21 by 21 pixels, 10 times
	Class Interval	Class Interval	Class Interval
Height (m)	8.5 – 62.85	8.5 – 62.84	8.5 – 62.84
Slope (°)	0.15 – 3.26	0.15 – 2.5	0.15 - 2
Curvature (°/m)	-0.015 – 0.07	-0.01 – 0.04	-0.01 – 0.04
TRI (m)	0.015 – 0.4	0.02 – 0.35	0.02 – 0.3
MRVBF	0.8 - 7	0.9 – 7.93	1.35 - 8
MRRTF	0.38 – 9.87	0.35 – 9.87	0.38 – 9.53

The analysis of the spatial distribution of morphometric variable classes is useful to help understanding the output maps generated using the two methods (combinatorial OR and maximum entropy) as will be shown in the next section.

Regarding the first variable, a clear increase of heights from SE to NW can be noticed. Height values at the boundaries between the *Barreiras* Formation and the Quaternary plain are characterized by abrupt changes and could be clearly identified. The boundary between the *Barreiras* Formation and the basement is less sharp and seems to be controlled by a NE-SW structure.

The results for the variables slope, curvature and TRI showed up very similar, allowing a relatively efficient distinction between the *tabuleiros* of the *Barreiras* Formation and the Quaternary plain, especially regarding the variables slope and TRI. In the areas of contact between the *Barreiras*

Formation deposits and basement rocks, limits are less clear and the curvature seems more efficient.

The Multiresolution Index of Valley Bottom Flatness (MRVBF) showed better results in the distinction between the *Barreiras* Formation deposits and the Quaternary plain. One possible explanation is a greater flattening of the Quaternary areas, raising their classification level far above the valleys in the *tabuleiros*. This index is not so efficient in distinguishing between the *Barreiras* Formation and the basement, which can be attributed to the fact that the valleys in the *tabuleiros* are increasingly less flattened and narrower as it approaches the contact with the basement.

The Multiresolution Index of Ridges Top Flatness (MRRTF) can be regarded as the less efficient variable in distinguishing between *tabuleiros* of the *Barreiras* Formation and the domains of the basement and the Quaternary plain. The distinction between the *Barreiras* Formation and the basement, based on the MRRTF index, is impaired due to the characteristically transitional morphology of the tops in the contact area. Regarding the distinction with Quaternary plain, this domain also presents very flattened morphology, similar to the tops of the *tabuleiros*.

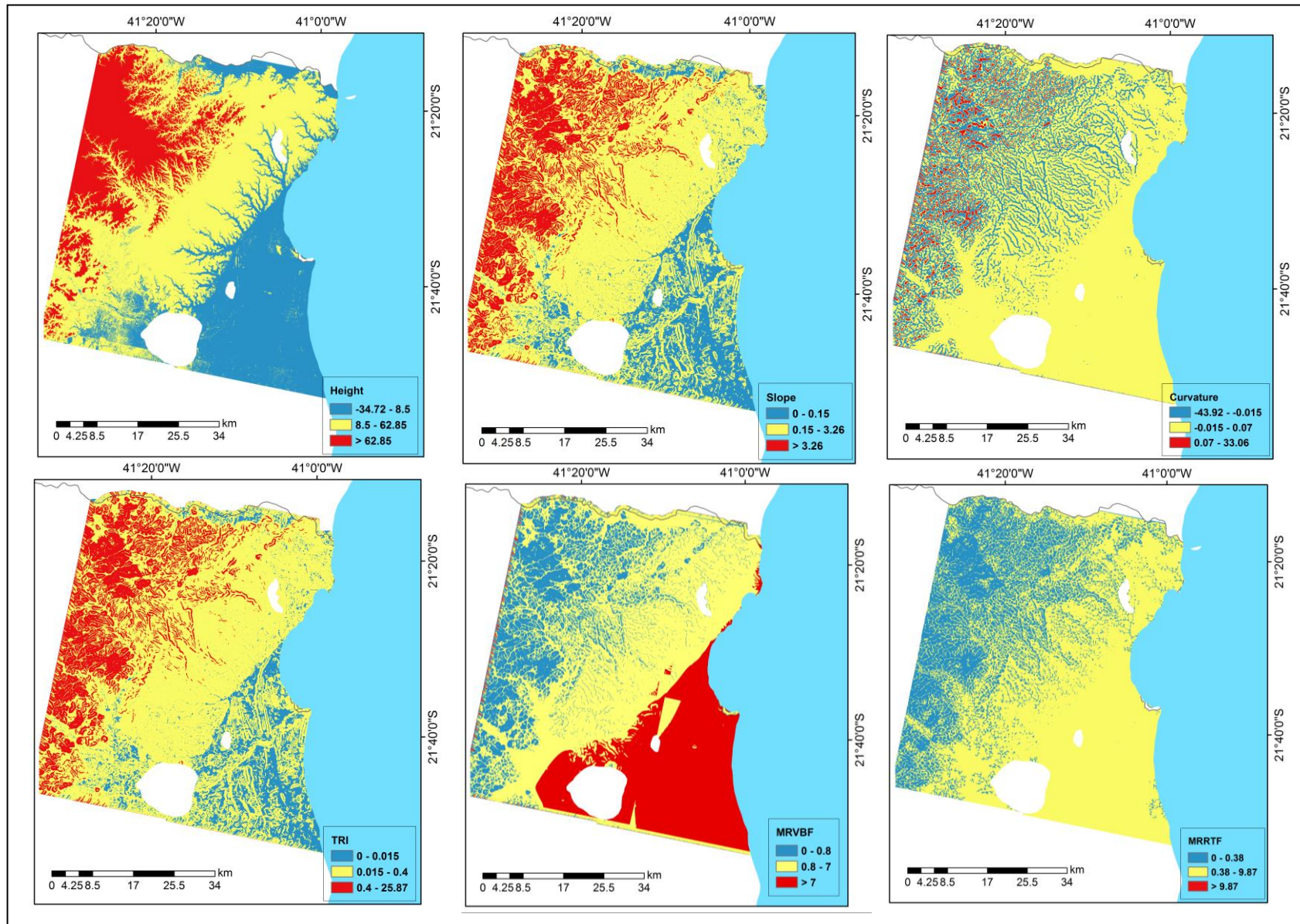


Figure 36: Morphometric variables derived from DSM surface smoothed 10 times with window size of 15 by 15 pixels: Height; Slope; Curvature; Terrain Roughness Index (TRI); Multiresolution Index of Valley Bottom Flatness (MRVBF) and Multiresolution Index of Ridges Top Flatness (MRRTF). The main intervals related to *Barreiras* Formation, but not exclusively, are represented by the yellow color.

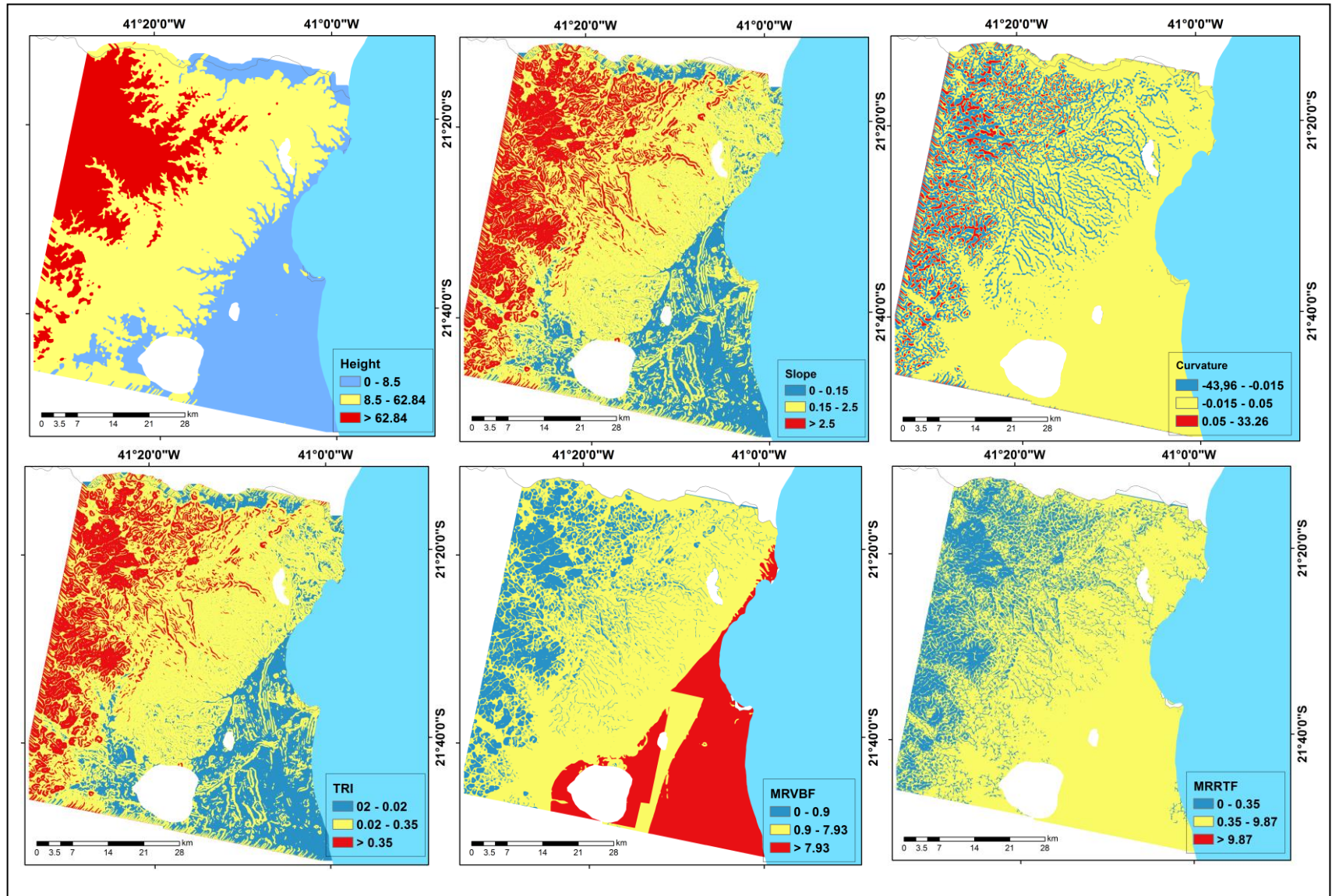


Figure 37: Morphometric variables derived from DSM surface smoothed 14 times with window size of 15 by 15 pixels: Height; Slope; Curvature; Terrain Roughness Index (TRI); Multiresolution Index of Valley Bottom Flatness (MRVBF) and Multiresolution Index of Ridges Top Flatness (MRRTF). The main intervals related to *Barreiras* Formation, but not exclusively, are represented by the yellow color.

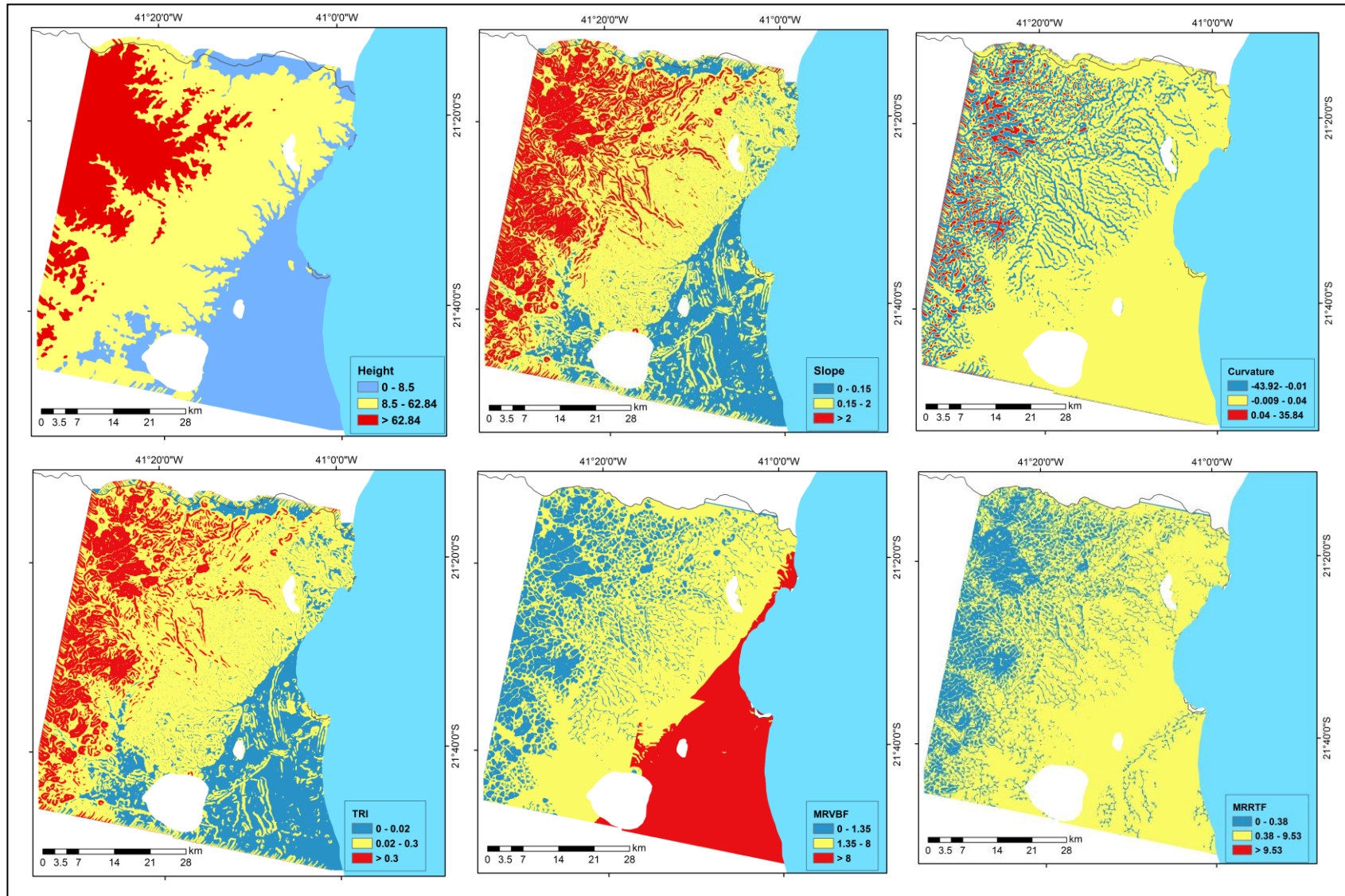


Figure 38: Morphometric variables derived from DSM surface smoothed 10 times with window size of 21 by 21 pixels: Height; Slope; Curvature; Terrain Roughness Index (TRI); Multiresolution Index of Valley Bottom Flatness (MRVBF) and Multiresolution Index of Ridges Top Flatness (MRRTF). The main intervals related to *Barreiras* Formation, but not exclusively, are represented by the yellow color.

6.3 Results of methods for identification of *Barreiras* Formation

In this section, the results obtained with the two methods used for mapping *Barreiras* Formation are presented. In order to evaluate the results obtained, three areas were particularly selected. These areas are the same that were highlighted in Figure 1, showing differences in tracing the contours of the limits of *Barreiras* Formation according to the maps of Silva & Cunha (2001) and Ribeiro (2010). The map produced by Chrismann (2014) in the same area of this research was used at this stage of the work as technical reference.

6.3.1 Results obtained using the method of combinatorial OR

6.3.1.1 DSM smoothed 10 times with window size of 15 by 15 pixels

The results from combinatorial OR shown in Figure 39 to 42 were obtained upon the surface smoothed 10 consecutive times with FOCALMEAN filter, using the window dimensions of 15 by 15 pixels.

The class intervals related to *Barreiras* Formation for each morphometric variable analyzed in all tests with this smoothed surface are shown in Table 12. It is to be noted that the intervals vary according to the DSMs smoothed surfaces, imposing new classifications as different surfaces were adopted. The height class interval of basement, between the values 62.86 and 540.28, was used in some tests.

The map generated with the combination of variables height, slope, curvature, and indices TRI, MRVBF and MRRTF is shown in Figure 39. The biggest differences appeared in the area A2, on the limit between *Barreiras* Formation and basement.

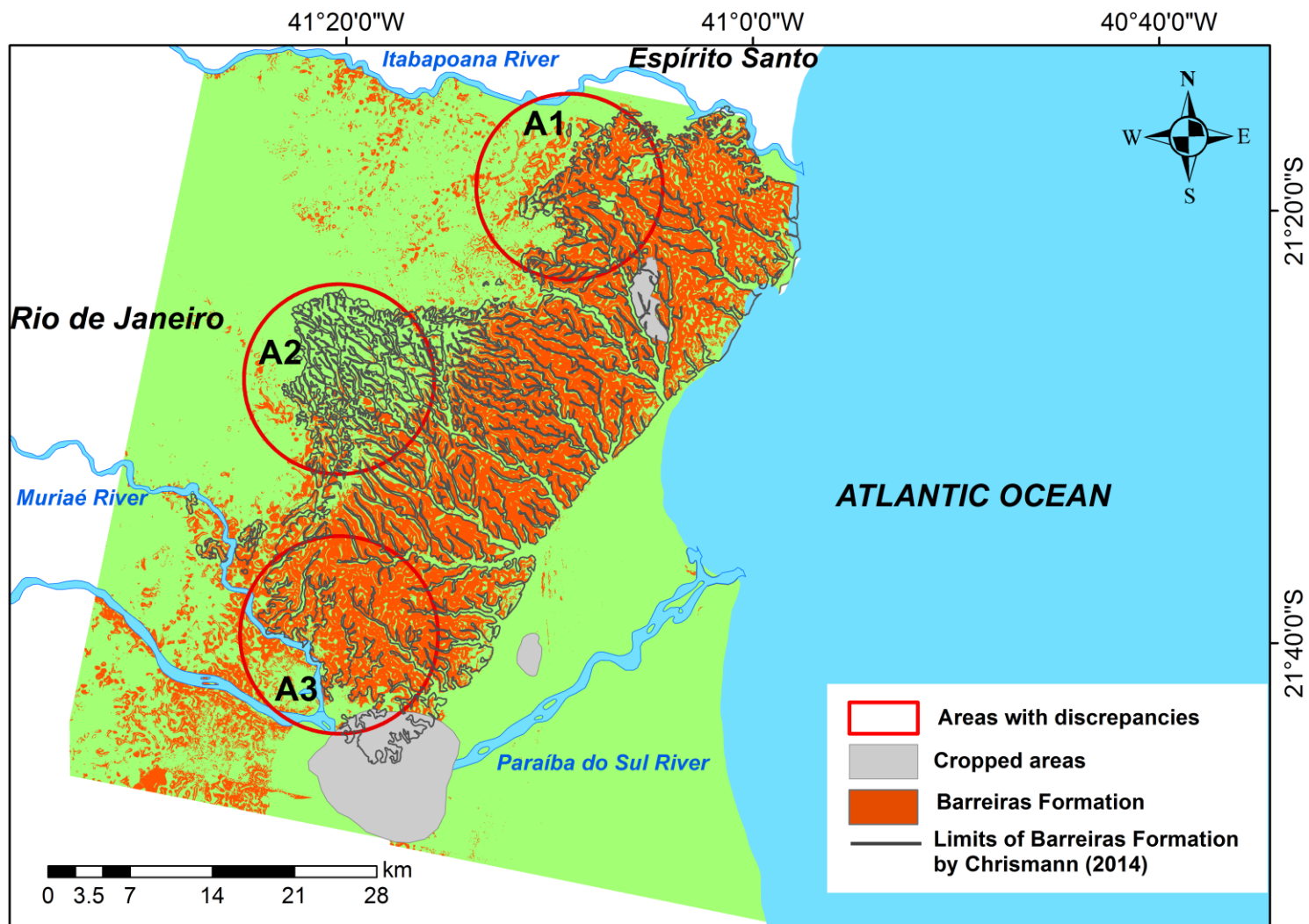


Figure 39: Map of *Barreiras* Formation generated from the combination of morphometric variables height, slope and curvature, and indices TRI, MRVBF and MRRTF, performed upon DSMs smoothed with a window size of 15 by 15 pixels and 10 iterations.

Chrismann (2014) noticed variations in the degree of fluvial dissection along the NE-SW axis, where the southern and northeastern portions present a lower degree of dissection, while the central region, which includes the A2 region, is more dissected and concentrated fairly higher density drainage. This region has been described as having the greatest extent of *Barreiras* Formation in NW-SE direction, reaching the foothills of the main basement topographic high in the study area. In the same region, Ribeiro (2010) and Ribeiro & Mello (2011) identified NW-SE topographic highs and lows, documenting important morphotectonic features printed on the *tabuleiros* of *Barreiras* Formation. According to these authors, the uneven distribution of these deposits evidences neotectonic topographic compartmentalization.

In the area of contact between the *Barreiras* Formation and the Quaternary plain, the combination of variables shown in Figure 39 worked successfully as to the determination of the limit of these units. It can be associated to the relatively continuous distribution of these deposits in such area (Chrismann, 2014).

While with the visual interpretation method it is possible to notice the small variations in the pattern of *tabuleiros* of *Barreiras* Formation, semi-automatic methods such as the one proposed in this research, use models that represent the overall geomorphological characteristics to infer results on the identification of these deposits. From this premise, it was chosen to examine, in isolation, some variables that could be contributing to the discrepant results in the area A2.

The first variable analysed was the height. The definition of height classes is an important resource for the identification of several topographical compartments and individualization of a set of landforms. The range of height used took into consideration the heights recorded in the region for most of the *Barreiras* Formation deposits: interval between 8m and 62m. However, the elevation of some blocks due to the neotectonic deformation raised the height of these deposits to a level that surely was not included in the class interval defined for the test and, therefore, were not recognized as *Barreiras* Formation. The range of heights assigned in this test failed to model the reality of the landscape.

The MRRTF and MRVBF indices represent aspects related to the morphology of the tops and valley bottoms respectively. As the area A2 presents itself as more dissected relief, which however is not a characteristic morphology of *Barreiras* Formation, with flat tops and valleys, it is understandable that these indices did not contribute to the identification of *Barreiras* Formation, since the values of these indices would be closer to the values of the basement of steeper hills and deeper valleys.

Based on these initial results, it was decided to conduct new tests that will be presented as follows.

The next test was performed excluding the height variable. Analysing again the three regions (A1, A2 and A3), there was an increase in the number of areas identified as *Barreiras* Formation in the areas A1 and A2 (Figure 40), while area A3 did not change significantly. Likewise there was an increase of areas identified as *Barreiras* Formation in the basement domain. This fact is justified because when the interval related to the height of the *Barreiras* Formation was removed, there was no more restriction and the deposits outside of this interval could be identified.

However, the complete exclusion of the height variable affected the results in the region close to the coast, showing a false emergence of *Barreiras* Formation in some areas of the *Paraíba do Sul* River coastal plain. Due to the continuous distribution of *Barreiras* Formation deposits in the coastal region and their elevation of about 8 m or more as compared to the Quaternary plain, the variable height plays an important role to differentiation of these units while the other variables, combined together, were not able to differentiate both of them. In summary, the results of this test showed that the complete exclusion of the variable height compromised the results of the differentiation of *Barreiras* Formation from the Quaternary deposits.

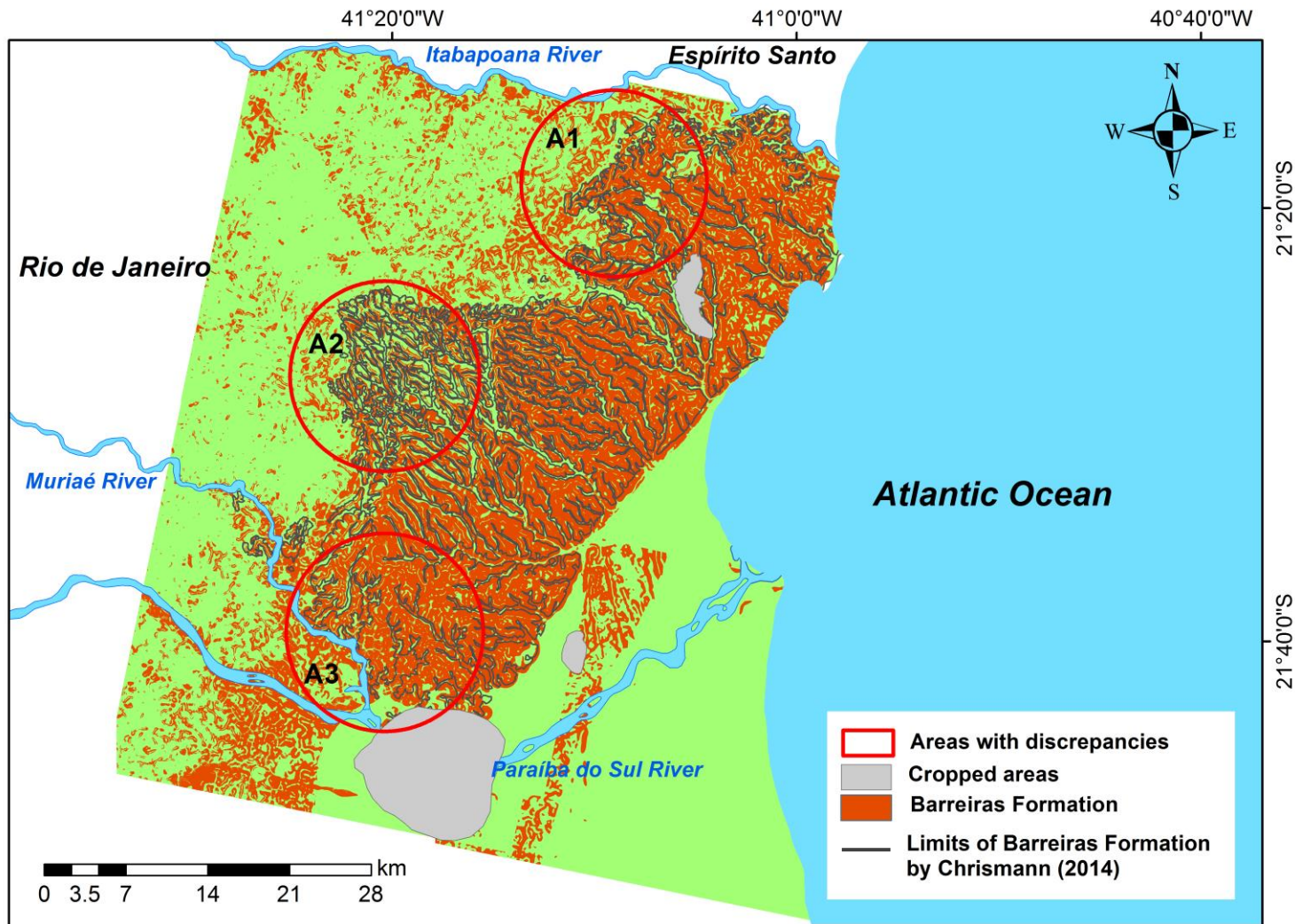


Figure 40: Map of Barreiras Formation generated from the combination of morphometric variables slope and curvature, and indices TRI, MRVBF, MRRTF, performed upon DSMs smoothed with a window size of 15 by 15 and 10 iterations.

The following test included again the height variable, which has now been reclassified, including the interval class of *Barreiras* Formation and basement, between the values 62.86 and 540.28, but excluding the height interval of Quaternary plain.

The result (Figure 41) doesn't show the areas identified as *Barreiras* Formation on the Quaternary plain, which was certainly caused by the exclusion of the height range related to the Quaternary deposits. In a visual analysis, the regions A1 and A2 remained almost unchanged from the previous test as well as the areas identified as *Barreiras* Formation in the basement domain. Although both height intervals (*Barreiras* Formation and basement) are included in the test, the combination of other variables has helped to distinguish *Barreiras* Formation from basement.

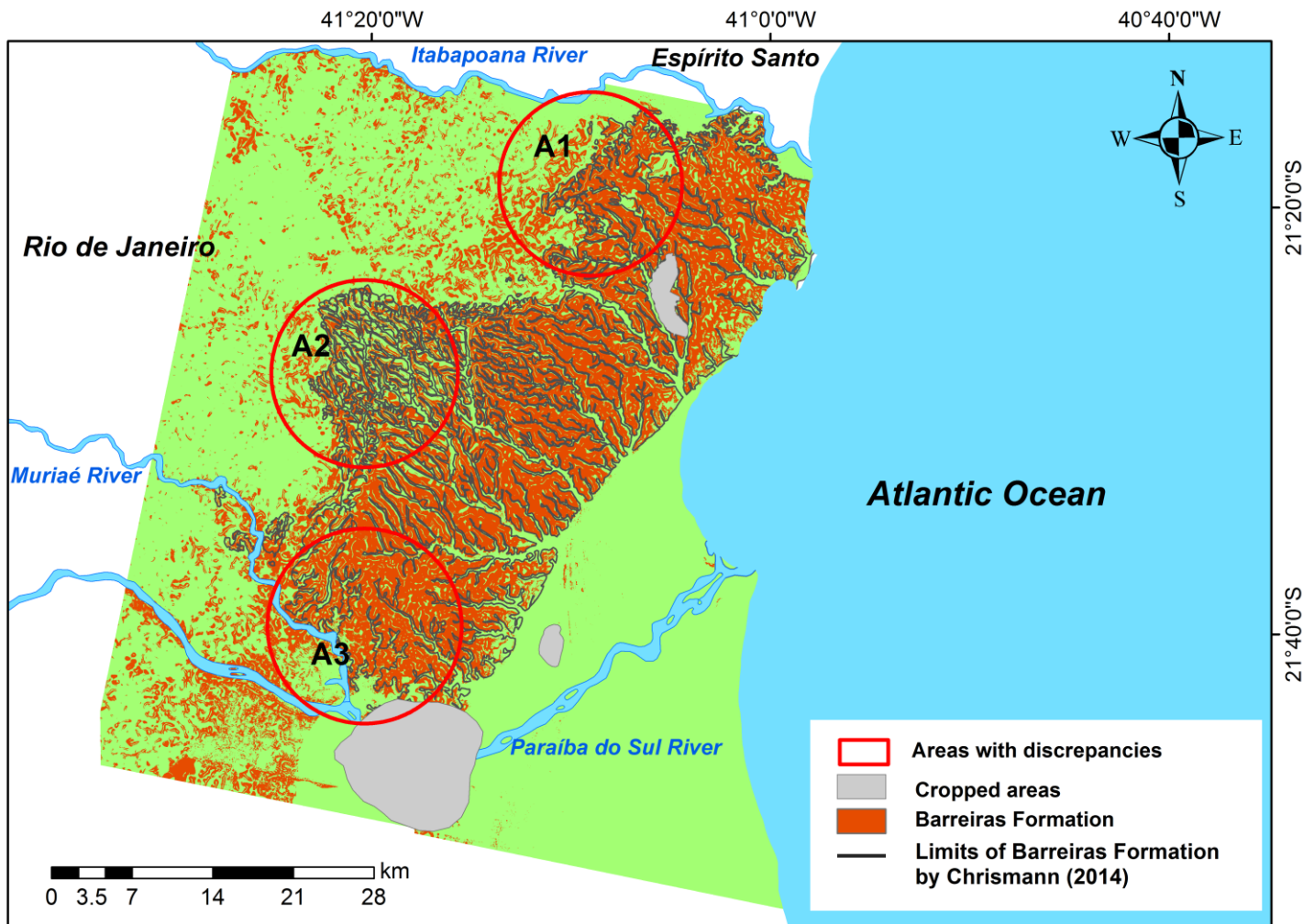


Figure 41: Map of *Barreiras* Formation generated from the combination of morphometric variables height, with two classes (*Barreiras* Formation and basement), slope and curvature, and indices TRI, MRVBF and MRRTF, performed upon DSMs smoothed with a window of 15x15 pixels and 10 iterations.

The last test with the surface smoothed with a window of 15 x 15 pixels and 10 iterations was conducted with the combination of the variables height, slope, curvature and terrain roughness index (TRI), excluding the MRVBF and MRRTF indices. This decision was based on the fact that both indices have been developed using DEM resolution of 25m. Although Gallant & Dowling (2003) presumed that the relationship between the steepness levels, DEM resolution and the MRVBF and MRRTF values are not varying between landscapes and with different DEM resolutions, it was not possible to adjust the parameters for DEMs with resolution of 10m. In this last test, the height variable was classified in the same way as in the previous test (including the intervals related to the basement).

In a visual analysis, there was a very slight increase of *Barreiras* Formation areas in the transition region between *Barreiras* Formation and basement, and some isolated occurrences upon Quaternary plain (Figure 42). This result could be explained by the fact that the *Barreiras* Formation deposits are more dissected in contact with the basement area, presenting a shape of hilly tops and narrow valleys instead of flat tops and valleys.

Based on the visual interpretation of this result, two additional tests were carried out using the same combination of variables height (including intervals related to *Barreiras* Formation and basement), slope, curvature and terrain roughness index, but then employing other smoothed surfaces, one obtained by using window 15 by 15 pixels and 14 iterations and the other one by using a window of 21 by 21 pixels and 10 iterations.

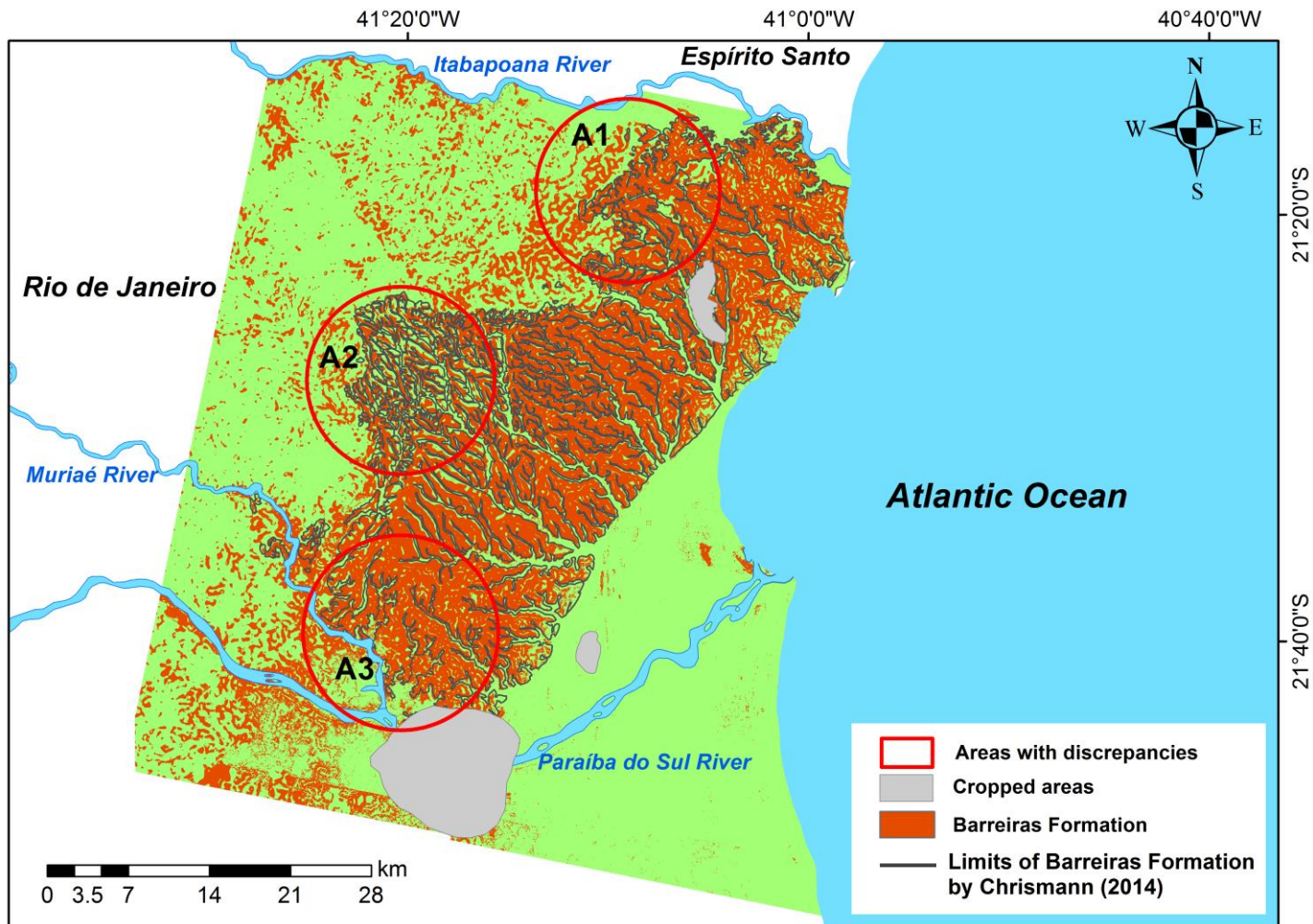


Figure 42: Map of *Barreiras* Formation generated from the combination of morphometric variables height, with two classes (*Barreiras* Formation and basement), slope and curvature, and TRI, performed upon DSMs smoothed with a window of 15x15 pixels and 10 iterations.

6.3.1.2 DSM smoothed 14 times with window size of 15 by 15 pixels

The intervals classes related to *Barreiras* Formation for each morphometric variable analysed, employing FOCALMEAN filter, 14 iterations and window dimension of 15 by 15 pixels are shown in Table 12. The height range of basement, between the values 62.85m and 494.68m is also included in this test.

As the surface used in this test was smoothed with the same window size, changing only the number of iterations from 10 to 14 times, the result showed no significant changes (Figure 43).

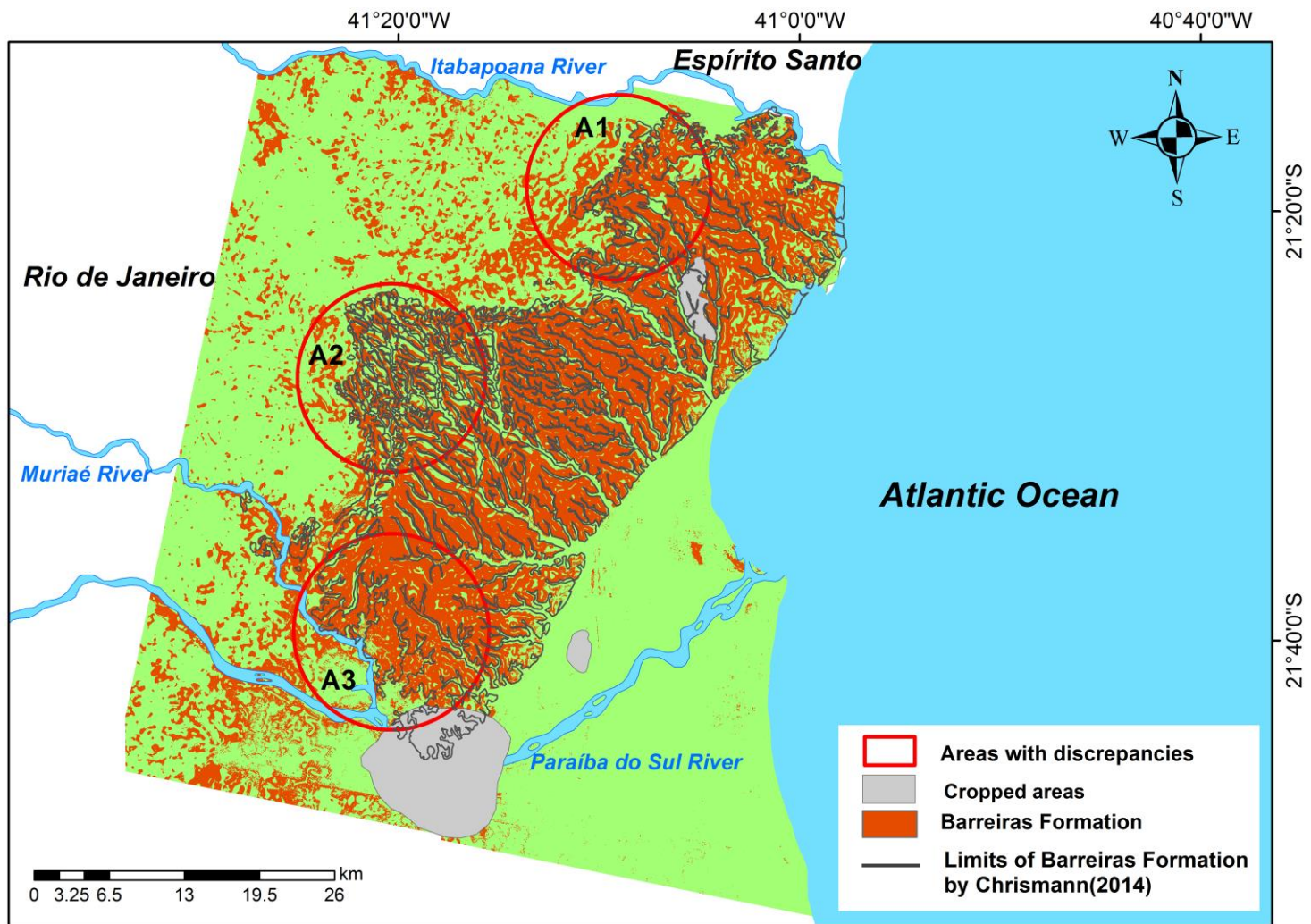


Figure 43: Map of *Barreiras* Formation generated from the combination of morphometric variables height, with two classes (*Barreiras* Formation and basement.), slope, curvature, and TRI, performed upon DSMs smoothed with a window of 15x15 pixels and 14 iterations.

6.3.1.3 DSM smoothed 10 times with window size of 21 by 21 pixels

The result presented in Figure 44 shows little changes compared to the previous results, even when using a larger window of 21 by 21 pixels, including the range of classes of variables presented in Table 12. This fact is due to the flatness of the study area, resulting in values very similar in all tests.

6.3.2 Results of tests using the method of maximum entropy

The class intervals used for classifying morphometric variables using the three smoothed surfaces of DSMs showed no significant differences, which indicates little variation in the degree of smoothing between the three surfaces (15x15, 10 times; 15x15, 14 times; and 21x21, 10 times). For this reason only the surface smoothed with an intermediate degree (window size of 15 x 15 pixels and 14 iterations) was chosen for the following tests, using the maximum entropy method.

The combination of the variables height, slope, curvature and terrain roughness index (TRI) was adopted for these tests for simplicity sake.

By using the Maxent model method, differently from the previous method, there was no need to include class intervals of morphometric variables and indices. The values of height, slope, curvature and terrain roughness index were obtained directly from the raster files (generated for each of the above mentioned variables) at the respective locations of the sample points.

A couple of different tests were performed by varying the number of sample sets used to represent the occurrences of *Barreiras* Formation in order to evaluate the behavior of the model used by the Maxent software. In the first test, samples collected in field surveys performed in this research and in previous researches in the study area were used. In two other tests, samples were obtained from the identification of *Barreiras* Formation upon orthoimages generated in this research.

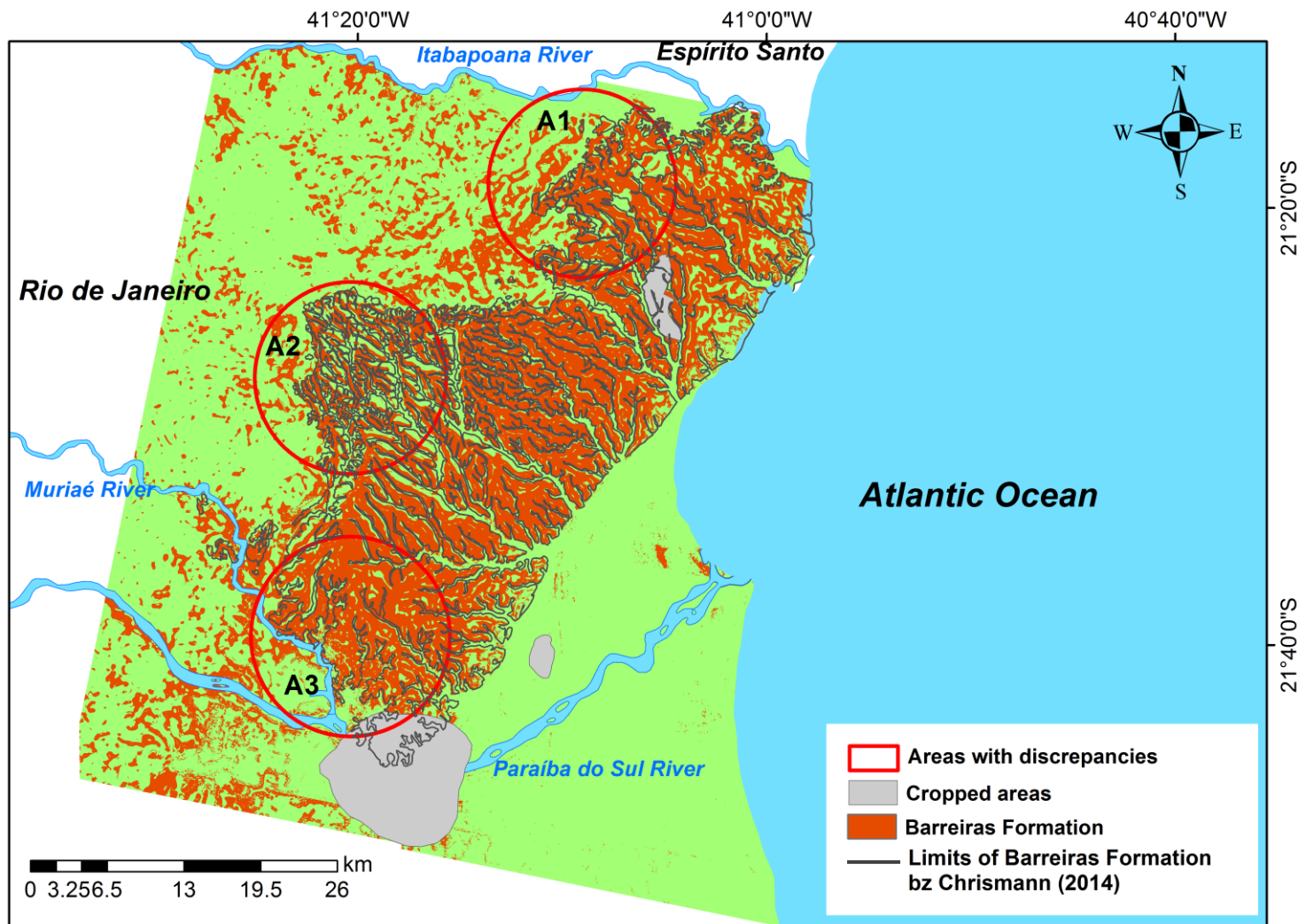


Figure 44: Map of *Barreiras* Formation generated from the combination of morphometric variables height - with two classes (*Barreiras* Formation and basement), slope and curvature, and TRI, performed upon DSMs smoothed with a window of 21x21 pixels and 10 iterations.

6.3.2.1 Samples collected in field surveys

In this test, a set of 67 points were used. The set of points had been measured in the study area as well as obtained from previous researches from Morais (2001) and Ribeiro (2010).

By evaluating the same three highlighted areas (A1, A2 and A3) already analysed in the previous method, it was found that for the areas A1 and A2 the probability of the occurrence of *Barreiras* Formation was above 50% (Figure 45). In the area A3 as well as in the northeastern portion of the study area, where the *Barreiras* Formation presents its typical morphological characteristics of *tabuleiros* (flat tops and low degree of fluvial dissection), problems were identified.

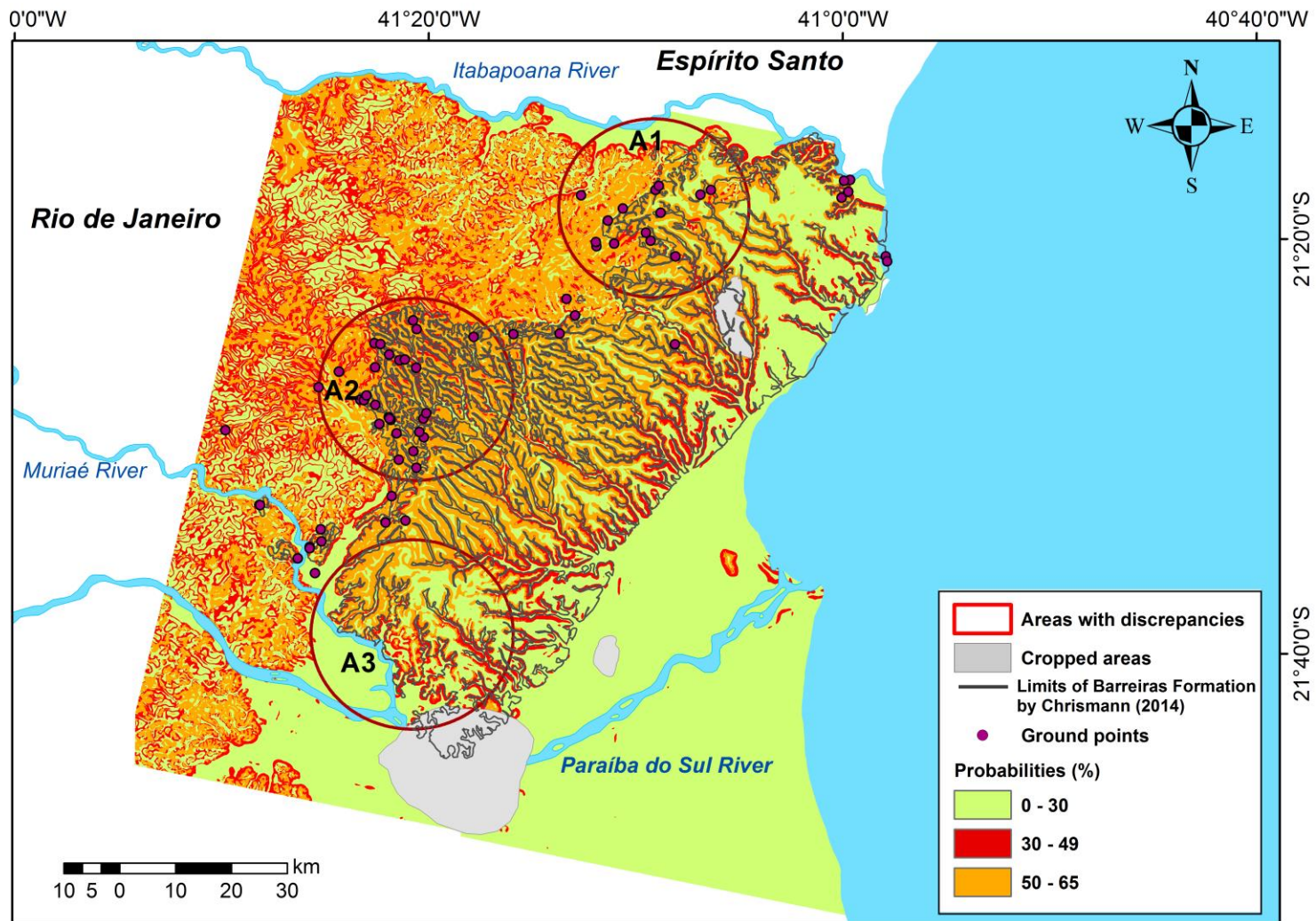


Figure 45: Probability map of *Barreiras* Formation distribution generated by Maxent software, using 67 sample points collected in the field.

The majority of sample points gathered in the field was located in the transition zone between the *Barreiras* Formation and the basement. This distribution was planned seeking to expand the field survey in the contact area between the *Barreiras* Formation and the basement, where the morphology of *Barreiras* Formation is not the most typical. As the values of each morphometric variable used as input for the Maxent model were obtained at the location of these points, it can be concluded that even having been identified in the field as *Barreiras* Formation, these values did not properly model the *Barreiras* characteristics, since in this region (transition zone), this unit presented itself highly dissected, showing relief different from the typical one of *Barreiras*.

The result of the grid of prediction generated by the Maxent model was an overestimation of the occurrence of *Barreiras* Formation (above 50%) in the northwestern part of the study area, which is already known as the basement. This result was based on the values of each morphometric variable in the transitional area, whose values are similar to the hills of the basement.

In the northeastern and southern/southwestern portion of the study area, in contact with the Quaternary plain, the Maxent model estimated a probability of *Barreiras* distribution below 30%, although in these areas the most striking morphological characteristics of this unit can be found. Likewise, the values of the morphological variables gathered from the sample points used in this test didn't represent properly the characteristics of *Barreiras* Formation.

The jackknife graph for this set of samples (Figure 46) shows the curvature variable with the smallest contribution in relation to the other variables, whose contributions are relatively with the same proportions. One possible explanation for the smaller contribution of the curvature variable is probably that most of the sample points used in the model were located close to the basement (transition area between the *Barreiras* Formation and basement) where the curvature values are much higher than 0 due to steeper slope of the hilly relief. For this reason, the model could not identify most of the areas near the coast and thus their contribution to the model process was reduced.

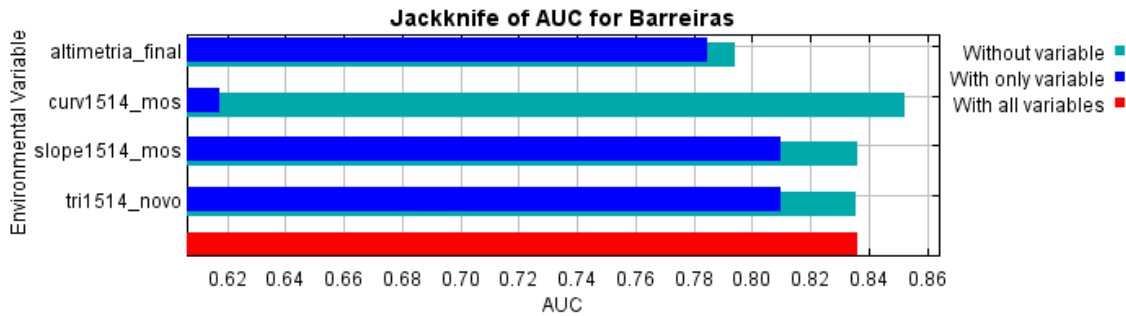


Figure 46: Jackknife graph of Area Under the Curve (AUC), showing the importance of each variable to generate the probability map of *Barreiras* Formation distribution from 67 samples collected in the field.

In the case of height variable, the graph shows that removing this variable would bring a lower gain for the model. In theory this means that the variable has the largest amount of information compared to the other variables. In this case, this is understandable because all other variables are derived from the height variable. However, this graph should be evaluated with caution, especially if the variables are highly correlated as is the case in this study.

The result reflects, in summary, the importance of choosing the location of points in the sample set, as discussed by Elith et al. (2011). The chosen samples showed bias, being more concentrated at the contact between the basement and the *Barreiras* Formation, inducing an inadequate result.

6.3.2.2 Set of samples collected from desktop

The next tests were performed using sample points whose coordinates were obtained from the identification of *Barreiras* Formation upon orthoimages generated in this research. Two set of samples were produced: one containing 46 sample points and the another one containing 151 points.

The first result (Figure 47), using 46 points, shows that the areas A1 and A3 presented the contour closest to the available geological maps (Figure 1). In the area A2, most dissected and uplifted deposits of *Barreiras* Formation were assigned with percentages between 30% and 49%, considered in this study as not being *Barreiras* Formation. This result is the same recorded to the area which is already known as basement.

Even with a small amount of points, the model was able to distinguish between deposits of *Barreiras* Formation and Quaternary plain. Some

occurrence mistakes, with a probability between 30% and 49%, appeared in the Quaternary region.

The result of this test shows the importance of preparing the sample data as parameters to the adequacy of the model and subsequent interpretation of the results, as highlighted by Elith et al. (2011). In this test, the choice of some sample points more evenly distributed over the investigated area enabled the model to more correctly identify even such *Barreiras* Formation deposits whose identification probability had been below 30% in the previous test as had been the case in the northeastern and southern/southwestern portions of the study area.

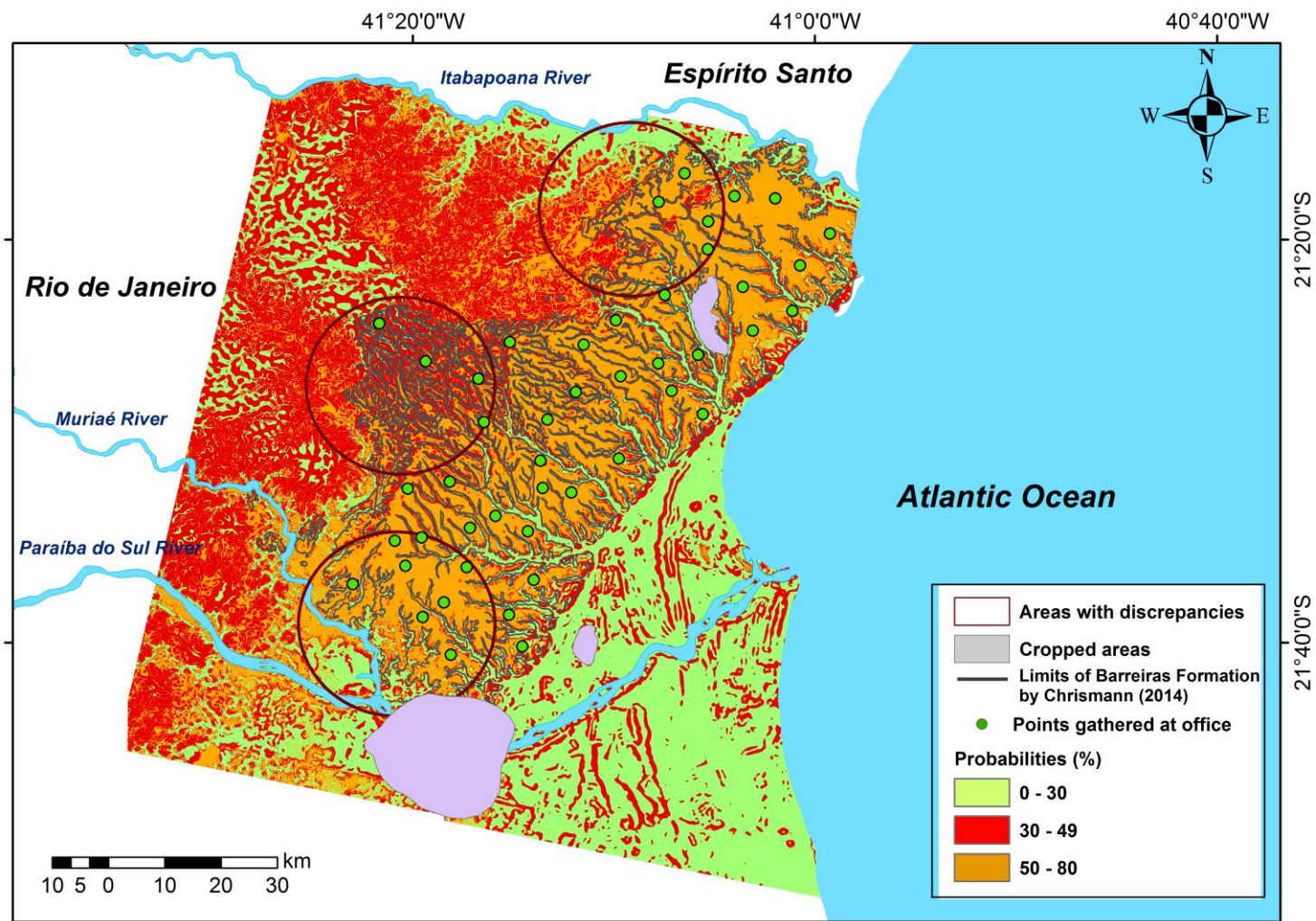


Figure 47: Probability map of *Barreiras* Formation distribution generated by Maxent software, using 46 samples collected from desktop

The jackknife graph of variable contribution to this distribution of points showed a higher contribution of the curvature variable than in the previous test, since the points were better distributed over the areas presenting flatter tops (Figure 48).

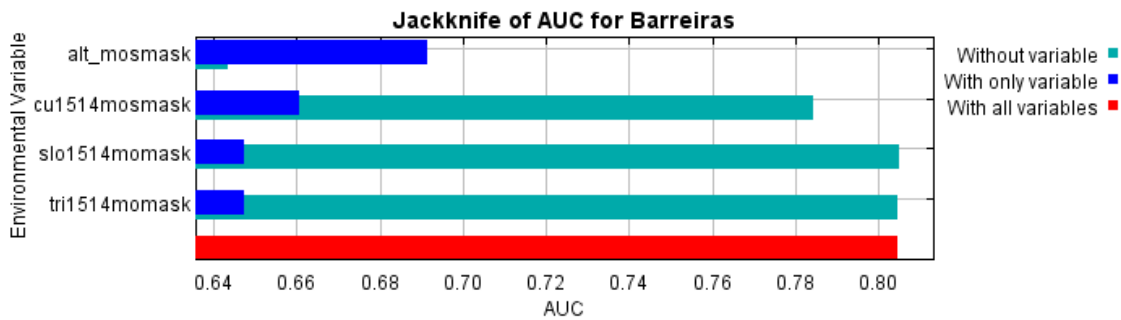


Figure 48: Jackknife graph of Area Under the Curve (AUC), showing the importance of each variable to generate the probability map of *Barreiras* Formation distribution from 46 samples collected in the field.

The second test using points collected from the desktop was performed using a set of samples containing 151 representative points of the *Barreiras* Formation.

The increase in the number of points as well as a more even distribution of these points brought benefits in terms of the map visualization to the entire region, especially for the A2 region, as shown in Figure 49. It should be noticed that in the northwestern region of the study area, the percentage of probability being *Barreiras* Formation is below 30% which is a more realistic result compared to the results of previous tests because it is a basement area. Some remaining occurrences above 50% can be found probably in regions where the basement has morphological characteristics similar to the *Barreiras* Formation, as is the case in the northwestern region already investigated during the survey field.

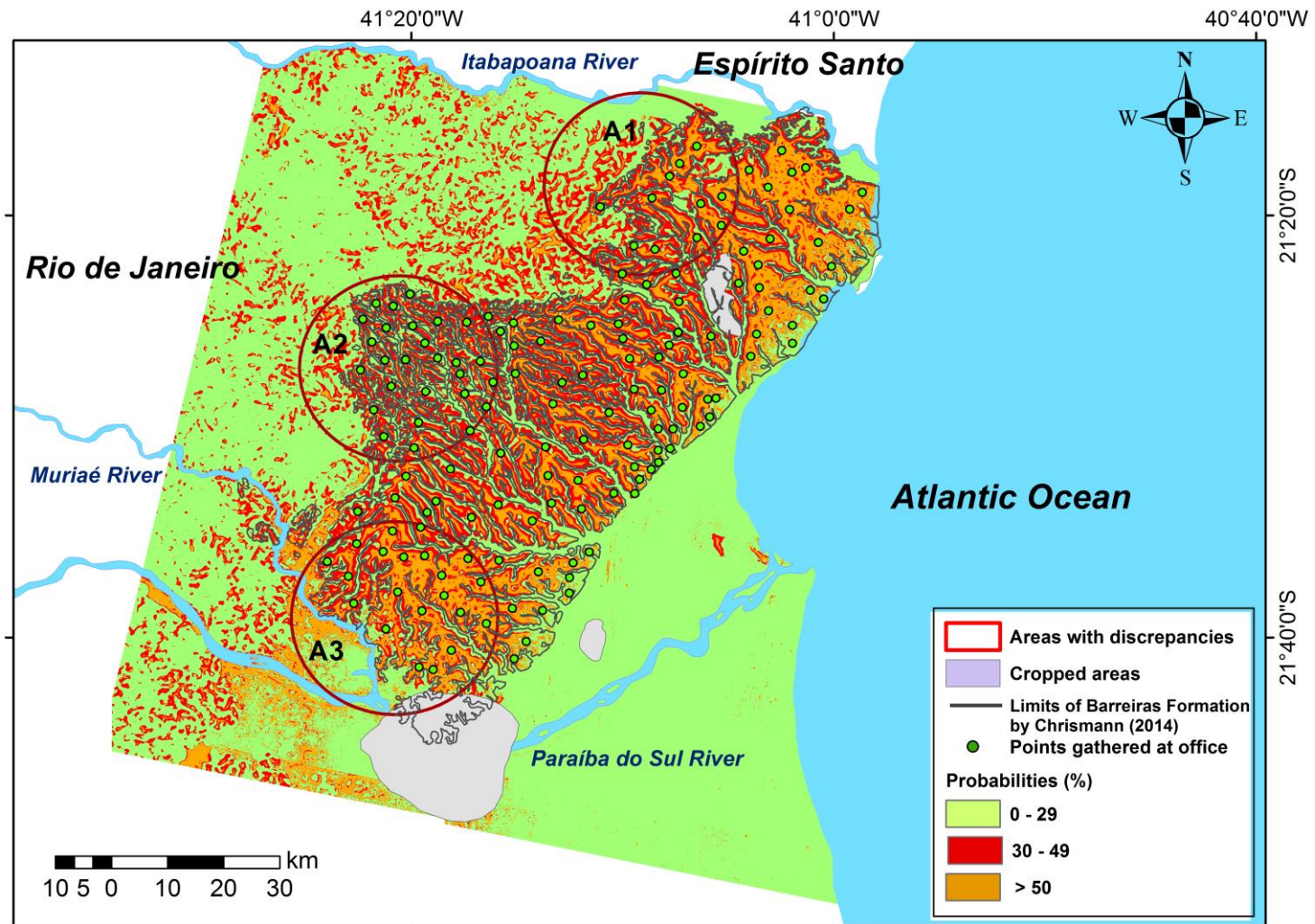


Figure 49 Probability map of *Barreiras* Formation distribution generated by Maxent software, using 151 samples collected from desktop.

The jackknife graph, shown in Figure 50, now presented a decrease in the importance of the height variable. On the other hand, according to the graph, its withdrawal will result in the lower gain for the model.

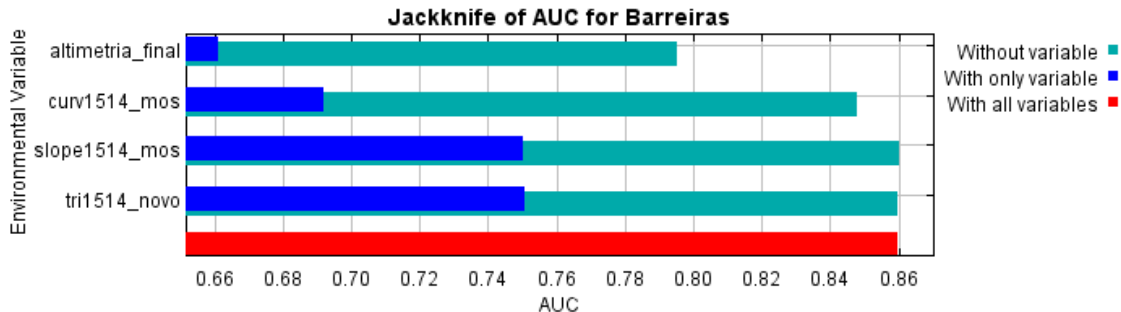


Figure 50: Jackknife graph of Area Under the Curve (AUC), showing the importance of each variable to generate the probability map of *Barreiras* Formation distribution from 151 samples collected in the field.

6.3.3 Evaluation of methods for identification of *Barreiras* Formation

Although both methods have made use of morphometric variables combination for the identification of *Barreiras* Formation, they are quite different. A discussion based on the characteristics of each method is presented in Table 13.

The first method uses combinatorial OR function to combine different raster files containing information about the morphometric variables. Because it is a relatively simple combination, it becomes easier to be used by any user. In contrast, the second method (maximum entropy) employs a more complex mathematical formulation to be understood by users with limited knowledge in statistics. The absence of specific documentation about the Maxent software makes it difficult to understand how to suit the various parameters to the desired application.

The combinatorial OR method does not require a set of points representing the occurrence of the *Barreiras* Formation. However, the morphometric variables must be classified prior to their combination. The final results of each combination are quite dependent on this classification. As this is an empirical classification, an important problem concerns the identification of values associated with transition zones. In the maximum entropy method is necessary to use a set of points representing the *Barreiras* Formation and the

model solution is much more dependent on the quality and distribution of these points than the amount. In this method, the values of each variable are automatically obtained at each sample point. As there is no possibility of working with absence data in this model, it is necessary to have a set of samples that are representative of the feature that you want to model, with no bias (for example, areas with higher number of points than others). Areas with bias have stronger effect in models that work only with presence data than models that work with presence and absence data.

The first method (combinatorial OR) has a limitation in relation to the number of possible variables being combined at one time, on the order of twenty. Moreover, the complexity in the interpretation of results is directly proportional to the number of variables used. In this study it is not a problem because the number of morphometric variables needed to represent *Barreiras* Formation should not exceed this limit. The method of maximum entropy, besides having no limit on the number of variables, provides various graphics output that allows a more userfriendly evaluation of the results.

The method of combinatorial OR can be applied in any other region outside the domain of the study area. Small adjustments in the class intervals of morphometric variables may be needed in case of minor variations, for example in the relief of *Barreiras* Formation in other regions. In contrast, the maximum entropy assumes the use of new sampling points within the new area. This requirement brings important limitations regarding the cost, time and, in case of a widely distributed unit such as *Barreiras* Formation, it becomes quite complex to ensure a good distribution of points.

Finally, the result obtained by using the combinatorial OR method corresponds to a map with the boundaries of the representation of the *Barreiras* Formation. In the second method (maximum entropy), the final result is a distribution map of *Barreiras* Formation, being a representation of the probability percentage of occurrence of the feature under study.

Table 13: Main characteristics of the combinatorial OR and maximum entropy methods.

COMBINATORIAL OR	MAXIMUM ENTROPY
Relatively simple method, using the logical OR operator.	More complex mathematical formulation to be understood for users with little knowledge in statistics.
No need for a set of sample points representing the <i>Barreiras</i> Formation.	Need for a set of sample points showing the occurrence of the <i>Barreiras</i> Formation.
Requires previous morphometric variables classification according to intervals that represent <i>Barreiras</i> Formation.	The geomorphometric variables do not require previous classification.
The results of the variables combination are strongly dependent on previous classification.	The final result is more dependent on the quality and distribution of sampling points than the proper quantity thereof.
Shows limit on the number of variables that can be used in each combination (maximum 20).	There is no limit on the number of variables to be used for model execution.
The complexity in evaluating the results is proportional to the number of variables used in each combination.	The model provides various output graphics for the interpretation of results.
Can be applied in any area outside the boundaries of the survey area, assuming that the <i>Barreiras</i> Formation shows similar characteristics.	Need new sampling points located within the new area to be investigated.
The final result is a map with the boundaries of <i>Barreiras</i> Formation.	The final result is a map of the distribution of <i>Barreiras</i> Formation.

6.4 Results of the output maps validation

All output maps were evaluated in comparison to the map produced by Chrismann (2014) using spatial correlation analysis. The percentages of

correlated and uncorrelated areas between all the output maps and the reference map are shown in Figures 51, 52 and 53.

The three output maps generated with combinatorial OR upon DSM surface smoothed 10 times with windows of 15 by 15 pixels, using the different selected combinations of morphometric variables, present percentages of correlated areas (*Barreiras* and not *Barreiras*) equal to 83%, 78% and 82% (Figure 51). The uncorrelated areas (False Negative and False Positive) correspond respectively to 17%, 22% and 18%.

The next three output maps that were validated (Figure 52) show the same combination of variables (height, slope, curvature and TRI), performed using three different smoothed surfaces. The results show no variation in the percentage of correlated (81%) and not correlated (19%) areas between the output maps and the reference map.

The last results were obtained using the output maps generated with maximum entropy method (Figure 53). They show percentages of correlated areas below 81% in all maps (71%, 80% and 78%). The not correlated areas show percentages of 29%, 20% and 22%. Although the latter map has displayed the lowest percentage of false positive (3%), it also has the highest percentage of false negative (19%) and lower percentage of true positive (9%). This result is probably due to the selected sample points (151) despite being better distributed, it was not sufficient to represent main aspects of *Barreiras* Formation.

Comparing all results together, the first map generated with the combinatorial OR method upon the DSM surface smoothed 10 times and window size of 15 by 15 pixels showed the best result (Figure 51 a). The correlated areas were 83% and the total of not correlated areas was 17%. In the not correlated areas, the false negative of 9% was concentrated exactly upon the *Barreiras* Formation deposits which were uplift due to tectonic, which is a very consistent result. Furthermore, the percentage of 8% of false positive was lesser when compared to other results.

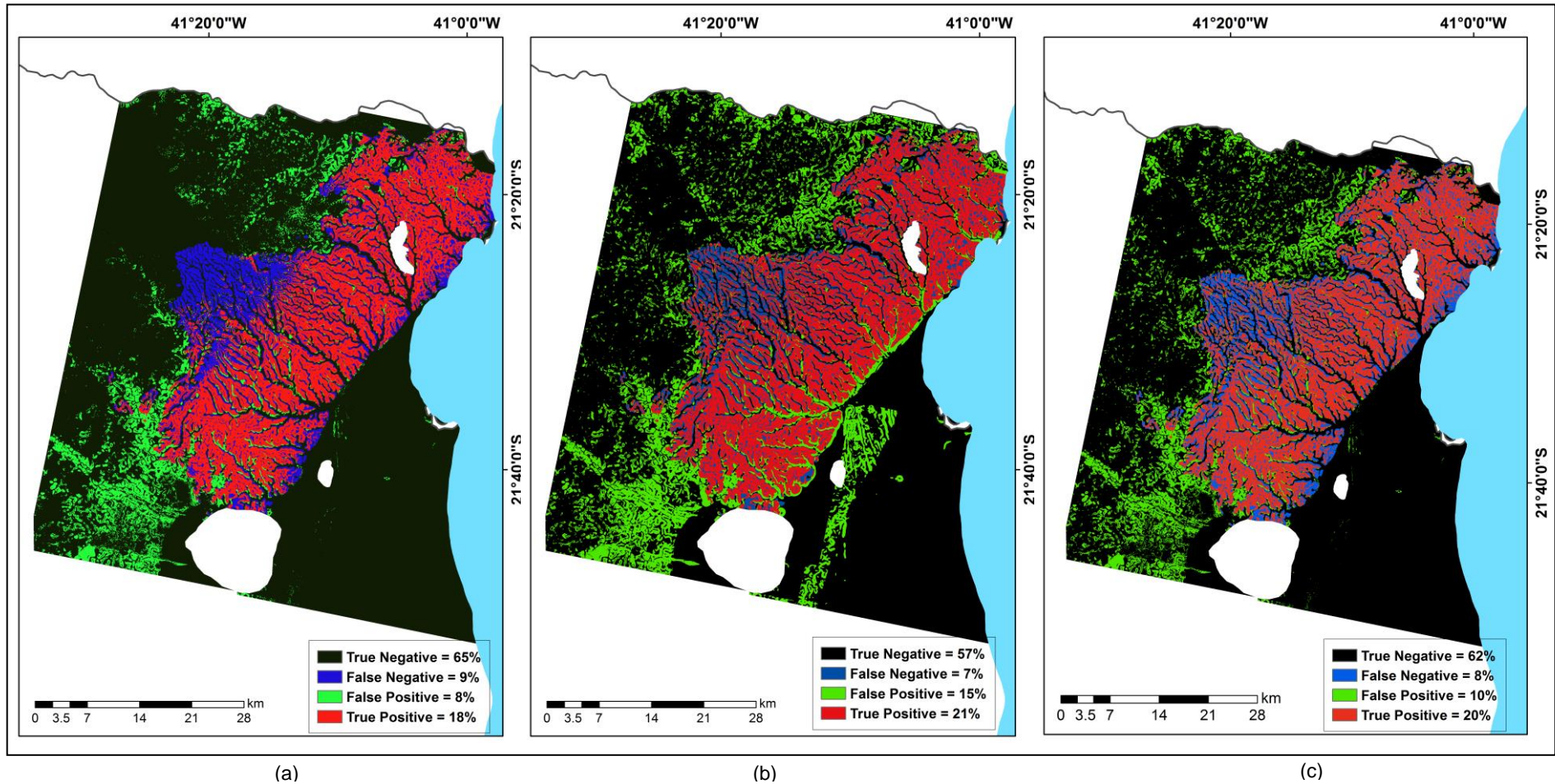


Figure 51: Validation through spatial correlation analysis of the maps generated with combinatorial OR method upon DSM surface smoothed 10 times with windows 15 by 15 pixels, using the morphometric variables: (a) height, slope, curvature, TRI, MRVBF and MRRTF; (b) slope, curvature, TRI, MRVBF and MRRTF; and (c) height (*Barreiras* and basement interval classes), slope, curvature, TRI, MRVBF and MRRTF.

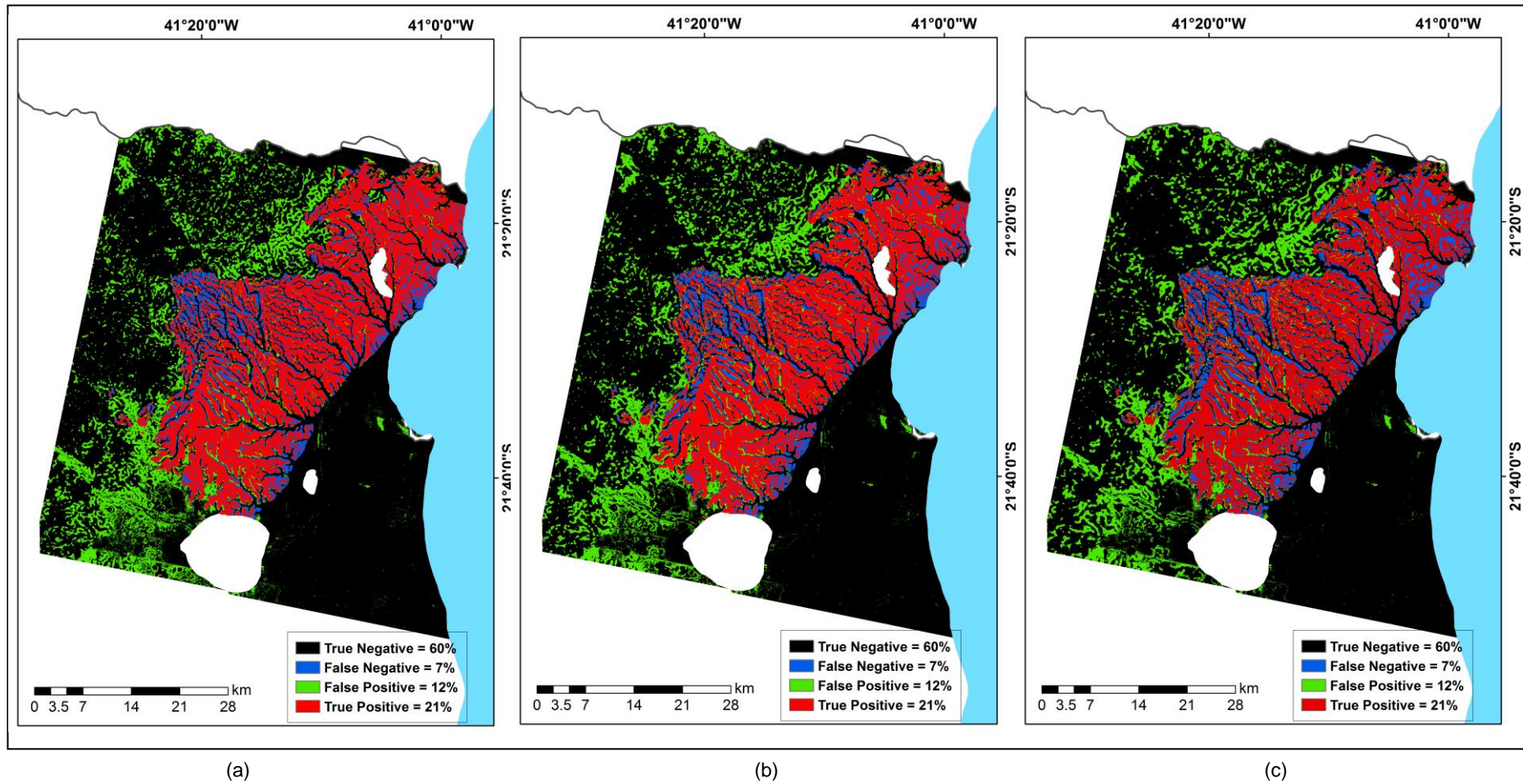


Figure 52: Validation through spatial correlation analysis of the maps generated with combinatorial OR method using the morphometric variables: height (*Barreiras* and basement interval classes), slope, curvature and TRI. (a) DSM surface smoothed 10 times with windows of 15 by 15 pixels; (b) DSM surface smoothed 14 times with windows of 15 by 15 pixels; and (c) DSM surface smoothed 10 times with windows of 21 by 21 pixels.

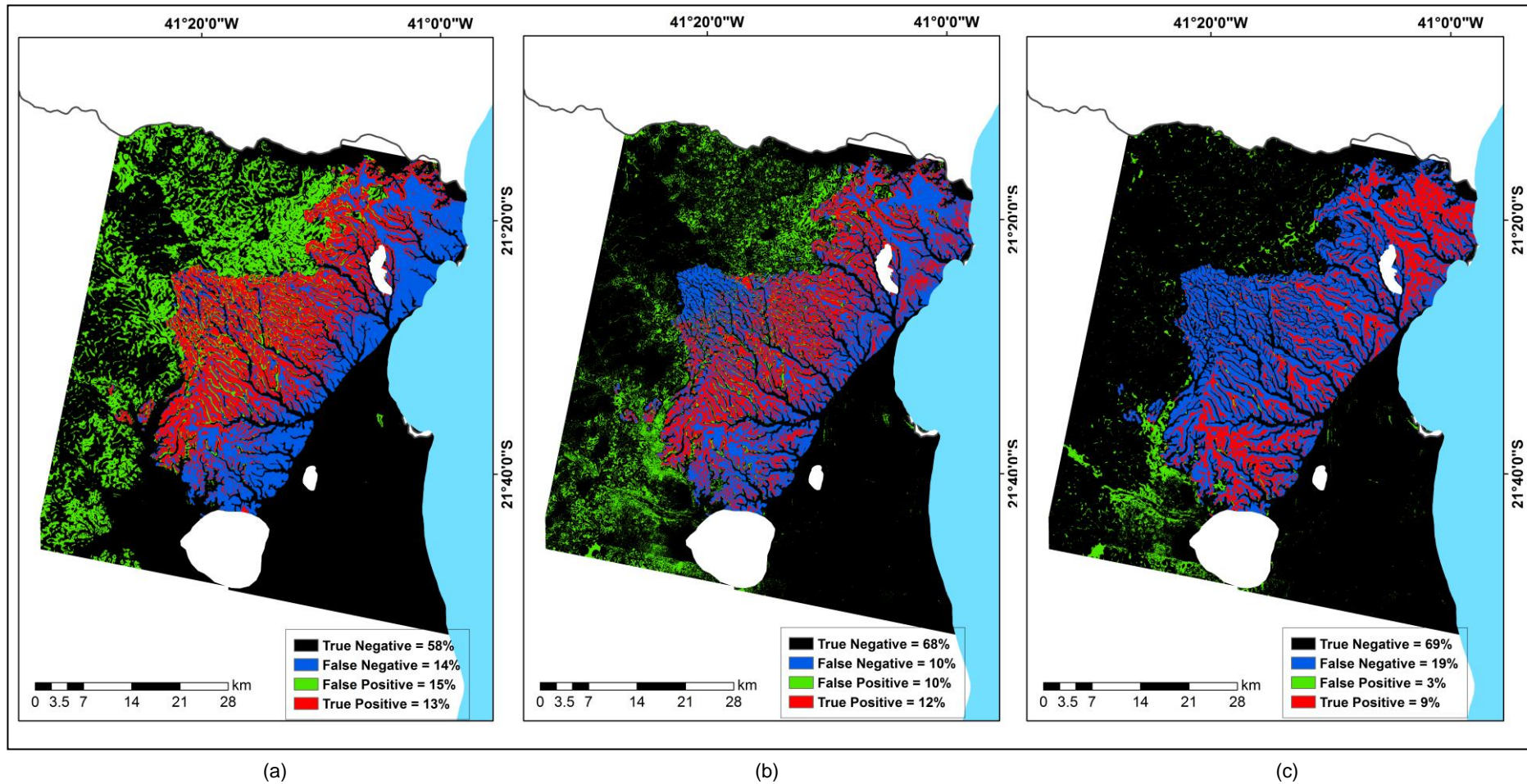


Figure 53: Validation through spatial correlation analysis of the maps generated with maximum entropy method using the morphometric variables: height (*Barreiras* and basement interval classes), slope, curvature and TRI for the DSM surface smoothed 14 times with windows of 15 by 15 pixels. (a) Samples collected in field surveys; (b) 46 sample points collected from desktop; and (c) 151 sample points collected from desktop.

6.5 Results of map visualization

The comparison between the best result obtained in the validation of all maps that were generated in the present study (the map generated with the combinatorial OR method upon the DSM surface smoothed 10 times and window size of 15 by 15 pixels – Figure 51a) and the reference map (Chrismann, 2014) shows many more similarities than differences. An important similarity concerns especially the layout of the valleys that dissect the *Barreiras* Formation deposits (Figure 54). The biggest difference is exactly in the A2 area, where the morphological characteristics of the *Barreiras* Formation deposits could not be verified due to neotectonic deformation. Other difference is noted in A1 area near the contact with the basement, where the areas identified by the output map generated in this research are more extensive than those identified by Chrismann (2014) using visual interpretation. In this region (A1), isolated occurrences of these deposits were identified.

In order to evaluate the gains obtained with the use of high resolution imagery, a comparison between the best output map generated in this research and the map of Ribeiro (2010), obtained from the SRTM DEMs with 90m spatial resolution, was carried out (Figure 55). In the map generated by this study, it is possible to identify the *Barreiras* Formation dissected by a greater amount of deep valleys, which is more realistic and was expected due to the resolution (10m) of the DSMs used. Once more, the biggest difference is in the A2 area and it can be related to neotectonic deformation that changes the typical morphological characteristics of *Barreiras* Formation. Another important difference lies in the A1 area, where the areas identified as *Barreiras* Formation by Ribeiro (2010) are more extensive than the areas identified in the present study and by Chrismann (2014). In this area, isolated occurrences were identified with the method used in the present study.

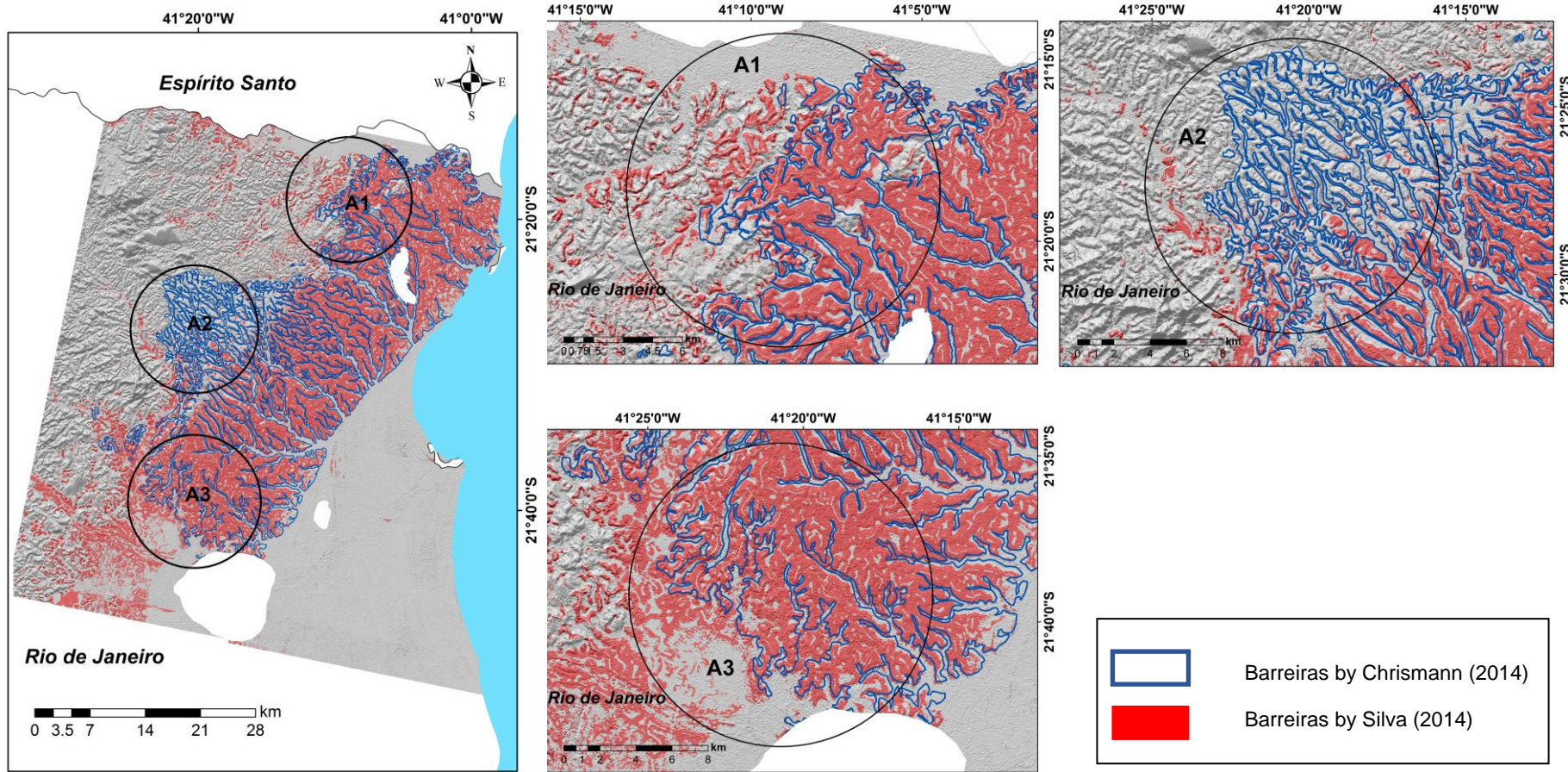


Figure 54: Comparison between Silva (2014) and Chrismann (2014) maps and details of discrepancy areas (A1, A2, A3).

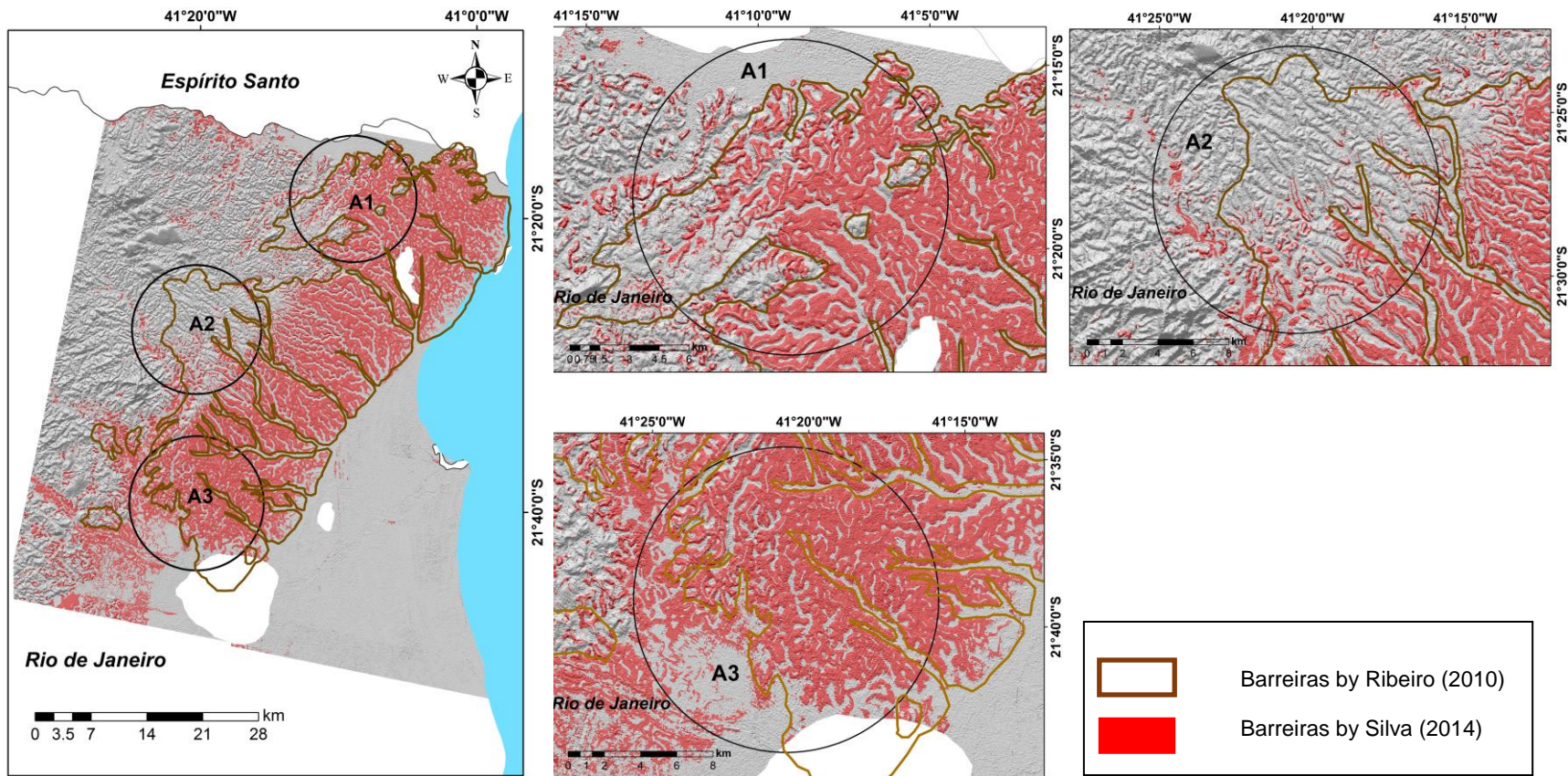


Figure 55: Comparison between Silva (2014) and Ribeiro (2010) maps and details of discrepancy areas (A1, A2, A3).

7 CONCLUSIONS

The main objective of this study was achieved, being successfully tested a process of semi-automatic identification and detailed mapping of the *Barreiras* Formation deposits based on morphometric analysis of digital surface models (DSMs) from high resolution optical satellite imagery.

As *Barreiras* Formation has a wide spatial distribution on Brazilian coastal region, the possibility of application of this methodology in other regions represents a gain in terms of time compared to mapping by using the traditional field survey methods in detailed scale. Furthermore, this methodology can also be applied to map other sedimentary geological units that have similar characteristics like the *Barreiras* Formation.

Regarding the identification of the *Barreiras* Formation deposits, the major challenge was, essentially, the use of images with spatial resolution of the order of 2.5m to classify a feature of wide spatial distribution. It has imposed a more regional analysis, although employing a high-detail resolution. The alternative applied to overcome this issue was employing a low-pass filter for the successive smoothing of the DSMs in order to obtain a surface with reducing the number of gray levels and attenuation of high frequencies (noise), besides the generalization of geomorphometric variable information.

The smoothing of DSMs did not cause major problems regarding the identification of the *Barreiras* Formation limits because this unit is associated with a very flat and extensive morphology. The deep and flat valleys embedded in this morphology could be very well represented in the output maps.

Although the acquisition for free of the ALOS/PRISM images has contributed to the development of this research, technological advances in Remote Sensing imply the decreasing cost of high-resolution images, representing a gain in terms of cost and benefits to further projects. The use of optical satellite imagery for areas with little vegetation cover, as was the case in this research is recommended. In areas with medium vegetation cover, the application of the same methodology using laser profiling for generating DEMs can be suggested, while P-band radar are recommended for areas with dense vegetation.

The method of morphometric variables combination using combinatorial OR appears to be more appropriate for the main purpose of this research because it can be extrapolated to other regions with only small adjustments in interval values of variables. The maximum entropy method proved to be valid to assist the survey field planning aiming for the identification of *Barreiras* Formation deposits, directing visits to sites whose results had higher percentages of probability of the occurrence of such geologic unit.

Regarding particular issues already highlighted in the proposition of this study (see section 1.4 The Research Methods), now, at this stage of this research study, the following answers can be provided.

1. What is the effective quality of DSMs automatically generated from high spatial resolution images by using the model of rational functions in terms of its cartographic precision to achieve the Brazilian Cartographic Standards and for being used in the geomorphological analysis?

The usage of the rational functions model with the RPCs coefficients supplied with the ALOS-PRISM images made possible the generation of DSMs and orthoimages with a reduced number of control points and achieved a quality compatible with the Brazilian Cartographic Standards for vertical and horizontal mapping in a scale of 1: 25,000, Class A. Using the mathematical model of rational functions, fewer control points were required. There was no need for additional measuring points on the field. The quantity of pre-existing control points was sufficient for the vertical and horizontal accuracy control of the DSMs and orthoimages generated, due to their good spatial distribution in the images. This has important repercussions in terms of cost and time in developing research projects like the one conducted here. .

Moreover, the use of the rational function model enabled more quickly and accurately the generation of cartographic maps at a scale of 1: 25,000 for the northern region of the State of Rio de Janeiro, in accordance with the Brazilian Cartographic Standards. This represents a gain in terms of systematic mapping in detail scale, which is still poorly available in Brazil.

2. What processes need to be made upon the DSMs to reach the stage of the generation of geomorphometric variables?

As mentioned beforehand, the presence of noise in the DSMs as well as the excess of information generated in the step of morphometric variables derivation due to the high resolution images made it necessary to smooth successively the DSMs. The filters used in this step of work allowed not only the noise attenuation but also the necessary generalization of the morphometric variables information for the purpose of a regional analysis of the feature investigated. The results obtained indicate the adequacy of the simple averaging technique (FOCALMEAN) of the ArcGIS FocalStatistics tool.

3. What geomorphometric variables are most appropriate to represent the morphology of the *Barreiras* Formation?

The variables height, slope and curvature and the terrain roughness index, multiresolution index of valley bottom flatness and multiresolution index of ridges top flatness showed the best results for the identification of *Barreiras* Formation regarding their morphological characterization.

The height values associated with *Barreiras* Formation could be easily checked as intermediaries between the basement and the Quaternary deposits. In the areas where the *Barreiras* Formation did not present its common morphological characteristics, due to neotectonic deformation, the method could not identify the *Barreiras* Formation properly.

The flat tops that are a morphological characteristic of the *Barreiras* Formation were evident from the analysis of the slope and curvature values that were very close to 0. Similarly, the low surface roughness of the morphology associated with the *Barreiras* Formation can be contrasted with a higher roughness of the basement domain.

The Multiresolution Index of Valley Bottom Flatness (MRVBF) and the Multiresolution Index of Ridges Top Flatness (MRRTF) were less efficient in the distinction of *Barreiras* Formation in the transition area to the basement

domain. This fact is due to the narrower valleys as well as the more hilly tops of these deposits in the mentioned region.

The combination of those variables together has indicated the possibility to distinguish the *Barreiras* Formation from other regional geological units in other locations since the deposits present their usual morphological characteristics.

Other morphological aspects could also help to distinguish between *Barreiras* Formation deposits and basement domain, such as drainage orientation, drainage density, drainage patterns and basin elongation ratio. These aspects were not included in the analysis due to several limitations of the functions used to generate the respective hydrological variables. These limitations of the functions to represent the reality prevented to show aspects of the *Barreiras* Formation visually so perceptible as surface gently sloping to the sea, drainage network with lower density than the basement and the subparallel drainage pattern.

4. What are the gains achieved with the use of high spatial resolution images, compared to the level of detail of the topic to be mapped, if compared to available maps in regional scale?

As was to be expected, the use of high resolution imagery showed substantial gains in identifying the *Barreiras* Formation, when compared to available maps in regional scale. This can be clearly seen in the visual comparison of the map generated in this study with that one produced by Ribeiro (2010) in terms of the most detailed outline contour of its limits and the identification of smaller dissected valleys. The differentiation of these deposits and the basement in areas where the latter one appears more weathered with morphological characteristics similar to those of the *Barreiras* Formation deposits also represented a gain for the methodology proposed. In consequence, the field surveys for the identification of *Barreiras* Formation can be concentrated in areas where this unit lies modified of their usual morphology, resulting in savings in terms of required time and expenses on field surveys.

For future studies within the same approach the use of multispectral images and classification procedures is recommended in an attempt to improve the identification of the *Barreiras* Formation limits, especially in transition areas with the basement.

REFERENCES

- ALBRECHT, J. (2007): **Key Concepts & Techniques in GIS**. London. SAGE Publications Ltd.. 103 pp.
- ALMEIDA, F.F.M.; AMARAL, G.; CORDANI, U.G.; KAWASHITA, K. (1973): **The Precambrian evolution of the South American cratonic margin south of the Amazon river**. In: NAIRN, A.E.M.; STEHLI, F.G. (eds.) **The Ocean Basins and Margins**, New York. Plenum. 411- 446.
- ALMEIDA, F.F.M.; HASUI, Y.; NEVES, B.; FUCK, R.A. (1981): **Brazilian structural provinces: an Introduction**. **Earth Science Review**, 17:1-29.
- ANDRIOTTI, J.L.S. (2003): **Fundamentos de estatística e geoestatística**. São Leopoldo. Editora Unisinos. 165 pp.
- ARONOFF, S. (1989): **Geographic Information System: a management perspective**. Ottawa. WDL Publications. 294 pp.
- BANG, K.I.; JEONG, S.; KIM, K. (2003): **Modification of sensor model parameters with a few GCPs**. In: ASPRS Annual Conference, 3-9 May, Anchorage, Alaska. 6.
- BEZERRA, F.H.R.; MELLO, C.L.; SUGUIO, K. A (2006): **Formação Barreiras: Recentes Avanços e Antigas Questões**. Geologia USP (Série Científica), São Paulo, V.6, n. 2. 1-4.
- BIZZI, L.A.; SCHOBENHAUS, C.; VIDOTTI, R.M.; GONÇALVES, J.H. (eds.). (2003): **Geologia, Tectônica e Recursos Minerais do Brasil: Texto, Mapas e SIG**. Brasília. CPRM. 4 CD-ROM.
- BRASIL (1984): **Decreto nº 89.817 de 20 de junho de 1984. Instruções Reguladoras das Normas Técnicas da Cartografia Nacional** [online]. Diário Oficial da União. Brasília, in <http://www.concar.ibge.gov.br/indexf7a0.html?q=node/41>. Access on 10 Nov. 2013.
- BRÊDA, T.C. (2012) : **Análise Multiescalar da Formação Barreiras na Área Emersa da Bacia de Campos, entre Búzios e Campos dos Goytacazes** (RJ). Dissertation (Master in Geology) – Instituto de Geociências, Universidade Federal do Rio de Janeiro. 117f.

- BURROUGH, P.A.; MCDONNELL, R.A. (1998): **Principles of Geographical Information Systems**. 2. ed. Oxford: Oxford University Press. 333 pp.
- CARVALHO, A.M; TOTTI, M.E.F.(orgs). (2006): **Formação histórica e econômica do Norte Fluminense**. Rio de Janeiro: Garamond, FAPERJ. 328 pp.
- CEFETES (2012): **Correlação de Imagens. Apostila de Fotogrametria**. Available at: <ftp://ftp.cefetes.br/Cursos/Geomatica/.../cap4.pdf>. Access on 28 Oct. 2012.
- CEPERJ. O (2014): **Estado do Rio de Janeiro e seu ambiente**. Available at: http://www.ceperj.rj.gov.br/ceep/info_territorios/ambiente.html. Access on 12 Jan. 2014.
- CHENG, P.; TOUTIN, T. (2001): **Orthorectification and DEM generation from high resolution satellite data**. In.: ACRS - Asian Conference on Remote Sensing, Singapore. 1203-1208.
- CHRISMANN, J. (2014): **Mapeamento da Formação Barreiras na Região Norte Fluminense, entre os Rios Paraíba do Sul e Itabapoana**. Monografia (Monograph in Geology). Universidade Federal do Rio de Janeiro, Rio de Janeiro. 49 pp.
- CHRISTOFOLETTI, A. (1980): **Geomorfologia**. 2. ed. São Paulo: Edgard Blücher, São Paulo. 188 pp.
- COELHO, L.C.T.; BRITO, J.L.N. (2007): **Fotogrametria Digital**. Rio de Janeiro: Ed UERJ. 196 pp.
- CORREIA, J.D. (2008) : **Metodologia para Mapeamento Semi-Automático de Feições Depositionais Quaternárias por Imagens Orbitais de Alta Resolução Espacial: Médio Vale do Rio Paraíba do Sul**. (PhD in Geology) – Instituto de Geociências, Universidade Federal do Rio de Janeiro, Rio de Janeiro. 665 pp.
- COSTA, E.R. (2006): **Geração automática de Modelos Digitais de Terreno a partir de Imagens de Câmaras Digitais**. (Master in Cartographic Sciences) – Faculdade de Ciências Cartográficas, Universidade Estadual de São Paulo, Presidente Prudente. 139 pp.
- CRÓSTA, A.P. (1992): **Processamento Digital de Imagens de Sensoriamento Remoto**. Campinas: IG/UNICAMP. 170 pp.

- DANTAS, M.E. (2000): **Mapa geomorfológico do Estado do Rio de Janeiro**. In: CPRM. Geomorfologia do Estado do Rio de Janeiro. Brasília: CPRM, 63. CD-ROM.
- DODGE, M.; McDERBY, M.; TURNER, M. (eds). (2008): **Geographic Visualization: Concepts, Tools and Applications**. Chichester, England: John Wiley & Sons, Ltd.. 319 pp.
- ELITH, J.; PHILLIPS, S.J.; HASTIE, T.; DUDIK, M.; CHEE, Y.E.; YATES, C.J. (2011): **A Statistical explanation of MaxEnt for ecologists**. Blackwell Publishing Ltd, 43–57. (Diversity and Distributions).
- EL-SHEIMY, N.; VALEO, C.; HABIB, A. (2005): **Digital terrain modelling – acquisition, manipulation and applications**. Boston/London: Artech House, 257 pp.
- EARTH OBSERVATION RESEARCH CENTER (EORC); JAPAN AEROSPACE EXPLORATION AGENCY (JAXA) (2007): **PRISM**. In: About ALOS. 2007. Available at: <<http://www.eorc.jaxa.jp/ALOS/en/about/prism.htm>>. Access on 13 Oct. 2012.
- ESRI. (2013a): **ArcGIS Help 10.1**. Available at: <http://resources.arcgis.com/en/help/main/10.1/index.html#//018p00000008000000>. Access on: 05 Jul. 2013.
- ESRI. (2013b): **Understanding-curvature-rasters**. Available at: <http://blogs.esri.com/esri/arcgis/2010/10/27/understanding-curvature-rasters/>. Access on: 05 Jul. 2013.
- ESRI. (2013c): Spatial Analyst: **Advanced GIS Spatial Analysis Using Raster and Vector Data**. Available at: http://www.esri.com/library/whitepapers/pdfs/arcgis_spatial_analyst.pdf. Access on: 05 Jul. 2013.
- FELGUEIRAS, C. A.; CÂMARA, G. (1999): **Modelagem numérica do terreno**. In: CÂMARA, G.; DAVIS, C.; MONTEIRO, A. M. V. (orgs.). Introdução à ciência da geoinformação. São José dos Campos: INPE, Chapter 7. Available at: <<http://www.dpi.inpe.br/livros.php>>. Access on: 05 Sept. 2013.
- FELICÍSIMO, A. M. (1994): **Modelos digitais del terreno: introducción aplicaciones en las ciencias ambientales**. Oviedo: Universidad de Oviedo,

1994. Available at: <<http://www.etsimo.uniovi.es/~feli>>. Access on: 15 Sept. 2013.

FERREIRA, V.R.; SOUZA, P.M.; PONCIANO, N.J.; CARVALHO, A.J.C. (2003): **A fruticultura como alternativa para a produção familiar no âmbito do PRONAF nos municípios de Campos dos Goytacazes e São Francisco do Itabapoana**. Revista Brasileira Fruticultura, Rio de Janeiro. 436–439.

GALLANT, J.C.; WILSON, J.P. (2000): **Primary topographic attributes**. In: Terrain Analysis: Principles and Applications. New York: Chapter 3, 51-85.

GALLANT, J.C.; DOWLING, T.I. (2003): **A multiresolution index of valley bottom flatness for mapping depositional areas**. **Water Resources Research**. Available at: <http://onlinelibrary.wiley.com/doi/10.1029/2002WR001426/pdf>. Access on: 17 Feb. 2014.

GALLANT J.; DOWLING, T.; AUSTIN, J. (2012): **Multi-resolution Valley Bottom Flatness (MRVBF, 3" resolution)**. CSIRO. Data Collection. 10.4225/08/512EF27AC3888, 2012. V. 2. Available at: <https://data.csiro.au/dap/landingpage?pid=csiro:5681>. Access on: 17 Feb. 2014.

GDTA (1992): **Physical bases in remote sensing**: V. 1.2. Toulouse.127 pp.

GOMES, L.M.; REIS, R.B.; CRUZ, C.B.M. (2009): **Análise da cobertura florestal da Mata Atlântica por município no Estado do Rio de Janeiro**. In: XIV Brazilian Symposium for Remote Sensing (2009), Natal, São José dos Campos: INPE. 3849-3857.

GRUEN, A.; KOCAMAN, S.; WOLFF, K. (2007): **Geometric Validation of ALOS/PRISM IMAGES**. ETH, Conference Paper.

HEILBRON, M.; PEDROSA-SOARES, A.C.; CAMPOS NETO, M.C.; SILVA, L.C.; TROUW, R.A.J.; JANASI, V.A. (2004): **Província Mantiqueira**. In: MANTESSO-NETO, V.; BARTORELLI, A.; C. DAL RÉ CARNEIRO, C.; BRITO NEVES, BB (eds.) (2004): O Desvendar de um Continente: a Moderna Geologia da América do Sul e o Legado da Obra de Fernando Flávio Marques de Almeida. São Paulo: Editora Beca. Chapter. XIII, 203-234.

HENGL, T.; EVANS, I.S. (2009): **Mathematical and Digital Models of Land Surface**. In: HENGL, T.; REUTER, H.I. (eds.) (2009): *Geomorphometry Concepts, Software, Applications*. Developments in Soil Science, 1. ed., Amsterdam: Elsevier, V. 33, Chapter 2, 31- 63.

HENGL, T.; MacMILLAN, R.A. (2009): **Geomorphometry – A Key to Landscape Mapping and Modelling**. In: HENGL, T.; REUTER, H.I. (eds.) (2009): *Geomorphometry Concepts, Software, Applications*. Developments in Soil Science, 1. ed. Amsterdam: Elsevier, V. 33, Chapter 19, 433 - 460.

IBGE (2009): **Manual Técnico de Geomorfologia**. Rio de Janeiro: IBGE/Diretoria de Geociências, Departamento de Recursos Naturais e Estudos Ambientais, 2. ed., 175 pp.

IBGE. (2014 a): **Mapeamento sistemático em 1:25.000. 2014a**. Available at: ftp://geofp.ibge.gov.br/mapeamento_sistematico/base_vetorial_continua_escala_25mil/. Access on: 7 Jan. 2014.

IBGE. (2014b): **Mapeamento sistemático em 1:50.000**. Available at: ftp://geofp.ibge.gov.br/mapeamento_sistematico/. Access on: 7 Jan. 2014.

IBGE. (2014c): **Glossário cartográfico**. Available at: http://www.ibge.gov.br/home/geociencias/cartografia/glossario/glossario_cartografico.shtm >. Access on: 10 Jan. 2014.

IBGE. (2014 d): Figura 3.htm. Available at: <http://www.ibge.gov.br/home/geociencias/geodesia/fig3.htm>>. Access on: 18 Feb. 2014.

IWATA, T. (2003): **Precision geolocation determination and pointing management for the advanced land observing satellite (ALOS)**. In: *Geoscience and Remote Sensing Symposium (2003): IGARSS'03*. 2003 IEEE International, V. 3, 1845- 1848. Available at: <http://ieeexplore.ieee.org/stamp/stamp.jsp?tp=&arnumber=1294269&isnumber=28603> >. Access on 05 Sept. 2012

JACOBSEN, K. (2005): **Photogrammetry and Geoinformation Trends for Large Scale Mapping: Map Middle East**. Dubai. Available at: http://www.ipi.uni-hannover.de/uploads/tx_tkpublikationen/jac_MapME05.pdf. Access on: 14 Jan. 2014.

JAPAN AEROSPACE EXPLORATION AGENCY (JAXA) (2004): **ALOS Hardware**. In: ALOS (2004). Available at: <http://alos.jaxa.jp/2/alos_hard-e.html>. Access on: 05 Sept. 2012.

JAPAN AEROSPACE EXPLORATION AGENCY (JAXA) (2007): **Advanced land observing satellite “DAICHI” (ALOS)**. In: Missions-Satellites and Spacecraft (2007). Available at: <http://www.jaxa.jp/projects/sat/alos/index_e.html>. Access on: 05 Sept. 2012.

JENSEN, J.R. (2011): **Sensoriamento Remoto do Ambiente: Uma Perspectiva em Recursos Terrestres**. 2. ed. São José dos Campos: Parêntese. 598 pp.

LEICA PHOTOGRAMMETRY SUITE (LPS) (2008): **Automatic Terrain Extraction**, User's Guide. Leica Geosystems Geospatial Imaging (2008). 154 pp.

LILLESAND, T.M. & KIEFER, R.W. (1994): **Remote Sensing and Image Interpretation**. New York: John Wiley & Sons, Inc.. 750 pp.

LI, Z.; ZHU, Q.; GOLD, C. (2005): **Digital terrain modeling: principles and methodology**. Boca Raton, Florida: CRC Press. 318 pp.

MACHADO-SILVA, A. J. F. (1988): **Modelos de correção geométrica para imagens HRVSPOT**. (Master in Applied Computation) – Instituto Nacional de Pesquisas Espaciais, São José dos Campos. 223 pp.

MARTIN, L.; SUGUIO, K.; DOMINGUEZ, J. M.L.; FLEXOR, J. (1997): **Geologia do Quaternário costeiro do litoral norte do Rio de Janeiro e do Espírito Santo**. Belo Horizonte: CPRM. 112 pp.

MAUNE, D.F.; KOPP, S.M.; CRAWFORD, C.A.; ZERVAS, C.E. (2001a): **Introduction**. In: MAUNE, D. F. (ed.). Digital elevation model technologies and applications: the DEM users manual. Bethesda, Maryland. The American Society for Photogrammetry and Remote Sensing (ASPRS), Chapter 1, 1-31.

MAUNE, D. F.; MAITRA, J. B.; MCKAY, E. J. (2001b): **Accuracy standards**. In: MAUNE, D. F. (ed.). Digital elevation model technologies and applications: the DEM users manual. Bethesda, Maryland: The American Society for Photogrammetry and Remote Sensing (ASPRS), Chapter 3, 61-82.

- MERCHANT, D. C. (1982): **Spatial accuracy standards for large scale line maps**. In: Technical Congress on Surveying and Mapping (1982): Proceedings V. 1, 222-231.
- MIKHAIL, E.M.; BETHEL, J.S.; McGLONE, J.C. (2001): **Introduction to Modern Photogrammetry**. New York: Editorial John Wiley & Sons. 496 pp.
- MITASOVA, H.; HOFIERKA, J. (1993): **Interpolation by regularized spline with tension**. II. Application to terrain modeling and surface geometry analysis. *Mathematical Geology*, V. 25, n. 6. Available at: <http://skagit.meas.ncsu.edu/~helena/gmslab/papers/MG-II-93.pdf>. Access on: 02 Dez. 2013.
- MONICO, J.F.G.; DAL PÓZ, A.P.; GALO, M.; SANTOS, M.C.; OLIVEIRA, L.C. (2009): **Acurácia e Precisão: revendo os conceitos de forma acurada**. *Boletim de Ciências Geodésicas, Sec. Comunicações, Curitiba*, V. 15, n. 3, 469-483.
- MOORE, I.D.; GEISSLER, P.E.; NIELSEN, G.A; PETERSON, G.A. (1993): **Soil attribute prediction using terrain analysis**. *Soil Science Society of America Journal*, V. 57, 443-452.
- MORAIS, R. M. O. (2001): **Estudo Faciológico da Formação Barreiras na Região entre Maricá e Barra de Itabapoana, Estado do Rio de Janeiro**. (Master in Geology) – Instituto de Geociências, Universidade Federal do Rio de Janeiro. 132 pp.
- MORAIS, R.M.O. (2007): **Sistemas Fluviais Terciários na Área Emersa da Bacia do Espírito Santo (Formações Rio Doce e Barreiras)**. (PhD in Geology) – Instituto de Geociências, Universidade Federal do Rio de Janeiro. 139 pp.
- MORAIS, R.M.O., MELLO, C.L., COSTA, F.O., SANTOS; P.F. (2006): **Fácies Sedimentares e Ambientes Depositionais Associados aos Depósitos da Formação Barreiras no Estado do Rio de Janeiro**. *Geologia USP (Série Científica)*, São Paulo, V.6, n. 2. 19-30.
- NIMER, E. (1972): **Climatologia da região sudeste do Brasil: introdução à climatologia dinâmica, subsídios à geografia regional do Brasil**. *Revista Brasileira de Geografia*, Rio de Janeiro, V. 34. 3-48.

- NIMER, E. (1979): Um **modelo metodológico de classificação de climas**. Revista Brasileira de Geografia, Rio de Janeiro, V.41, n. 4. 59-89.
- NUNES, F.C.; SILVA, E.F.; VILAS BOAS, G.S. (2011): **Grupo Barreiras: Características, Gênese e Evidências de Neotectonismo**. Boletim de Pesquisa e Desenvolvimento. EMBRAPA. 194 pp.
- OLIVEIRA, L.F. (2011): **Análise de Modelos Digitais de Superfície Gerados A Partir de Imagens de Sensor PRISM/ALOS**. (Master in Civil Engineering), Faculdade de Engenharia Civil, Universidade Federal de Viçosa. 163 pp.
- PAPARODITIS, N.; POLIDORI, L. (2002): **Overview of digital surface models**. In: KASSER, M.; EGELS, Y. (eds) (2002): Digital Photogrammetry. London/New York: Taylor & Francis, 2002, Chapter 3. 160-164.
- PARANHOS, P. (2000): **Artigo modificado de Tese de Dissertação: São João da Barra, apogeu e crise no porto do açúcar do norte fluminense**. Available at: <http://www.historica.arquivoestado.sp.gov.br/materias/anteriores/edicao08/materia02/texto02.pdf>. Access on: 5 Jan. 2014.
- PCI GEOMATICS (2009a): **Geomatica OrthoEngine User Guide – Version 10.3**. Ontario, Canada: PCI Geomatics Enterprises.
- PCI GEOMATICS (2009b): **Focus User Guide - Version 10.3**. Ontario, Canada: PCI Geomatics Enterprises.
- PHILLIPS, S.J.; DUDIK, M.; SCHAPIRE, R.E. (2004): **A Maximum Entropy Approach to Species Distribution Modelling, Proceedings of the Twenty-First International Conference on Machine Learning**. 655-662.
- PHILLIPS, S.J.; ANDERSON, R. P., SCHAPIRE, R.E. (2006): **Maximum entropy modeling of species geographic distributions**. *Ecological Modelling*, 190, 231-259.
- PHILLIPS, S.J. & DUDIK, M. (2008): **Modelling of species distributions with Maxent: New extensions and a comprehensive evaluation**. *Ecography*, 31,161-175.
- PIKE, R.J.; EVANS, I.S.; HENGL, T. (2009): **Geomorphometry: A Brief Guide**. In: HENGL, T. & REUTER, H.I. (eds) (2009): Geomorphometry

Concepts, Software, Applications. Developments in Soil Science, 1. ed. Amsterdam: Elsevier, V. 33, Chapter 1. 3-30.

RAMALHO, R. S. (2005): **Diagnóstico do Meio Físico como Contribuição ao Planejamento do Uso da Terra do Município de Campos dos Goytacazes.** Thesis (PhD in Ecology and Natural Resources) - Universidade Estadual do Norte Fluminense (UENF), Campos dos Goytacazes. 108 pp.

RAMIREZ, J. R; ALI, T. (2003): **Progress in metrics development to measure positional accuracy of spatial data.** International Cartographic Conference (ICC), Durban, South Africa, 1763-1772. Available at: http://icaci.org/documents/ICC_proceedings/ICC2003/Papers/221.pdf. Access on 31 Jan. 2014.

RANA, S. (2006): **Use of plan curvature variations for the identification of ridges and channels on DEM.** In: INTERNATIONAL SYMPOSIUM ON SPATIAL DATA HANDLING, 12-14, July 2006, Vienna, Austria. Available at: <http://eprints.ucl.ac.uk/2105/>. Access on: 25 Nov. 2013.

REUTER, H.I.; HENGL, T.; GESSLER, P.; SOILLE, P. (2009): **Preparation of DEMs for Geomorphometric Analysis.** In: Hengl, T. & Reuter, H.I. (eds) Geomorphometry Concepts, Software, Applications. Developments in Soil Science, ELSEVIER, 2009. V. 33, chapter 4, 87- 120.

RIBEIRO, C. S. (2010) : **Influência da Tectônica Pós-Deposicional na Distribuição da Formação Barreiras entre o Rio Paraíba do Sul (RJ) e o Rio Doce (ES).** (Master in Geology) – Instituto de Geociências, Universidade Federal do Rio de Janeiro. 165 pp.

RIBEIRO, C.S.; MELLO, C.L. (2011) : **Deformação Neotectônica dos Tabuleiros Costeiros da Formação Barreiras entre os Rios Paraíba do Sul (RJ) e Doce (ES) na Região Sudeste do Brasil.** In: XIII Congresso da Associação Brasileira de Estudos do Quaternário. 9 -14 Oct. 2011, Búzios, Rio de Janeiro. Available at : http://www.abequa.org.br/trabalhos/Carolina_RIBEIRO_ABEQUA2011_Neotectonica.pdf. Access on: 15 Nov. 2013.

RICHARD, J.A., JIA, X. (1999): **Remote Sensing Digital Image Analysis: an Introduction.** 3. ed. Berlin, Heidelberg, New York, Barcelona, Hong Kong, London, Milan, Paris, Singapore, Tokyo: Springer. 363 pp.

RILEY, S.J., DeGLORIA, S.D.; ELLIOT, R. A (1999): **Terrain ruggedness index that quantifies topographic heterogeneity**, Intermountain Journal of Sciences, vol. 5, No. 1-4.

RIZZINI, C.T. (1979): **Tratado de Fitogeografia do Brasil. Aspectos ecológicos**. São Paulo: Hucitec/Edusp, V. 2. 327 pp.

ROSSETTI, D.F. (2006) : **Evolução Sedimentar Miocênica nos Estados do Pará e Maranhão. Geologia USP (Série Científica)**, São Paulo, V.6, n.2. 7-18.

SAADI, A.; BEZERRA, F.H.R.; COSTA, R.D.; IGREJA, H.L.S.; FRANZINELLI, E. (2005) : **Neotectônica da plataforma brasileira**. In: SOUZA, C.R.G.; SUGUIO, K.; OLIVEIRA, A.M.S.; OLIVEIRA, P.E. (eds) Quaternário do Brasil. Ribeirão Preto: Holos, Cap. 10. 211-234.

SABINS, F.F. (2000): **Remote Sensing – Principles and Interpretation**. 3. ed. USA: Waveland Press, Inc.. 494 pp.

SHARY, P.A.; SHARAYA, L.S.; MITUSOV, A.V. (2002): **Fundamental quantitative methods of land surface analysis**. Geoderma, n. 107, 1-32.

SILVA, L.C.; CUNHA, H.C.S. (2001): **Geologia do estado do Rio de Janeiro**. Brasília: CPRM, CD-ROM.

SMITH, M.J. (2010): **Statistical analysis: a comprehensive handbook of statistical concepts, techniques and software tools**. University College London. 46. Available at: <<http://www.statsref.com/StatsRefExtract.pdf>>. Access on 15 Jan. 2014.

SUGUIO, K.; NOGUEIRA, A.C.R. (1999): **Revisão crítica dos conhecimentos geológicos sobre a Formação Barreiras do Neógeno e o seu possível significado como testemunho de alguns eventos geológicos mundiais**. Revista Geociências, São Paulo, V. 18, n. 2. 461-479.

SUMMERFIELD, M. A. (1991): **Global geomorphology**. London: Longman Press, 537 pp.

TAKAKU, J.; TADONO, T. (2009): **RPC generations on PRISM/AVNIR-2 level 1B2 images**. In: ALOS PI Symposium. Kailua-Kona, Hawaii, USA. Available at: <http://www.asf.alaska.edu/sites/www.asf.alaska.edu/pi_symp/files/documents/presentations/Takaku_J._optcalval_RPC.pdf>. Access on : 31 Jan. 2012.

- TAO, V.; HU, Y.(2004): **RFM: An open sensor model for cross sensor mapping**. In: ASPRS Conference, 23-28 May, Denver, USA, 2004. 9 pp.
- TOMMASELLI, A.M.G.; MEDEIROS, N.G. (2010): **Determination of the indirect orientation of orbital images using control straight lines**. In: The Photogrammetric Record, V. 25, n. 130, 159–179.
- TOTTI, M.E.F.; CARVALHO, A.M.; ALTOE, A.P. (2002): **Indicadores de qualidade de vida nas cidades das regiões Norte e Nordeste fluminenses**. In: Boletim nº 8 do Observatório Sócioeconômico da Região Norte Fluminense. Campos dos Goytacazes. 22 pp.
- TOUTIN, T. (1995): **Multisource data integration: comparison of geometric and radiometric methods**. International Journal of Remote Sensing, v. 16, n. 2795-2811. 15 pp.
- TOUTIN, T. (2004): **Review article: geometric processing of remote sensing images: models, algorithms and methods**. International Journal of Remote Sensing, V. 25, n. 10, 1893-1924.
- TOUTIN, T. (2006): **Comparison of 3D physical and empirical models for generating DSMs from stereo HR Images**. Photogrammetric Engineering & Remote Sensing, Bethesda, V. 72, n. 5, 597-604.
- TOUTIN, T.; CHÉNIER, R.; CARBONNEAU, Y. (2002a): **3D models for high resolution images: examples with QuickBird, Ikonos and Eros**. In: ISPRS SYMPOSIUM. Proceedings... Ottawa, Canada, 8-12 July 2002. V. 43, part 4. 547-551.
- TOUTIN, T.; CHÉNIER, R.; CARBONNEAU, Y.; ALCAÏDE, N. (2002b): **3D mapping with high resolution images**. In: 22. EARSeL SYNPOSIUM. Prague, 1 CDROM.
- VALERIANO, M.M. (2003): **Curvatura vertical de vertentes em microbacias pela análise de modelos digitais de elevação**. Revista Brasileira de Engenharia Agrícola e Ambiental, Campina Grande, V. 7, n. 3, 539-546. Available at: <<http://www.scielo.br/pdf/rbeaa/v7n3/v7n3a22.pdf>>. Access on: 15 Jul. 2012.
- VALERIANO, M.M. (2005): **Modelo digital de variáveis morfométricas com dados SRTM para o território nacional: o projeto Topodata**. In: XII

SIMPÓSIO BRASILEIRO DE SENSORIAMENTO REMOTO, 16-21 Abr 2005, Goiânia. São José dos Campos: INPE, 2005. 3,595-3,602. 1CD-ROM.

VALERIANO, M.M.; MORAES, J.F.L. (2001): **Extração de rede de drenagem e divisores por processamento digital de dados topográficos**. In: X SIMPÓSIO BRASILEIRO DE SENSORIAMENTO REMOTO, 21-26 Abr 2001, Foz do Iguaçu. São José dos Campos: INPE, 2001. 517-524.

VALERIANO, M.M.; CARVALHO JÚNIOR, O.A. (2003): **Geoprocessamento de Modelos Digitais de Elevação para Mapeamento da Curvatura Horizontal em Microbacias**. Revista Brasileira de Geomorfologia, Ano 4, N° 1, 17-29, Available at: http://www.ugb.org.br/home/artigos/SEPARATAS_RBG_Ano_2003/Revista4-1_Artigo03_2003.pdf. Access on: 15 Jul. 2012.

WOLF, P. R; DEWITT, B. A. (2004): **Elements of photogrammetry: with applications in GIS**. 3. ed. New York: McGraw-Hill. 608 pp.

ZEVENBERGEN, L. W.; THORNE, C. R. (1987): **Quantitative analysis of land surface topography**. Earth Surface Processes and Landforms, V. 12, 47-56.